AN EFFICIENT APPROACH TO EVALUATE SEISMIC PERFORMANCE AND RELIABILITY OF WOOD SHEAR WALLS

by

JIANZHONG GU

B.Eng., Shanghai Jiao Tong University, 1992
M.A.Sc., Shanghai Jiao Tong University, 2001

A THESIS SUBMITTED IN PARTIAL FULFILLMENT OF
THE REQUIREMENTS FOR THE DEGREE OF

DOCTOR OF PHILOSOPHY

in

THE FACULTY OF GRADUATE STUDIES

(Forestry)

THE UNIVERSITY OF BRITISH COLUMBIA

August 2006

ABSTRACT

Performance-based engineering and design aim to achieve multiple performance levels under different hazard levels. There is a need to define and quantify structural performance in a reliability based format for managing risk and uncertainty.

The tedious process of nonlinear dynamic analysis of shear walls requires an efficient tool to predict the drift with acceptable accuracy. A simplified mechanics-based analog model was developed for such purpose. The similarities of the load-displacement curves of individual nail connectors and shear walls indicate it may be possible to represent the shear wall behaviour with a large pseudo nail. To develop a pseudo nail model, a nonlinear optimization problem which minimizes the error of prediction is involved. Five search methods were implemented in solving the optimization problem: hill climbing, random search, genetic algorithm, simplex and artificial neural network. The input of the model is the load-displacement relationship of the structure subject to a half cyclic static load with the decreasing curve after peak load. Results from laboratory tests and validated models of two types of regular panel shear walls were used to verify the accuracy of this model. Good agreement was obtained.

The uncertainty of structural performance is attributed to many sources of randomness. The combined effect of earthquake intensity and ground motion records, were considered in this thesis where wall drifts were considered as the performance measure. The drift demand distribution of a structure was formulated and a popular format of reliability procedure was discussed. A new reliability procedure based on conditional distribution at given earthquake records was established. Another procedure,

the Monte Carlo method considering weighted ranking, was proposed to improve the efficiency of simulation when intensity measure is arbitrarily sampled. The construction of confidence curves is also presented for the analysis of structural performance.

Both the pseudo nail model and the reliability procedures were implemented to calculate the reliability indices of eight types of Japanese walls. The results can be used for engineering practice and to guide the modification of building code.

TABLE OF CONTENTS

LIST OF TABLES

LIST OF FIGURES

ACKNOWLEDGEMENT

I would like to express my gratitude to my supervisor, Dr. Frank Lam. His guidance and financial assistance are essential to the accomplishment of my studies. His precious advice and opinion have greatly shaped my view toward the research work of this thesis as well as the general topic of timber engineering.

I would also like to appreciate my advisory committee member, Dr. R. O. Foschi, for his generosity to share his time with invaluable instruction and source codes. I would like to extend my thanks to my advisory committee member, Dr. H. G. L. Prion, for his guidance and help in the past years.

I would like to thank all of my colleagues and friends for their help in the past years.

To my wife, Haiying Zhou

my daughter, Hengtong Gu

my son, Patrick Hengyi Gu

and my parents, Hailin Gu and Huiying Ma

CHAPTER 1. INTRODUCTION

1.1 General

Wood is the primary building material used in low-rise construction in both North America and Japan. In typical wood platform frame construction, 38 mm thick members are used as frames; plywood or oriented strand board (OSB) panels as sheathing; and deeper dimension lumber or engineered wood products as joists and beams. Nail connectors are the principal fasteners used to connect various structural components. Lateral resistance against wind and seismic forces is provided by the diaphragms and shear walls. In Japan, diagonal brace and metal hardware are commonly used to reinforce traditional mortise-and-tenon connections in their post and beam buildings.

Generally, light frame structures are believed to perform well under earthquakes due to the high ratio of strength to weight for wood materials and the high ductility of nail connections. It was reported (Diekmann 1997) that a non-engineered wood house survived the 1906 San Francisco earthquake even though fault rupture caused a 4.8 meter offset in the front garden of the house. In modern wood construction, complex and irregular plans and elevations are becoming more common. This type of construction tends toward structural eccentricity and load path issues that may show more pronounced damage from earthquakes (Zacher 1994). The 1994 Northridge earthquake and the 1995 Kobe earthquake are two examples of recent earthquakes causing enormous damage to densely populated urban areas. The aftermath of these earthquakes has led to a greater level of interest; consequently, increased resources are being invested in the study of the seismic performance of wood structures. The 1994 Northridge earthquake had a

magnitude of 6.7. It did not cause a lot of collapses but the insured loss was as high as $10 billion US dollars, and it created an insurance crisis in the region. The 1995 Kobe earthquake had a moderate magnitude of 6.8. However, its epicenter was located close to the ground surface. Consequently, ground accelerations and velocities affected many buildings, causing damage to 150,000 wooden structures, and resulting in collapses, fire and significant loss of life. The 1995 Kobe earthquake inflicted grave emotional and psychological trauma to Japanese society (Prion and Filiatrault 1996, Foliente 1997).

These two recent tragedies illustrate the destructive consequences of failing to meet the prime design objective of modern seismic resistance structural design, i.e., to prevent building collapse especially under long return period events, and to minimize damage under moderate shorter return period earthquakes. Performance-based engineering considers multiple performance and hazard levels. It is recognized that performance-based engineering and design need to be defined and quantified in a reliability-based format. Many countries, including Canada and Japan, are revising their design codes in order to meet the criteria of performance-based design. The performance analysis of wood structures is one of the primary steps needed to achieve the objectives of modern codes.

Japan is one of the important markets for the British Columbia (BC) softwood lumber industry. To maintain Canada's market share in Japan against its competitors, the BC softwood industry and Canadian government have invested in collaborative research on the performance of Japanese post and beam structures. In Canada, the University of British Columbia (UBC) is actively participating in this program. Through the academic activities and the collaboration between UBC and the Japan Building Research Institute

(BRI), both sides are sharing information and working together to develop performance based design procedures for Japanese wood structures.

1.2 Objective and Scope

The structural performance of wood shear walls relates to many sources of uncertainty, including wood properties and earthquake ground motions. The level of variation of these sources makes it almost impossible to conduct reliability-based performance analysis with experimental studies. Analytical tools calibrated against experimental results are typically used for reliability analysis.

UBC has developed several sets of finite element programs to analyze the response of wood frame structures (Foschi 1990, He 2002) and Japanese post and beam structures (Foschi 2004). In these programs, all components of structures were meshed to fine elements, including beam elements, panel elements and contact elements. The nail connection, which is believed to be the main source of the nonlinearity and pinching effect of the cyclic load-deformation curves in wood structures, was modeled with a beam surrounded by the nonlinear foundation and contact interface. A sub-program, HYST (Foschi 2000), can be employed to calculate the response of each nail connection.

A typical wood house has thousands of nails. When the house is subjected to earthquake load, the time-history analysis may have several thousand time steps, each of which can be divided into small load steps. At each load step, the response of every nail must be calculated by the HYST program. Iteration is usually necessary for such a nonlinear problem, and this requires repeating the calculation several times. Consequently it would be very time-consuming to calculate the earthquake response of

wood houses using the detailed finite element approach. Reliability based-analysis and design are especially challenging work for this kind of structural analysis.

The objective of this thesis is to propose a solution to earthquake reliability analysis of wood structures. It includes a computationally-efficient model to evaluate the hysteresis behaviour of wood shear walls. The accuracy of the model should be acceptable for earthquake reliability analysis when compared with other simplified models. It also includes reliability analysis methods to deal with the uncertainty of structural performance.

There are three major contributions from this thesis. First, a simulation-based hysteresis model which has good accuracy and computational efficiency is developed. Second, two new formats of seismic reliability procedures are developed for performance-based earthquake engineering and design. Third, reliability indices of eight types of Japanese wood shear walls are presented for code provision consideration or further study.

Chapter 2 consists of a literature review for this thesis. Chapter 3 introduces the concept of the proposed shear wall model and its realization methods. Background and physical explanations are illustrated at the beginning, followed by an introduction of several search methods in solving the optimization problem. Chapter 4 describes the verification of the pseudo nail model with different configuration under different load protocols. Here, two examples of regular light frame shear walls with two different configurations of sheathing panels are presented. Chapter 5 discusses the procedures of seismic reliability analysis and three methods are presented to evaluate the structural probability of failure. The concept of confidence curves is also discussed. Chapter 6

involves an application of the shear wall model and reliability analysis procedures. The experimental results of eight types of Japanese walls are used as the input to calibrate the model, after which reliability analysis of each type of walls is conducted. Earthquake performance of the walls made from different species is compared. Chapter 7 presents the conclusions and recommendations for future study.

CHAPTER 2. LITERATURE REVIEW

2.1 Introduction

When structures are subjected to horizontal loads, such as earthquake or wind loads, relative lateral motions tend to occur between the different stories of the structures. The large horizontal inertia forces must be transferred to the ground by the structural components to avoid excessive structural displacement, fracture or even failure. These components are as important as the gravity load resistant components of the structure since all of the components provide the integrity needed for the structure to function as a shelter.

Basically three types of lateral load resistant systems are being used in wood structures: moment resistant connections, braced walls and shear walls.

1) Moment resistant connections are not commonly used in platform frame construction. Splitting along the grain is critical even though moment resistant connections can provide a large opening within a frame. Some applications of moment resistant connection are found in heavy timber post-and-beam construction in North America. Efforts are being made to decrease the splitting issue by use of innovative connection systems, such as the timber rivets (Hampson et al. 2003). Nevertheless, wide application of this type of system still has a long way to go.

2) Braced walls are one of the most efficient structural systems used to resist lateral load. Bracing members are the diagonal members inserted in the rectangular bays of frame. The bracing creates a stable triangulated frame to resist the lateral loads. Even numbers of braces are typically placed symmetrically on one side of

walls to resist the load from both directions. Traditionally knee bracing and cross bracing were widely applied to provide horizontal stiffness.

3) In North America, sheathed shear walls replaced braced shear walls in platform frame residential construction. A sheathed shear wall develops its in-plane structural rigidity through the in-plane shear capacity of the sheathing material which is connected to the framing lumber with nails. The sheathing material can be solid lumber sheathing, structural panels, gypsum wallboard or stucco. Sheathing materials and the fasteners connecting the sheathing to frames are the key components developing shear action in a wood frame construction. In this thesis, such shear walls will be referred to panel-sheathed shear wall in order to distinguish it from other types of walls.

In North America, sheathed shear walls are the most popular lateral resistant system in platform frame construction. In Japan and other eastern Asian countries, traditional construction style, consisting of the post and beam structures with wood to wood connections, such as mortise-and-tenon and wedge, are typically used. These wood-to-wood connections alone can be considered as semi-rigid connections with limited capacity to resist the applied moment caused by large seismic loads. As Japan is an earthquake-prone country, diagonal bracing has become popular to increase the resistance of structures under earthquake. Metal hardware has also been introduced to connect or reinforce the major post and beam members. In recent years, home builders are become increasingly interested in panel sheathed shear walls although the braced post and beam walls with metal fasteners are still being used. These combined lateral resistant systems

represent the current trend in the Japanese home building industry (Japan Housing and Wood Technology Center 1996).

According to the Canadian Wood Council, a shear wall is *an in-plane or plate-type structural element designed to transmit force in its own plane*. Herein, the terminology of shear wall in this thesis refers to all three types of lateral load resistant systems, including moment resistant connected frames, braced walls and sheathed shear walls. In fact, the shapes of the load-displacement relationships in the three types of systems are similar in form. It is not surprising therefore, that many models, such as BWBN model (Foliente 1993), apply to all three types of systems.

2.2 Modeling of Shear Walls

The structure of shear walls involves multiple types of members and connections. It is complicated to analyze the structural behaviour of shear walls. Research on the structural performance of shear walls under disaster load has been performed for many years. The shear wall modeling was summarized in many previous studies, such as those of Dolan (1989), BFRL report (1997), and Pardoen et al. (2003). The following sections summarize some of the research.

2.2.1 Simple Nonlinear Spring Models

The simple nonlinear spring model refers to models which describe the shear walls with one or several nonlinear springs. Under a dynamic load, one or multiple dampers are added to explain viscous damping. Basically, most of these models are single-degree-of-freedom system (SDOF). They are purely phenomenon-based descriptions of

experiments. The significant difference among these models is how to express the pinching effect under a reversed cyclic load.

Ewing et al. (1980) described a model of wood diaphragms supported on masonry walls under a seismic load. One pair of spring and damper was applied to simulate the response of each section of diaphragm. From the cyclic test results, the envelope curve of the nonlinear response was represented by a so-called second-order curve. Another multi-linear curve was added to describe the unloading curves from the backbone curve under cyclic load.

Stewart (1987) and Stewart et al. (1988) proposed a load-deflection hysteresis model for ductile nailed structures. This model used a tri-linear curve to represent the envelope curve of the reverse cyclic test results. The unloading curve was described as two straight lines which intersect at the displacement axis. An additional straight line expressed the reloading curve to explain the pinching effect.

Sakamoto and Ohashi (1988) suggested a lumped mass model for the earthquake response analysis of walls. Five lines connecting the origin, one specific point and four turning points outlined the envelope curve of the nonlinear spring. Two additional lines were added to formulate the unloading curve. The reloading curve had two additional lines, one of which had a slope varying with the starting point of reloading.

Ceccotti and Vignoli (1990) applied a piecewise linear hysteresis model to DRAIN-2DX, a commercial finite element program, to evaluate the seismic behviour of semi-rigid timber joints. This model employed six straight lines to describe the nonlinear load-displacement relationship of wood members. This model was later applied to calibrate

the force reduction factor in the National Building Code of Canada for shear walls (Ceccotti and Foschi 1998) and wood buildings (Ceccotti and Karcabeyli 2002).

Yasumura (1990) developed a SDOF lumped mass model to perform time-history earthquake response analysis for braced frames. A bi-linear slip model was used to describe the load-displacement hysteresis loops from cyclic tests. This spring model used five independent values for the slope of lines under different loading stages: one for loading on the primary curve before yield, one for loading on the post yielding primary curve, one for unloading from primary curve, one for reloading with a soft spring and one for loading with a hard spring toward a previous peak. A more complicated model was developed to analyze the earthquake performance of wooden frame shear walls (Yasumura 2000).

The Bouc-Wen-Baber-Noori model (BWBN, Bouc 1967, Baber and Wen 1981, Baber and Noori 1986) is a distinct SDOF model used to analyze the earthquake performance of structures. Unlike other models using multiple straight lines or curves to simulate the inelastic and pinching effect, this model expresses the hysteresis loop through a set of differential equations. 13 parameters are involved in the differential equations. Foliente (1993) proposed to use this model to conduct the stochastic analysis of wood systems.

Kawai (1998) proposed a combined model with a series of straight lines considering the effect of slip. The model used six parameters to define different levels of stiffness at different loading stages. Three additional parameters were used to locate the starting and ending points of lines. An assumption of this model is that the experienced maximum displacement after peak load on one side would be the limit for the other side. The

parameters of the model were obtained from the cyclic test results. Then a dynamic analysis using the same set of model parameters can be conducted to predict results from shaking table tests and pseudo dynamic tests.

2.2.2 Simplified Analytical Models

To add to the current knowledge of the phenomenon-based description of shear walls, many attempts were also carried out to analyze the load-displacement relationship of shear walls with analytical methods. Shear walls are heavily redundant since they are always connected with more connections than that of statically-determinate systems. To simplify the analysis, some researchers tried to describe the shear walls with several degree-of-freedoms (DOFs). Typical assumptions of these models are straight (or rigid) frame members, rigid sheathing panels, and three to five DOFs for the shear wall. Some models involve energy conservation to establish equilibrium equations.

Tuomi and McCutcheon (1978) calculated the racking strength of nailed walls. The key assumptions of their work include: (1) the frame distorts as a parallelogram while the sheathing panel remains rectangular; (2) the nail connector is linear; (3) distortions and deflections are small, so that the deformation of each nail can be expressed as the function of corner distortion. An energy method was applied to calculate the racking strength. Robertson (1980) stated that the Tuomi and McCutcheon model (1978) cannot reflect the effect of wall length and vertical weight. This model was further improved upon to formulate an equivalent wall model in which all nails were represented by two diagonal springs in order to calculate the effect of openings (Itani et al. 1992). McCutcheon (1985) further modified this model with nonlinear nail connectors.

Easley et al. (1982) published another simplified model to explicitly calculate the shear deformation. Their method was originally developed for corrugated metal shear diaphragms. In this work, shear strain was decomposed into two parts: shear strain in the individual panels and shear strain due to the localized deformations at the fasteners. It was also assumed that shear forces in vertically arranged nail fasteners are in the vertical direction and those in top and bottom nail fasteners have both vertical and horizontal force components. The vertical forces of these nail fasteners were only proportional to the distance to the vertical center line of each panel. A set of formulae were given to predict the deformation of shear walls. The results were reported to be acceptable for engineering design when compared with finite element method results and test results.

Gupta and Kuo (1985) proposed a simple numerical model for nonlinear analysis. Four degree-of-freedoms for a single panel wall were used to describe the relative angle between horizontal edge frames (top and bottom plates) and panels, the relative angle between vertical edge studs and panels, the shear angle of vertical studs, and the magnitude of the sinusoidal shape of the studs. Each panel had an additional one DOF. The results were compared with experiments by Easley et al. (1982) and satisfactory agreement was observed. It can also be noted that the assumption of the sinusoidal shape of studs is not necessary to obtain acceptable results. In principle, this model is similar to the works of Tuomi and McCutcheon (1978) and Easley (1984). The difference among these models is the number of DOF used to describe the movement of frames and sheathing panels. The diagonal displacement between frames and panels was the only DOF in the Tuomi and McCutcheon's work (1978). Two DOFs expressed the sway angle of frames and the angle of panels relative to the frames in Easley's work (1982). In

a later work, Gupta and Kuo (1987) improved on the model by considering the uplift deformation of studs caused by horizontal load.

Källsner (1984) proposed an elastic calculation model for shear walls. He used the assumptions of rigid frames, rigid panels and elastic nail connections. The system had four DOFs including: frame rotation angle, panel rotation angle and displacement of the panel center. Minimal potential energy method was applied to the variables of DOFs. Källsner and Lam (1995) improved upon this model with the consideration of plastic deformation. Lower bound and upper bound methods were used to estimate the plastic load-carrying capacity of walls.

Another extension of simplified models was developed by Filiatrault (1990). It is a simple numerical model for the analysis of earthquake excitations. The deformation of the frame was defined by the lateral displacement of the top plate (1 DOF). Each sheathing panel was depicted as rigid-body translations and rotation (3 DOF) and symmetric shear deformation (1 DOF). In total, each wall had 4N+1 DOF (N is the number of sheathing panels). This number is significantly less than that of the general finite element method. The load slip characteristic of the nail connector is same as in Dolan's model (1989). Good agreement between analytical and experimental results was observed. Folz and Filiartrault (2001) improved this model to simulate reversed-cyclic tests and calibrate a single-degree-of freedom nonlinear dynamic system. This model was widely used in the CUREE-Caltech Woodframe Project (www.curee.org).

Dinehart and Shenton (2000) developed a dynamic model based on the observation that, at small displacement amplitudes, the hysteresis curve of a nail connection is elliptical in shape. Then the sheathing-to-stud connections were modeled using a linear

viscoelastic element. The results showed that this model fit the experimental results well at small displacement and not badly at moderate displacement. In both the basic assumption and the formulae simplification, a small equivalent damping ratio was assumed.

2.2.3 Finite Element Models

Compared with simple analytical models, finite element models can consider the contribution of all structural members, including frame, sheathing, nail connectors and hold downs. Finite element models have much accuracy and robustness. They can consider the effect of sheathing openings and bending of frame members. The buckling effect was also considered in some models. The finite element based shear wall models can be easily expanded for 3D analysis of buildings.

Foschi (1977) developed a finite element program for diaphragms. In this model, the sheathing panels were expressed as 12-node orthotropic plane stress elements. The frame members were modeled as linear beam elements. The nail connectors were expressed as nonlinear springs. The analysis gave a good estimate for the load-deformation characteristics of the walls as compared with experimental results. This model was improved to incorporate detailed nail connectors in DAP3D (Foschi, 1990). Recently, Foschi (2000) improved the model by calculating the hysteresis response of individual fasteners with principles of mechanics and the finite element method. Based on Foschi's work, He (2002) developed a three-dimensional finite element program for wood light frame structures. This program incorporated both a static module and a dynamic module. The outstanding feature of this program lies in the potenetial to simulate the structural eccentricity and load path of the whole building under dynamic loads. Compared to the

shake table tests of shear walls and one-storey house conducted at University of British Columbia (Durham 1998, He, 2002), good agreement of He's program was shown.

Itani et al. (1984) developed a finite element model where the nail connector was modeled as joint elements that are similar to smeared nonlinear springs. Each two-node joint element was expressed by a 10x10 stiffness matrix corresponding to different nodal displacement of frame and sheathing elements. The predicted results were verified with test results and good agreement was reported (Itani et al. 1984, Cheung et al. 1988).

Dolan (1989) developed a finite element model of shear walls that contains following elements: 1) beam elements for the frame members; 2) bilinear corner connector elements for the connection between the framing members; 3) plate elements for the sheathing panels; 4) sheathing connector elements consisting of nonlinear 3-D spring elements for the fasteners; and 5) bilinear bearing connector elements for the gap between adjacent sheathing panels. Beside the assumption proposed by Foschi (1977), Dolan used following assumptions: 1) contact elements are used between adjacent sheathing panels; 2) after peak load, the load decreases to zero linearly; 3) the exponential type functions are used to express the pinched loops; 4) the viscous damping is proportional to the mass. The results of this model compared well with test results. A dynamic program, DYNWALL, was also developed to compare with shake table test results. Good agreement was observed between numerical and experimental results for some cases.

Kasal et al. (1992a) developed two finite element models with commercial finite element program, ANSYS. The first is a detailed substructure model. In this model, studs and sheathing were modeled as two-dimensional shell elements with linear orthotropic properties. The joints were represented by two nonlinear springs clustered at

common nodes for sheathing and studs, with one for withdraw and another one for shear resistance. Gap elements were placed between sheathing panels. The other simple model utilized nonlinear diagonal springs to represent the shear behavior of walls (Kasal et al. 1992b). This assumption was based on DOF condensation technique. Satisfactory agreement between these two models was reported.

2.3 Experimental Tests of Shear Walls

The structural behaviour of wood shear walls is well-recognized for its complexity. The materials, connectors, geometry and load condition strongly affect the performance of shear walls. Experimental tests of shear walls help engineers understand how individual structural components act together to exhibit the structural behaviour. The test results can help to point to improvements and design recommendations, which can be used in engineering practice.

Over the past decades, many researchers have conducted numerous full size shear wall tests with the combination of different size, materials, opening and fastener spacing. Typical size of tested shear walls is 2.44 m x 2.44 m (8 feet x 8 feet), such as those in experiments conducted by Dolan (1989), Tissell (1993) and Durham et al. (2001). Large size shear walls were also investigated by some researchers, such as Karacabeyli and Ceccotti (1996), Lam et al. (1997) and Pardoen et al. (2003). Detailed bibliographies on some of the older full size shear wall tests were written by Carney (1975) and Peterson (1983). The research after 1982 was summarized by the BFRL report (1997), Pardoen et al. (2003) and van de Lindt (2003). Most of these bibliographies only covered the research on shear walls made with regular 38 mm x 89 mm members and sheathing panels. Few of them (van de Lindt 2003) mentioned some work that was done

concerning Japanese traditional construction. This thesis summarizes some published work on Japanese post-and-beam walls.

Yasumura (1990) conducted a series of reversed cyclic tests of braced frames. The frames had a width of 3800 mm and a height of 7500 mm. Large size glulam beams and columns were used. Steel plates were used to connect the wood members both with and without pins. The test results were used to obtain parameters of a hysteresis model.

Sugiyama et al. (1988) examined a series of racking tests for braced walls. Eleven walls with different geometry of bracing and siding were tested. It was found that the load-carrying capacity of the structure is larger than that of the summation of individual braced walls.

Kakaoka and Asano (1988) conducted photoelasticity tests to study the performance of frames and joints for Japanese traditional structures. Isochromatic lines from small scale tests with wedge joints were compared to show the difference between different frame and sheathing configurations. Some rotational deformation curves of joints were also shown. Data from the tests were used to analyze a frame structure.

Hirashima (1988) studied the earthquake response of a two-storey Japanese post-and-beam house. The house had a width of 3.64 m, a length of 7.28 m and a height of 5.46 m. In the first stage test, the house was tested cyclically with amplitude of 1% of storey height. During the following three months, the house experienced 21 earthquakes and its response was recorded for analysis. Finally, a forced vibration test was conducted to identify the resonance frequency. The test results from different test stages were found to be consistent with each other.

Hayashi (1988) reported his racking resistant tests of conventional walls with plywood sheathing panels. The tested walls had a dimension of 1.8 m x 2.55 m for S-series and 1.792 m x 2.514 m for SN-series. Each series had 12 walls with different opening ratios and locations. The test results revealed that stiffness and strength ratio decrease with the increase of opening ratio.

Kawai (1998) tested 16 types of shear walls that followed traditional Japanese post-and-beam construction. Most of the walls had the dimension of 3.64 m x 2.79 m. Twelve types of the specimen were sheathed with plywood, gypsum or siding boards. Six others were diagonally braced. Monotonic, cyclic and pseudo-dynamic loading tests were conducted for each type of wall.

Yasumura (2000) conducted tests on a series of wooden frame shear walls in accordance to Japanese construction standards. These walls had the length of 1.72 m or 2.73 m and the height of 2.44 m. They were tested under monotonic load, reversed cyclic load and pseudo dynamic load. Varying wall configurations including different opening, nail spacing, hold downs, sheathing orientation and sheathing blocking were considered. The test results were used to compare the structural performance of the various wall configurations and to verify some theoretical models.

Yamaguchi et al. (2000) conducted a series tests on 2.44 m x 2.44 m shear walls made with 38 x 89 mm Canadian S-P-F lumber and 9.5 mm Canadian plywood. A total of 12 specimens were studied under different loading rates of monotonic and reversed cyclic tests, pseudo dynamic tests and shake table tests. It was found that the force-deformation behaviour of light frame shear walls was influenced by the rate of displacement and the test protocols.

UBC conducted some experimental studies on the performance of Japanese walls. The walls consisted of three types: two-brace walls, four-brace walls and OSB sheathed walls. Beside traditional mortise–and-tenon connection, metal hardware was used in the construction of the walls to reinforce the connection. Twelve specimens with the dimension of 2.62 m x 2.70 m were tested under monotonic and reversed cyclic load. Three load protocols were applied to compare the effect to test results. This work was reported in a master's thesis (Stefanescu 2000).

2.4 Seismic Reliability Analysis of Wood Structures

Traditional design methods for shear walls are based on limited experiments and the force reduction factor method. The factors of the design equations, applied to nominal loads or resistances, are normally calibrated or optimized to approximately achieve target reliabilities over a sufficiently large, representative number of "calibration points or design cases". As a consequence, the actual reliabilities achieved by these design equations may vary from situation to situation and may deviate substantially from the targets for cases other than the original calibration points (Foschi 2003).

Performance of buildings is expressed with regard to the suitability of the building for function and occupancy, the extent to which life-safety is protected, and the necessity or practicality of effecting repairs on the structure and restoring it to service (SEAOC 1995). FEMA 273 (1997) defines earthquake hazard level with occurrence probability in 50 years. Four levels, 50%, 20%, 10% and 2% of occurrence probability in 50 years, were specified as the hazard levels. The corresponding mean return periods of these hazard levels are, respectively, 72, 225, 474 and 2475 years. The last two were particularly defined as Basic Safety Earthquake 1 and Basic Safety Earthquake 2, based on their

levels of importance. The building performance levels were described as Operational, Immediate Occupancy, Life Safety and Collapse Prevention. The structural performance levels were expressed by limiting damage states and drift limitation. Drift limitation of 3% for Collapse Prevention, 2% transient or 1% permanent for Life Safety and 1% transient or 0.25% permanent for Immediate Occupancy, is recommended for wood structures.

Performance-based design was promoted for the uniform design performance objectives considering multiple performance and hazard levels. Due to the uncertainty of seismic levels and corresponding resistance levels, performance-based design needs to be defined and quantified in a reliability based or probabilistic format.

Ceccotti and Foschi (1998) presented a structural reliability procedure to evaluate the force reduction factor for wood shear walls adopted in the NBCC. First, the shear walls of a four-storey residential building were designed following NBCC provisions for the city of Vancouver. Then nonlinear dynamic analysis was conducted with DRAIN-2DX to obtain the peak drift. The parameters of the hysteresis model came from the test data at Forintek Canada Corporation. The reliability indices were then calculated with RELAN (Foschi et al. 1988). The results showed that the current force reduction factor in NBCC may be adequate.

Foliente et al. (2000) conducted seismic reliability analysis of 0.91 x 2.45 m shear walls with a modified BWBN model. The applied mass was calculated following modified BRANZ procedure. The artificially generated ground motion records were scaled to the levels of 50%, 10%, 5%, 2% and 1 % occurrence probability in 50 years. The reliability index was found to depend on the assumed displacement capacity

determined from the static cyclic test, and the intensity of earthquakes used to generate the displacement spectrum.

Foschi et al. (2002) presented an approach to reliability calculations in performance-based design, using an importance sampling simulation. A structural database (force and displacement) was generated by finite element tools. The target reliability levels were calculated with localized interpolation from a response database. This method was incorporated with RELAN (Foschi et al. 1988) & IRELAN (Li and Foschi 1998). In the work which followed (Zhang and Foschi 2003, Foschi 2003), artificial neural network technology replaced localized interpolation to construct the response surface for reliability evaluation and seismic design. Due to the variation of the frequency content of earthquakes, two databases were built to represent average and standard deviation of the structural response over a large suite of earthquake records based on four variables representing perimeter and field nail spacing, the mass carried by the wall and peak ground acceleration of earthquake. Multiple performance levels, including serviceability, moderate damage and tearing force, were considered. Performance-based design of multiple objectives was realized through solving an optimization function which minimizes the deviations between the achieved reliabilities and the targets. A program, EQWALL, integrated with RELAN, IRELAN and DAP3D, was available for the design of shear walls.

Rosowsky (2002) reported his work in reliability-based seismic design conducted under Task 1.5.3 of the CUREE-Caltech Woodframe Project. The intention of this work was to propose a performance-based framework for the design. A suite of 20 ordinary ground motion records was selected to represent non-near fault ground motions in

southern California. These records were scaled to match the Uniform Building Code design requirements. Dynamic calculations were performed to give peak drift for each earthquake motion. Performance goals were calculated from the distribution of peak drift curves.

In van de Lindt and Walz's work (2003), 10 pieces of 1.2m x 2.4 m (4 x 8 ft) shear wall were tested to calibrate a hysteresis model. The result from each piece of wall was fitted to a nonlinear spring model. Then a SDOF system with each set of parameters was analyzed under 10 earthquake ground motion records. The peak drift from the time domain analysis was fitted to a Weilbull distribution. The reliability under different hazard levels was evaluated and a wide range of reliability index was reported. Another study by van de Lindt's (van de Lindt et al. 2005) examined the reliability indices of shear walls specified by American Forest and Paper Association/American Society of Civil Engineers 16 committee. Strength, rather than commonly used displacement, was chosen as the performance measure. This study examined a portfolio of shear walls under a set of 20 earthquake records (Krawinkler 2001). The calculated reliability indices ranged between 1.0 to 3.0 with a mean of 1.95 and a coefficient of variation of 0.30.

Li and Ellingwood (2004) presented a probabilistic methodology used in US Federal Emergency Management Agency supported SAC Steel Project to assess the performance of wood frame residential houses. SAC Project ground motions were used in the analysis and three hazard levels, 2%, 10 % and 50% exceeding probability in 50 years were considered. The maximum drift was predicted. The relationship between spectral

acceleration and demand (maximum drift) was fit to an exponential function, which can be the basis for further study.

Ellingwood et al. (2004) proposed a fragility analysis methodology of light frame wood construction subjected to hurricane and earthquake hazards. The analysis was demonstrated for selected common building configurations and constructions. It pointed out that the conclusion of fragility analysis under the control variable is easily understood by the general public than the more complicated concept of exceeding probability. Further validations were believed necessary before being application to building code improvements or loss assessment and insurance underwriting could be made.

2.5 Summary

Different shear wall models have been developed. The models and their input parameters depends on the type of wall under consideration, the type of test conducted, and the data fitting approach employed to characterize the wall performance. Simple nonlinear spring models fit the load-displacement behaviour of shear walls with a nonlinear spring. Simple analytical models use several DOFs to describe the nail slip between sheathing panels and frame members. Hysteresis models can also be calculated from mechanics principles and the finite element method, considering the contribution of the structural members. Generally speaking, the finite element models have good robustness to adjust to typical input displacement history or protocol at the cost of computational efficiency. The simple nonlinear spring models are the most efficient to evaluate the response while the fitted parameters of the models varies from different wall configurations. The simple analytical models are moderate in both computational efficiency and configuration-independence.

Seismic reliability analysis of wood structures is a new topic for performance based earthquake engineering. Some researchers used fragility method to analyze the earthquake performance of wood structures, such as Foliente et al. (2000), Rosowsky (2002) and Ellingwood et al.(2004). Some other studies (Foschi et al. 2002, Li and Ellingwood 2004) followed a traditional method for steel structures (Cornell et al. 2002). All of these methods calculated the probability of exceedance fully or partially from conditional probability distribution.

To conduct earthquake reliability analysis, two aspects of knowledge are required: an efficient model to predict the drift of structures with acceptable accuracy and appropriate methods to consider the combined effect of earthquake hazards and other sources of uncertainty. This thesis discusses the development of both aspects of knowledge.

CHAPTER 3. MODEL DEVELOPMENT

Shear walls have different combinations of materials, sizes and styles. The uncertainty of performance of shear walls depends on all aspects of the components, construction process and service condition. The relatively expensive experimental tests limit the geometry, load condition and the number of test specimen that can be considered. Theoretical modeling is important to better understand the intrinsic mechanism of shear wall performance under the expected uncertainty, so that the performance of general shear walls can be predicted and codified.

The objective of this chapter is to introduce a new shear wall model in which the mechanics based nail model is fitted to represent the behaviour of shear walls. Basically, the model is a nonlinear spring, which response is calculated from mechanics principles with a FEM program, HYST (Foschi 2000).

3.1 Initiation of Modeling

There are many similarities between the shapes of the load-deformation curve of individual nail connectors and that of shear walls (Figures 3.1 and 3.2). In both figures, the initial shape of load-displacement relationship is close to linear. With the increase of displacement, the nonlinearity becomes apparent. After reaching the ultimate or peak load, the load decreases while displacement continues to increase. The basic shape of pushover test curves of nails and shear walls are upwardly convex. The main difference between Figures 3.1 and 3.2 is the magnitude of units.

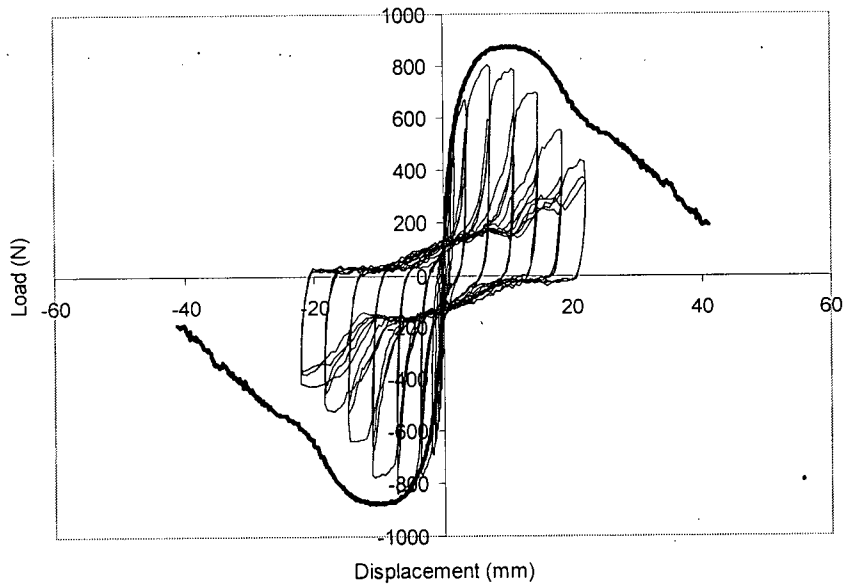

Figure 3.1 Load-displacement relationship from pushover and reversed cyclic loading of a nail connection test

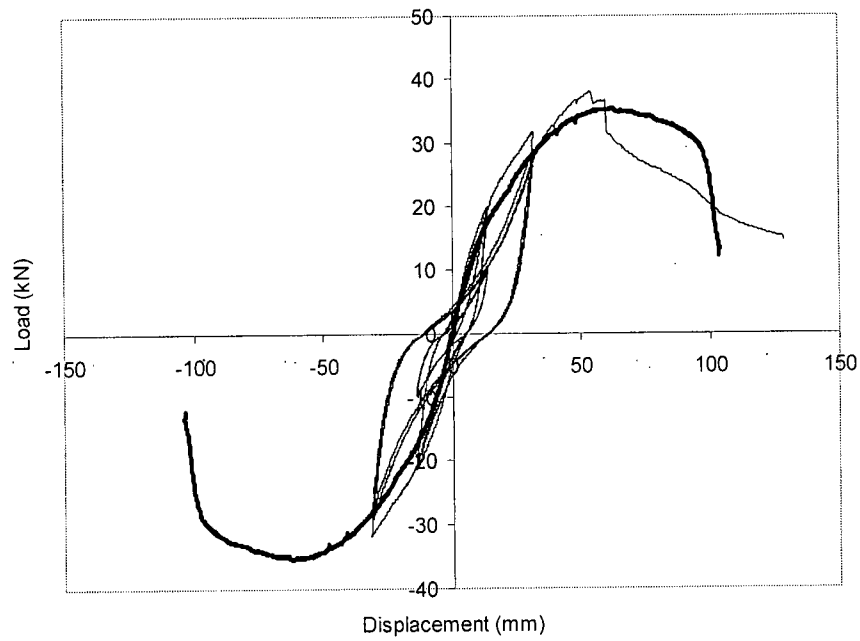

Figure 3.2 Load-displacement relationship from pushover and reversed cyclic loading test of a shear wall

3.1.1 Visual Expression of Shear Wall Mechanism

The similarities between the load-displacement relationship of shear walls and nail connectors can be explained by the mechanism of load transfer in wood frame shear walls. It is well recognized that the lateral response of shear walls is mainly governed by the characteristics of the panel-to-stud connections. The combined effect of the deformation from all the nails is superimposed together to exhibit an overall load-displacement curve of shear walls.

Figures 3.3 and 3.4 visually illustrate the relationship between the load-deformation curves of shear walls and nails. The frame is assumed to consist of pin jointed rigid straight members. When the wall is pushed by lateral force resisting wind or earthquake loads, the frame deforms in a parallelogram shape and the relatively rigid sheathing panel attempts to maintain the original shape. The shape difference between the frame and panel stretches the nail connectors. All of the components are integrated together through the connection of joints.

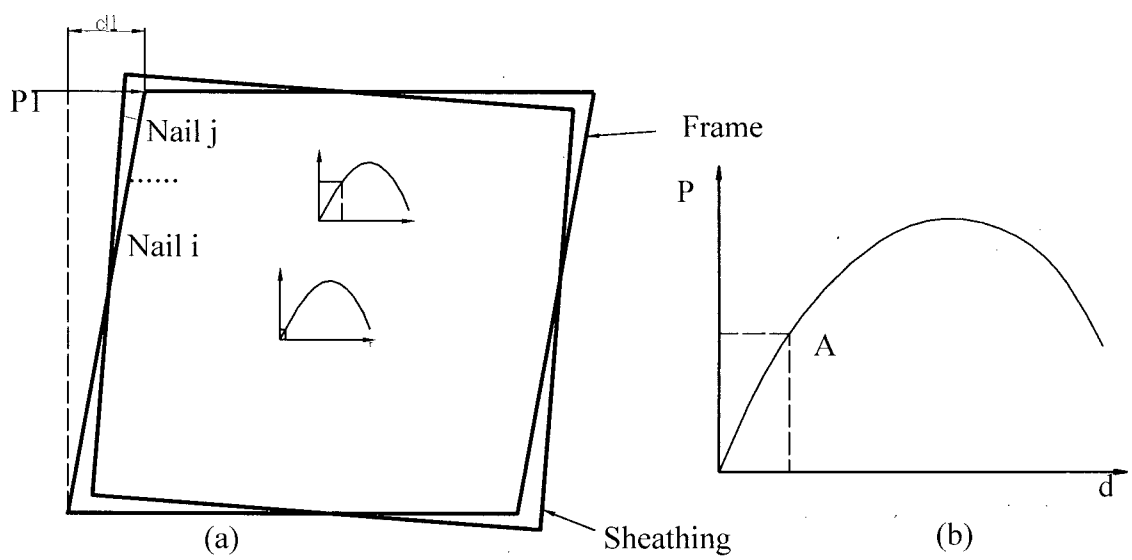

Figure 3.3 Initial stage of shear wall tests

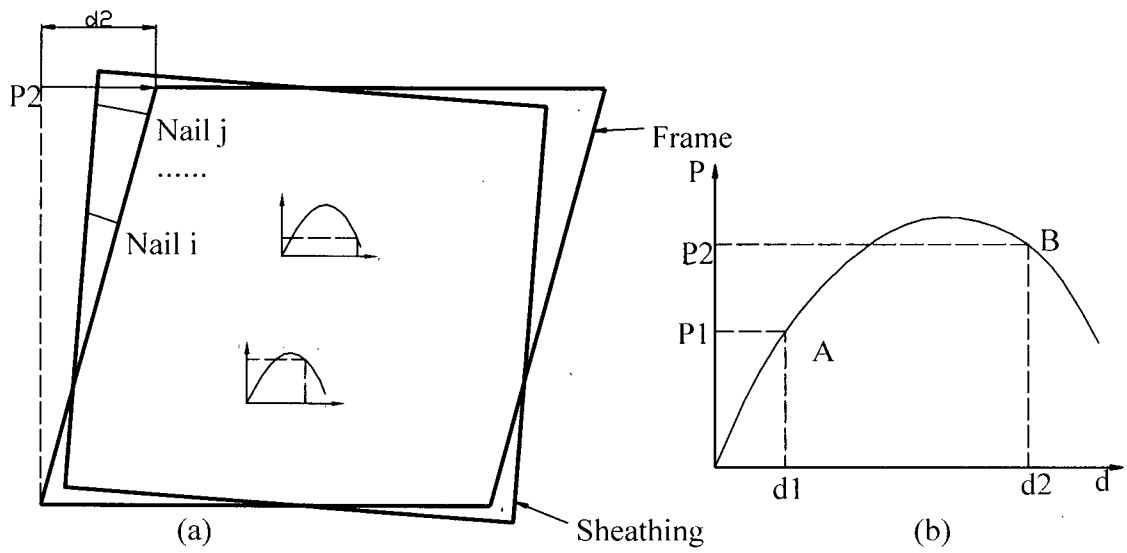

Figure 3.4 Secondary stage of shear wall tests

For illustration, two nails are plotted in Figure 3.3a, Nail i and Nail j at different locations. At the beginning, the applied force P_1, is small enough such that the nail forces are in the initial stage. The lateral displacement of the shear wall is noted as d_1. The current status is expressed as Point A in the load-displacement curve of the shear wall (Figure 3.3b).

When the pushover test continues, the gap between frame and sheathing increases but the load increment lags after displacement increment since the nails behave nonlinearly. That is, the slope of the load-displacement curve of the structure will decrease continuously with the increasing of displacement. Some of the nails may experience yielding of the steel or crushing of the surrounded wood medium both of which result in further decrease of resistance in the structure. This process will continue until the number of key nails experiencing the maximum load reaches a critical point after which

the shear wall cannot sustain further increase of lateral load. Point B in Figure 3.4b exhibits the status at this stage.

The approximate visual description illustrates that the load-displacement curve of a shear wall is the total contribution of an ensemble of nails. Its behaviour therefore is intrinsically related to the performance of single nail connectors.

3.1.2 Mathematical Expression with Finite Element Method

When the finite element procedure is applied to analyze the shear wall performance, the nodal forces can be finally expressed as the product of stiffness matrix and displacement vector (Foschi 1977, Filiatrault 1990):

$$\begin{bmatrix} k & A_{1\times n} \\ B_{n\times 1} & K_{n\times n} \end{bmatrix} \begin{pmatrix} d \\ R_{n\times 1} \end{pmatrix} = \begin{pmatrix} P \\ \mathrm{O}_{1\times n} \end{pmatrix} \tag{3.1}$$

where:

k is a variable (nonlinear function of nail slip and other materials);

A, B, K are sub-matrix (nonlinear functions of nail slip and other variables);

R is a vector representing nail slips;

d is the transverse displacement at the loading point (refer to Figures 3.3 and 3.4);

P is the applied load (refer to Figures 3.3 and 3.4);

O is a zero vector representing zero external forces at some nodes.

It should be stated that the stiffness matrix here refers to the secant stiffness. For nonlinear analysis of shear walls, generally there is no closed form expression of this matrix.

After simple calculation, one has:

$$d = k^{-1}(P + AK^{-1}Bd) \tag{3.2}$$

This equation indicates that the lateral shear wall displacement is a function of nail slips, other material properties and applied load. If the frames and sheathing panels are assumed to be rigid, the load-displacement relationship of shear walls is governed by the property of the nail connectors.

It can be concluded that the load-displacement curve of shear walls results from the total contribution of all nails as well as other materials. It can be considered as a "scaled" nail load-deformation curve representing the behaviour of a group of nails. This implies that it may be possible to find a pseudo nail connector with appropriate parameters to model the behaviour of shear walls.

3.2 Model Development

To simulate the load-displacement behaviour of shear walls, the selection of a representing nail model is important for the accuracy. Here a mechanics based nail model (Foschi 2000) was chosen as the analog. The finite element method is employed to describe the nonlinear behavior of the elasto-plastic properties of the nail, the nonlinear interaction between the nail and its surrounding wood medium and formation of the gap (Figure 3.5). In this figure, F represents the force applied to the top of the nail. When the nail head experiences a magnitude of displacement, Δ, the nail deforms to the shape as shown. The reaction of the surrounding wood medium is assumed to be a function p(w), which is the reaction force at unit length acted to nail with respect to the displacement, w. The embedding function p(w) has six parameters, K, Q_0, Q_1, Q_2, Q_3 and D_{max}, which allows for the degradation of strength and stiffness. K is the initial stiffness of the curve while Q_0 and Q_1 are the variables for an asymptote which illustrates the stage of the curve near the peak load. D_{max} is the displacement at the maximal load. Q_3 is a ratio of peak

load defining the shape of decreasing curve. Q_2 is the ratio of the peak load that is achieved at a deformation Q_3 multiplied by D_{max}. In this way, Q_2 and Q_3 define the shape of the decreasing or softening portion of the embedment relationship. Additional two parameters, D_i and L, are the diameter and length of the pseudo nail. So the reaction of wood medium, p(w) is expressed as:

$$p(w) = (Q_0 + Q_1 w)[1.0 - \exp(-Kw/Q_0)], \quad (\text{if } w \le D_{max}) \tag{3.3}$$

$$p(w) = p_{max} \exp[Q_4 (w - D_{max})^2], \quad (\text{if } w > D_{max}) \tag{3.4}$$

$$p_{max} = (Q_0 + Q_1 D_{max})[1.0 - \exp(-KD_{max}/Q_0)] \tag{3.5}$$

$$Q_4 = \log(Q_2)/[D_{max}(Q_3 - 1.0)]^2 \tag{3.6}$$

$$Q_2 = p/p_{max} \tag{3.7}$$

$$Q_3 = w/D_{max} \tag{3.8}$$

where

$p(.)$ is the resultant reaction force, force/length;

Q_0 is the intercept of the asymptote, force/length (refer to Figure 3.5);

Q_1 is the asymptotic stiffness, force/length^2 (refer to Figure 3.5);

K id the initial stiffness, force/length^2;

w is the displacement, length;

p_{max} is the maximum resultant reaction force, force/length;

D_{max} is the displacement at p_{max}, length.

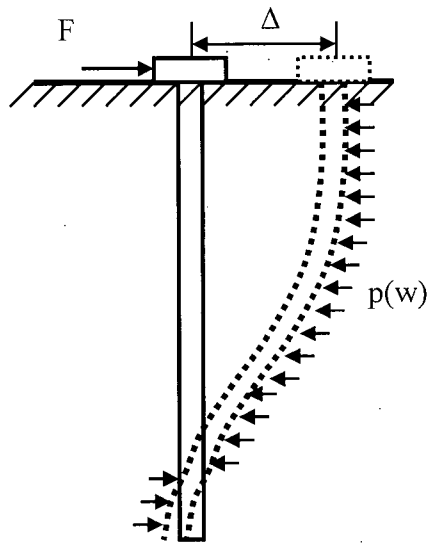

Figure 3.5 Typical mechanical connector (Foschi 2000)

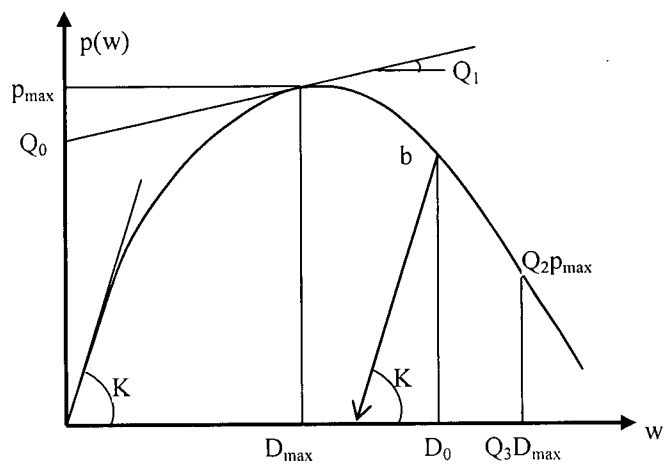

Figure 3.6 Embedment function of p(w) (Foschi 2000)

Under cyclic load, a set of reloading rules was defined

If ($w \le D_0$), then $p = 0$; (3.9)

If ($w > D_0$), then $p = \min[p_1 = K(w - D_0), p_2 = p(w)]$; (3.10)

If ($p = p_2$), then update D_0 : $D_0 = w - p / K$; (3.11)

If ($p = 0$) or ($p = p_1$), then D_0 unchanged. (3.12)

where

D_0 is the experienced maximum displacement before reloading (point "b" in Figure 3.5) .

Mechanical properties for the nail (modulus of elasticity and yield point) are those of mild steel. The unloading path is linear. This procedure has been implemented into a finite element program, HYST (Foschi 2000).

To represent the shear wall response with a pseudo nail such that it exhibits the same response of the representing shear walls, the selection of parameters is important. Compared with a physical nail connector, this pseudo nail model does not have real physical meaning of geometry. Beside the six parameters for HYST program, additional two parameters are required to identify its dimension: the length of the nail (L) and the diameter of the nail (D_i). Therefore, there are eight parameters in total: Q_0, Q_1, Q_2, Q_3, K, D_{max}, L and D_i, to be determined. To simplify the problem, Q_2 is set to 0.8. The rest seven parameters are to be identified as import to the HYST program for the representing pseudo nail model.

Since the pseudo nail model is not a real nail, it is difficult, if not impossible, to identify the parameters with traditional analytical method. Only simulation techniques are possible to find the appropriate parameters from the existing load-deformation curve of the pseudo nail model, or, of the shear walls. In other words, the challenge is to find parameters of the pseudo model from its known input and recorded output. Contrast to

traditional forward problems which determine the output from the known system parameters and given input, system parameter identification is an inverse problem.

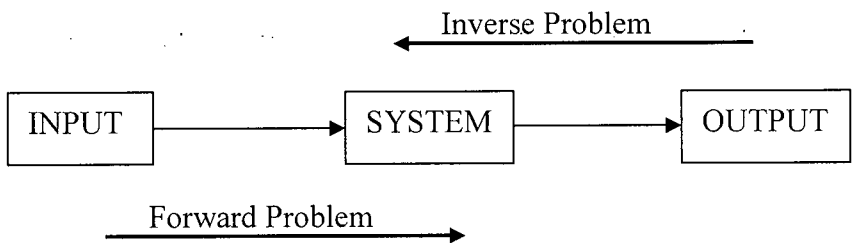

Figure 3.7 Forward and inverse problems

To solve the inverse problem, an optimization function is written to minimize the summation of square error between predicted and test data, shown as:

$$\min \varepsilon = \sum_{i=1}^{N} (F_{i,test} - F_{i,\mathrm{model}})^2 \tag{3.13}$$

where

i and N, are the ith and N^{th} discrete point, respectively;

$F_{i,test}$ is the value of force obtained from tests at the ith discrete point;

$F_{i,\mathrm{model}}$ is the value of force calculated from models at the ith discrete point.

This optimization function is subjected to variables of Q_0, Q_1, K, Q_3, D_{max}, L and D_i. These variables can be identified with different search methods.

3.3 Input Data Set

The number of input and output data sets, N, of the inverse problem may be great enough to calculate the parameters. Since there are seven parameters to be determined,

the minimum number of data sets, N, is seven. This is based on the assumption that all the seven sets of data are intrinsically independent.

Selecting seven implicitly independent data sets is difficult since the unknown parameters cannot determine the selection rules. More input data always consists of more system information. Ideally, the whole reversed cyclic test results are the best to feed into the optimization function (Equation 3.13), if computational efficiency is not of concern. For practical reasons, it is not necessary to fit the full set of reversed cyclic test results since much information from the test results is highly redundant with respect to the unknown variables of Q_0, Q_1, K, Q_3, D_{max}, L and D_i.

To capture the characteristics of loading and unloading paths with reasonable computational time, this model needs to be calibrated against the response of a shear wall subjected to a half cycle static load. This half cycle static load-deformation response can be obtained from an experiment or from a validated analytical calculation of wall response.

The maximum displacement of the input data should be more than the displacement at peak load. A post peak load of 80% maximum load is recommended for the input data. Furthermore, including the descending branch of the load-deformation curve is crucial for determination of the variable Q_3.

3.4 Search Methods

Equation 3.13 is a nonlinear optimization problem. The error function, ε, is not monotonic for most of seven variables, which means there are multiple local optima in the 8-dimensional (7 variables and their function) Euclid geometry. The optimization

does not have any explicit constraint condition. But some of them have to be positive to be assigned corresponding physical meaning, such as the length L and the diameter D_i.

Many search strategies are available to identify the best parameters of the optimization function. Basically, they can be classified into two groups: gradient based methods and non-gradient based methods.

3.4.1 Gradient Based Methods

The gradient based methods can be evolved from Taylor series expansion of a function. Consider the error function of seven variables in Equation 3.13:

$$\min \varepsilon = \varepsilon(X) = \varepsilon(Q_0, Q_1, K, Q_3, D_{max}, L, Di) \tag{3.14}$$

where

$$X = \begin{pmatrix} x_1 \\ x_2 \\ x_3 \\ x_4 \\ x_5 \\ x_6 \\ x_7 \end{pmatrix} = \begin{pmatrix} Q_0 \\ Q_1 \\ K \\ Q_3 \\ D_{max} \\ L \\ D_i \end{pmatrix}$$

The Taylor series expansion for this function, about the reference point X^*, is

$$\varepsilon(X) = \varepsilon(X^*) + \nabla\varepsilon(X)^T |_{X=X^*} (X - X^*) + \frac{1}{2}(X - X^*)^T \nabla^2 \varepsilon(X) |_{X=X^*} (X - X^*)$$

$$+ O[(X - X^*)^2] \tag{3.15}$$

where $\nabla\varepsilon(X)$ is the gradient which is defined as:

$$\nabla\varepsilon(X)=\begin{pmatrix}\frac{\partial\varepsilon(X)}{\partial x_1}\\ \frac{\partial\varepsilon(X)}{\partial x_2}\\ \frac{\partial\varepsilon(X)}{\partial x_3}\\ \frac{\partial\varepsilon(X)}{\partial x_4}\\ \frac{\partial\varepsilon(X)}{\partial x_5}\\ \frac{\partial\varepsilon(X)}{\partial x_6}\\ \frac{\partial\varepsilon(X)}{\partial x_7}\end{pmatrix}=\begin{pmatrix}\frac{\partial}{\partial Q_0}\varepsilon(\mathrm{Q}_0,\mathrm{Q}_1,\mathrm{K},\mathrm{Q}_3,\mathrm{D}_{\max},\mathrm{L},\mathrm{D}_i)\\ \frac{\partial}{\partial Q_1}\varepsilon(\mathrm{Q}_0,\mathrm{Q}_1,\mathrm{K},\mathrm{Q}_3,\mathrm{D}_{\max},\mathrm{L},\mathrm{D}_i)\\ \frac{\partial}{\partial K}\varepsilon(\mathrm{Q}_0,\mathrm{Q}_1,\mathrm{K},\mathrm{Q}_3,\mathrm{D}_{\max},\mathrm{L},\mathrm{D}_i)\\ \frac{\partial}{\partial Q_3}\varepsilon(\mathrm{Q}_0,\mathrm{Q}_1,\mathrm{K},\mathrm{Q}_3,\mathrm{D}_{\max},\mathrm{L},\mathrm{D}_i)\\ \frac{\partial}{\partial D_{\max}}\varepsilon(\mathrm{Q}_0,\mathrm{Q}_1,\mathrm{K},\mathrm{Q}_3,\mathrm{D}_{\max},\mathrm{L},\mathrm{D}_i)\\ \frac{\partial}{\partial L}\varepsilon(\mathrm{Q}_0,\mathrm{Q}_1,\mathrm{K},\mathrm{Q}_3,\mathrm{D}_{\max},\mathrm{L},\mathrm{D}_i)\\ \frac{\partial}{\partial D_i}\varepsilon(\mathrm{Q}_0,\mathrm{Q}_1,\mathrm{K},\mathrm{Q}_3,\mathrm{D}_{\max},\mathrm{L},\mathrm{D}_i)\end{pmatrix} \tag{3.16}$$

and $\nabla^2\varepsilon(X)$ is the Hessian matrix which is defined as:

$$\nabla^2\varepsilon(X)=\begin{pmatrix}\frac{\partial^2\varepsilon(X)}{\partial x_1^2} & \frac{\partial^2\varepsilon(X)}{\partial x_1 x_2} & \cdots & \frac{\partial^2\varepsilon(X)}{\partial x_1 x_7}\\ \frac{\partial^2\varepsilon(X)}{\partial x_2 x_1} & \frac{\partial^2\varepsilon(X)}{\partial x_2^2} & \cdots & \frac{\partial^2\varepsilon(X)}{\partial x_2 x_7}\\ \vdots & \vdots & \cdots & \vdots\\ \frac{\partial^2\varepsilon(X)}{\partial x_7 x_1} & \frac{\partial^2\varepsilon(X)}{\partial x_7 x_2} & \cdots & \frac{\partial^2\varepsilon(X)}{\partial x_7^2}\end{pmatrix} \tag{3.17}$$

Many search algorithms can be formulated from the Taylor series expanded at a local optimum. First order methods, such as Steepest Descent and Conjugate Gradient Method, truncate the second order Hessian while Quasi Newton methods involve both the gradient and Hessian.

All gradient based methods converge to a local optimum, which may not be the global optimum. Trial solutions to initiate the iteration are usually significant to achieve the global optimum.

The major difficulty to apply these methods is to generate the expression of gradient and Hessian in closed form. Since $F_{i,\mathrm{model}}$ is calculated from a nonlinear finite element

program, it is hard to explicitly express the gradient and Hessian and then evaluate them at specified points. Instead, the gradient and Hessian are generally approximated by finite difference which computes the values of the object function at small steps of dependent variables.

There is a dilemma in the choice of incremental steps of the variables for the determination of the gradient and Hessian. On one hand, the geometrical meaning of finite difference is a secant hyper-plane near the observed point. To represent the tangential hyper-plane of the gradient, incremental steps have to be as small as possible. On the other hand, truncation errors become significant for the generated gradient or Hessian when the incremental steps are very small. When the iteration reaches an optimum, the significant digits of adjacent function values are close to each other. Then the finite difference of these values deviates from the real situation, which results in divergence of the search.

3.4.2 Non-gradient Based Methods

Non-gradient based methods determine the search path without using the information of the gradient or Hessian. Many of these search methods are heuristic based, which improves the solution through incomplete available knowledge (Bolc and Cytowaki 1992). Some of them do not consider the search space, such as the hill climbing method. Others solely explore the search space without considering the object function values, such as the random search method. Finally, methods such as the genetic algorithm integrate the information from both search space and object functions (Michalewicz 1994). In this thesis, five algorithms were implemented to identify the parameters of the pseudo nail model.

3.4.2.1 Hill Climbing Method

Foschi (2000) developed a program of the hill climbing to find the parameters of his nail model from connector test results. This method starts from an initial point and sets it as the current point. During iteration, the values of neighboring points are evaluated. If the neighbor is better than the current one, it replaces the current one; otherwise the algorithm keeps the current point. The hill climbing method is easy to implement. But its efficiency is heavily affected by the nature of the problems. A good initial solution is important because the method converges to a local optimum. In this thesis, Foschi's program was modified to solve the optimization problem with seven parameters.

3.4.2.2 Random Search Method

A random search program was written by Foschi to identify the parameters of his nail model (Foschi 2000). This program generates all trial solutions within upper and lower boundaries randomly. Subsequent trials are limited to a given distance from the current best solution. If a trial is better than the current one, it updates the best solution; otherwise, it continues to search for a better solution. The key algorithm of the program is:

Step 0:

Generate some independent feasible random vectors and compare their functions. Pick up the best one as the initial current point.

Step 1:

Randomly generate a trial point within a prescribed distance from the current best point. If the trial point exceeds the boundaries, set it to the corresponding

boundary. Evaluate the function value at this point. If it is better than current one, then update the current one.

Step 2:

If the function value of current best point does not satisfy the prescribed stop criteria, goes to Step 1; else stop.

3.4.2.3 Simplex Method

The simplex method (Nelder and Mead 1965) was reported to succeed in identifying the parameters of a modified BWBN model (Foliente et al. 2000). Nelder and Mead's simplex considers the minimization of a function of n variables. $P_0, P_1, \ldots P_n$ are the (n+1) trial vectors in n-dimensional Euclid space. The function value at P_i point is denoted as y_i. Denote $[P_iP_j]$ for the distance from P_i to P_j and define:

$$y_h = \max_i(y_i) \quad (i = 0, n) \tag{3.18}$$

$$y_l = \min_i(y_i) \quad (i = 0, n) \tag{3.19}$$

$$\overline{P} = \frac{1}{n}\sum_{j \neq h} P_j \tag{3.20}$$

Consequently, the function values at y_l and y_l are denoted as P_h and P_l respectively. Three operations, reflection, contraction and expansion, are involved to generate a new point to replace P_h. The result of reflection is denoted as P^* and its co-ordinates are defined by the relation

$$P^* = (1+\alpha)\overline{P} - \alpha P_h \tag{3.21}$$

α is a positive constant, the reflection coefficient. It is defined as the ratio of the distance $[P^h \overline{P}]$ to $[P^* \overline{P}]$. This operation can be shown graphically (Figure 3.8). If y^* lies between y_h and y_l, then P_h is replaced by P^* and the search is started again.

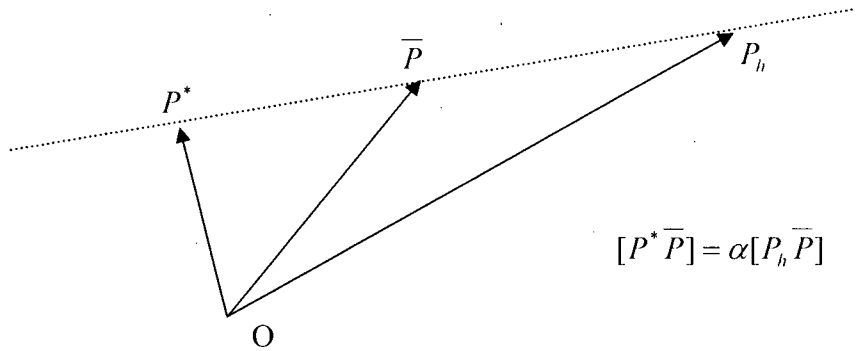

Figure 3.8 Reflection operation

If $y^* < y_l$, i.e. if reflection has produced a new minimum, then P^* is expanded to P^{**} by the relation

$$P^{**} = \gamma P^* + (1-\gamma)\overline{P} \tag{3.22}$$

The expansion coefficient γ is the ratio of the distance $[P^{**} \overline{P}]$ to $[P^* \overline{P}]$. It is greater than unity. Figure 3.9 shows the operation. If $y^{**} < y_l$, then P_l is replaced by P^{**} and the process is restarted. If $y^{**} > y_l$, the expansion fails and the process can be restarted after P_h is replaced by P^*.

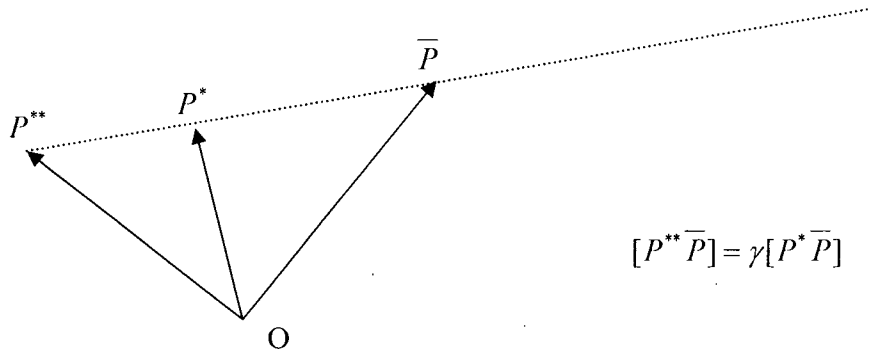

Figure 3.9 Expansion operation

If $y^{*} > y_{l}$ after reflection, a new $P_{h}^{'}$ is replaced by either old P_{h} or P^{*}, whichever has the lower function value. A new P^{**} is contracted by the relation

$$P^{**} = \beta P_{h}^{'} + (1-\beta)\overline{P} \tag{3.23}$$

The contraction coefficient β lies between 0 and 1 and is the ratio of the distance $[P^{**}\overline{P}]$ to $[P_{h}^{'}\overline{P}]$. If $y^{**} > \min(y_{h}, y^{*})$, replace all the P_{i}'s by $(P_{i} + P_{l})/2$ and restart the process. Otherwise, P^{**} replaces the P_{h} before the process is restarted.

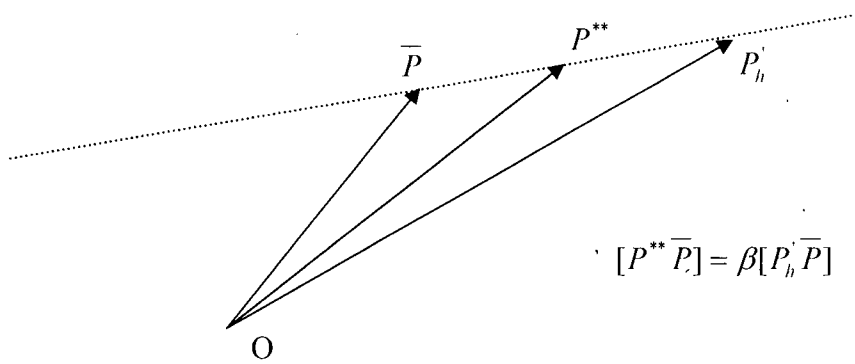

Figure 3.10 Contraction operation

Nelder and Read (1965) found that the strategy $\alpha=1$, $\beta=1/2$, $\gamma=2$ was the best. An open-source FORTRAN subroutine, MINIM (StatLib 2002), is used in this study to identify the parameters.

3.4.2.4 Genetic Algorithm

The Genetic algorithm (GA) is an adaptive heuristic search algorithm based on the mechanics of natural selection and natural genetics (Goldberg 1989). The fundamental concept of the algorithm is to mimic the Darwinian evolution process of the natural environments. Typical genetic operators include reproduction, crossover, and mutation. Encoding and decoding in strings are necessary before and after these operators.

The algorithm starts with a set of random solutions, or population. Each individual in the population is named as a "chromosome", which represents a trial solution to the problem. A chromosome has multiple genes, each of which corresponds to one variable of the problem. The chromosomes have to be expressed in forms of strings before operated. The process converting the problem into strings is encoding. Usually, but not necessarily, the string is expressed in binary.

Reproduction is a process in which individual strings are copied according to the relative ratio of their objective functions, or the fitness functions. The reproduction process imitates the natural selection of Darwinian survival of the fittest among creatures. The basic way to implement the reproduction operator is to create a biased roulette wheel where each current string in the population has a roulette wheel slot sized in proportion to its fitness for maximization problems. Figure 3.11 shows an example in which each chromosome (or solution), X(i), occupies an area A_i determined from the ratio of its fitness to the summation of the fitness of the population, i.e.,

$$A_i = \frac{f[X(i)]}{\sum_j f[X(j)]} \tag{3.24}$$

where

$f[X(i)]$ is the fitness of the problem for i^{th} chromosome.

Each spin of the roulette wheel generates one offspring. It is obvious that the chromosome with more fitness (more area on the wheel) has more opportunity to be chosen to generate offspring. The probability to be chosen is proportional to the area on the roulette wheel.

The operator following reproduction is crossover. The newly reproduced chromosomes are mated in pair at random. Each pair exchanges some portion of their genes. The starting location of the gene to be exchanged is randomly (typically in uniform distribution) determined. Figure 3.12 shows a pair of chromosomes swapped their string from the 5th to the 8th bit.

Mutation is a random change in the genetic material of a chromosome. Mutation alters one or more genes with a probability equal to the mutation rate, which is usually very low. In Figure 3.13, the 5th bit of the chromosome is flipped to 0 after mutation.

After new chromosomes are generated via the crossover and mutation operators, new reproduction can be conducted. The whole flowchart of the GA is expressed in Figure 3.14.

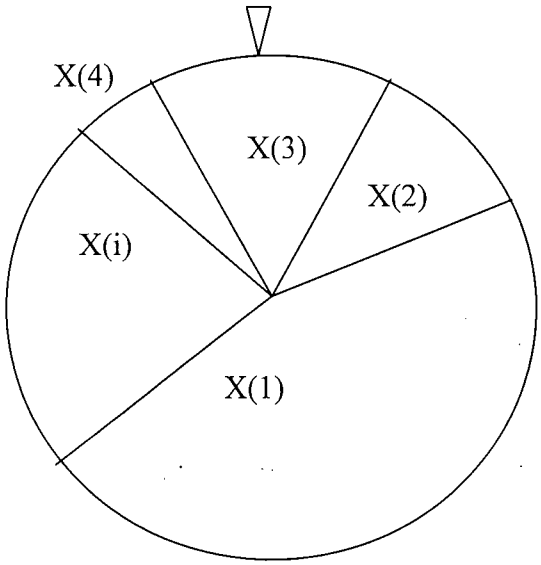

The occupied area A_i for x(i) equals to $\frac{f[X(i)]}{\sum_j f[X(j)]}$

Figure 3.11 Reproduction from roulette wheel

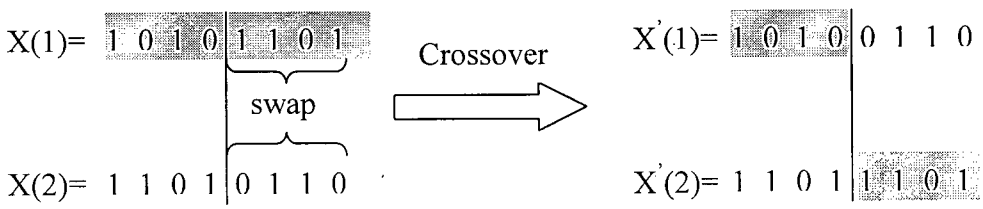

Figure 3.12 Crossover operator

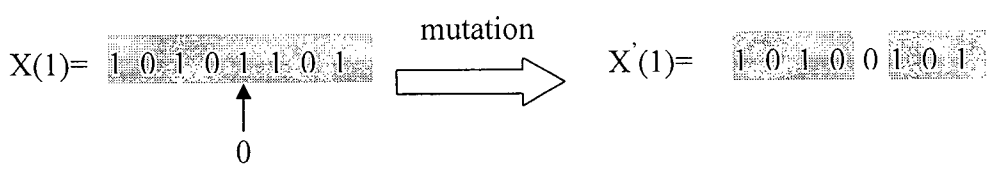

Figure 3.13 Mutation operator

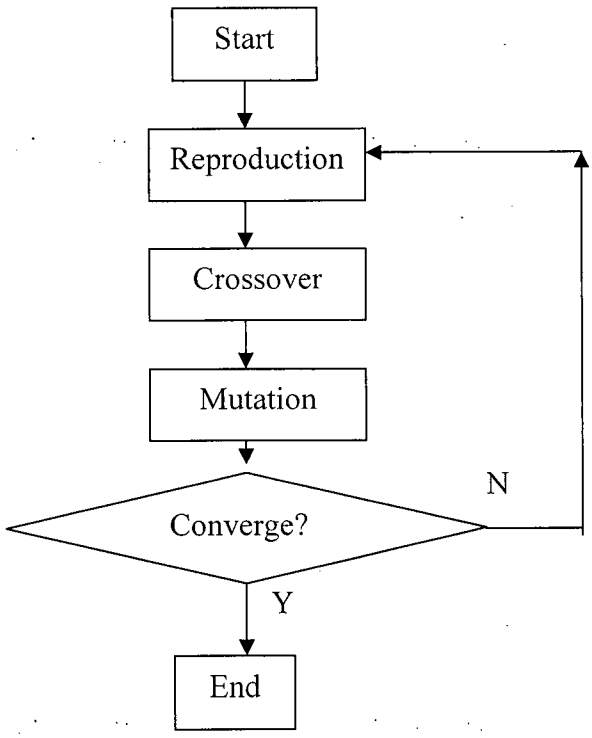

Figure 3.14 Flowchart of GA operators

This study employed an open-source FORTRAN program, PIKAIA (Charbonneau 2003) as a subroutine of optimization. This program was written for maximization problems because reproduction using the roulette wheel suits for such problems. The minimization problem expressed in Equation 3.13 is converted to an equivalent maximum problem, shown as:

$$\max(\frac{1}{\varepsilon}) = \frac{1}{\sum_{i=1}^{N}(F_{i,test} - F_{i,\mathrm{model}})^2} \tag{3.25}$$

This format of conversion keeps the positive sign of function value that is essential to compute the relative area on the roulette wheel. The singularity of the divisor is not a

problem here since numerical simulation can not obtain exactly the same results as the input ones.

3.4.2.5 Artificial Neural Network

The Artificial Neural Network (ANN) was inspired by the characteristics of biological nervous systems, such as the brain. The brain consists of a large number of highly interconnected processing elements called neurons. Each neuron is a specialized cell which can propagate an electrochemical signal. The neurons and the communication among neurons through electrochemical signal establish new connections or modification of existing connection which is the basis of learning function.

Artificial neural networks mimic the function of brain but they do not have the complexity as that of the brain. There are, however, two key similarities between biological and artificial neural networks. First the elements of both types of networks are simple computational devices that are highly interconnected. Second, the connections between neurons determine the function of the network. In the recent years, the power and usefulness of artificial neural networks have been demonstrated in many groups of applications, including clustering, classification and pattern recognition, function approximation and predication of dynamic systems.

Many types of artificial neural networks are available for solving different problems: perception, vector quantization networks, feed-forward neural networks, radial basis function networks and Hopfield networks. Each type of artificial neural networks has its own features and applies for different applications.

The artificial neural network is implemented here to extract the possible useful data from intermediate calculation results. The optimization methods, such as the random

search or simplex, have to run iteratively in order to obtain the final solution even though the final solution is not optimal. The incomplete data generated during the iteration process contains some valuable information. The artificial neural network is applied as a data mining tool to recover additional information.

The concept of this application is to find the parameters of the pseudo nail given its response curve, or the half cyclic static load-deformation curve of shear walls. A three-layer perception network is studied here with the topology shown in Figure 3.15.

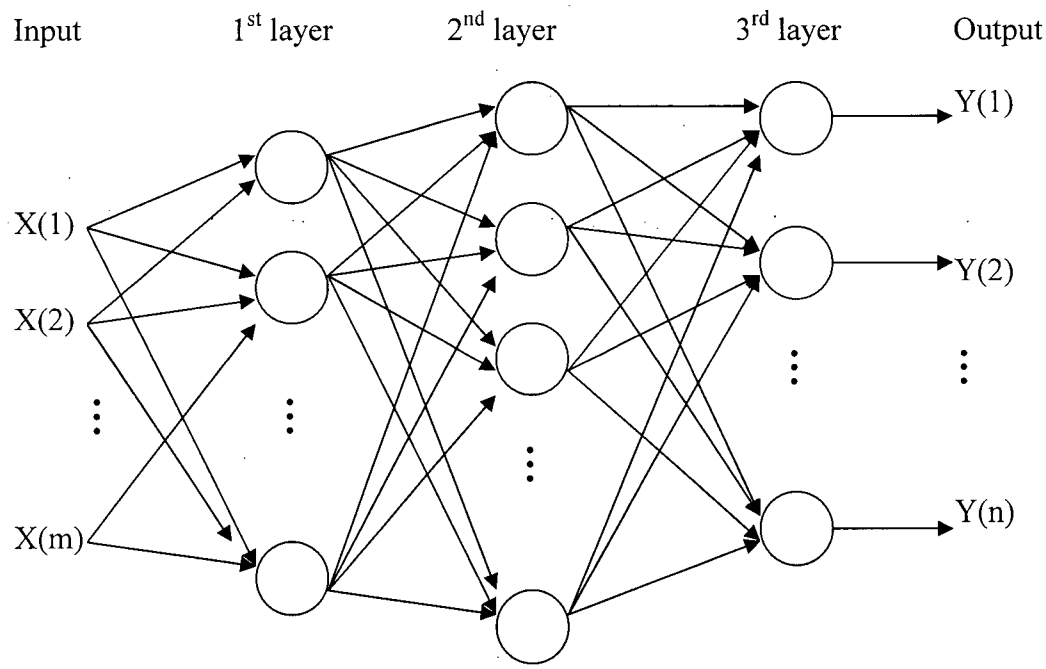

Figure 3.15 A three-layer network topology

The input of the studying neural network is the information of the response curve. But the response curves are typically composed of several hundreds of points. To reduce the number of independent input elements, five parameters, Q'_0, Q'_1, Q'_3, K' and D'_{max}, are used to characterize the shape of the response curve. The geometrical meaning of these

five variables is the same as that of the embedding function (Figure 3.6). So the input of the neural network has five elements. The output of the neural network of interest has seven elements, which are the seven variables to be optimized for the pseudo nail, i.e., Q_0, Q_1, K, Q_3, D_{max}, L and D_i. The transfer functions of neurons in the first and second layers are log-sigmoid, which is expressed as

$$a = \frac{1}{1+e^n} \tag{3.26}$$

where

n is the input of the neurons,

a is the output of the neurons.

The transfer functions of neurons in the third layer are linear, which can be expressed as

$$a = n \tag{3.27}$$

where

n is the input of the neurons,

a is the output of the neurons.

The multilayer perception network is trained by the back-propagation algorithm. The training method is Levenberg-Marquardt algorithm (Scales 1985), which is a variation of Newton's method. The training database is accumulated from the iteration process in running other methods (random, hill climbing, simplex and genetic algorithm) when many sets of trial solutions and their corresponding response curves are generated. The numbers of neurons in different layers vary from the training database. Typically, there are six, eight and seven neurons in the first, second and third layer, respectively.

3.5 Nonlinear Time-History Analysis

The representative pseudo nail is capable of predicting the nonlinear hysteresis behaviour of wood shear walls. Principally it is a nonlinear spring model which response is calculated with a finite element model. The dynamic response of the shear walls with such a nonlinear spring is calculated with a SDOF system, as illustrated in Figure 3.16. In this figure, the shear wall is represented by a nonlinear spring, whose response, F(x), is the function of drift x, as calculated by HYST (Foschi 2000). The shear wall carries a mass M on its top. C is the viscous damper of the system.

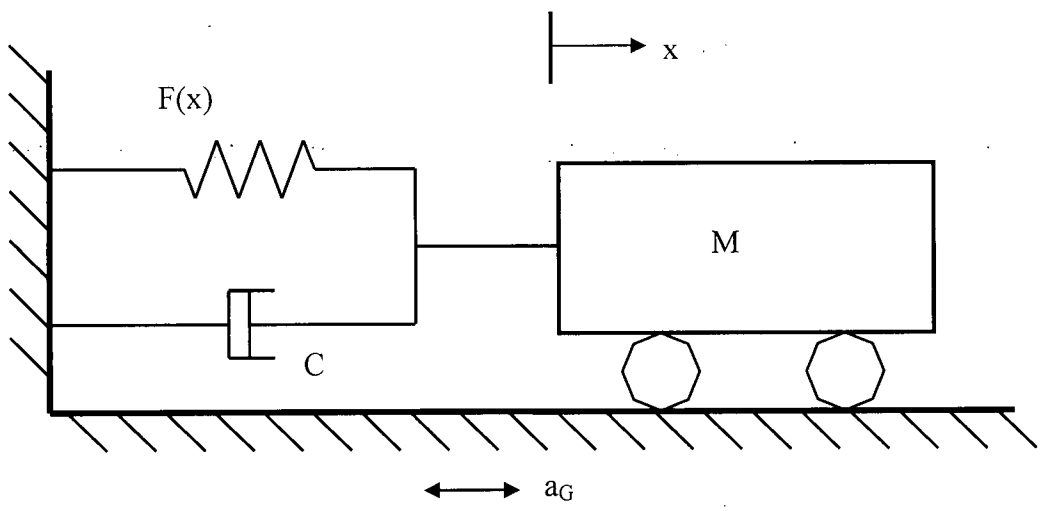

Figure 3.16 SDOF system for dynamic response

The governing equation of the SDOF system can be expressed as

$$M\ddot{x} + C\dot{x} + F(x) = -Ma_G \tag{3.28}$$

The second order differential equation is generally solved with direct integration methods (Bathe 1996). Houbolt method (Houbolt 1950), Newmark-β method (Newmark

1962) and Wilison-θ method (Wilson et al. 1972) are commonly used in engineering discrete analysis. The major difference of these methods is how to predict the acceleration or displacement in time. The implicit format of these methods requires iteration in solving the problems. This disadvantage does not stop their wide usage since their unconditional stability provides researchers with the flexibility in choosing the time step.

Newmark –β method is implemented in the study to analyze the dynamic equation 3.28. The assumptions of Newmark –β method are

$$\dot{x}(t+1) = \dot{x}(t) + [(1-\beta)\ddot{x}(t) + \beta\ddot{x}(t+1)]\Delta t \tag{3.29}$$

$$x(t+1) = x(t) + \dot{x}(t)\Delta t + [(\frac{1}{2} - \gamma)\ddot{x}(t) + \gamma\ddot{x}(t+1)]\Delta t^2 \tag{3.30}$$

where

t, $t+1$ are the solved time and next unknown time, respectively;

$x(.)$, $\dot{x}(.)$, $\ddot{x}(.)$ are the drift (relative displacement), velocity and acceleration, respectively;

β, γ are adjustable parameters.

Solving Equation 3.30 for $\ddot{x}(t+1)$ in terms of $x(t+1)$ and then substituting for $\ddot{x}(t+1)$ into Equation 3.29, one obtains equations for $\ddot{x}(t+1)$ and $\dot{x}(t+1)$, each in terms of the unknown displacements $x(t+1)$ only. Substituting these two relations into Equation 3.28 gives the expression of $x(t+1)$, after which $\ddot{x}(t+1)$ and $\dot{x}(t+1)$ can be calculated. The iterative procedure of Newmark–β method can be found in any text books about dynamics or finite element method (Bathe 1996). When programming these

procedures, the nonlinear response, F(x), is to be called or executed from another subroutine, HYST.

A popular format of Newmark–β method, the constant-average acceleration method, in which $\gamma = \frac{1}{4}$ and $\beta = \frac{1}{2}$, was used in the samples of the thesis.

3.6 Summary

A nonlinear single degree-of-freedom system, the pseudo nail model, was developed to simulate the dynamic behaviour of wood shear walls. This model used a nail analogue which response is evaluated with finite element method considering the nonlinear behaviour of nail shank, surrounded wood media and contact effect between nail and wood. Using nonlinear optimization methods, the parameters of the pseudo nail model can be calibrated with a half cycle result from reversed cyclic tests. With these parameters, the pseudo nail model can predict the behaviour of the representing shear wall under cyclic load or dynamic load.

Five optimization methods were implemented to identify the parameters, including hill climbing method, random search method, genetic algorithm, simplex and artificial neural network. Newmark–β method was used to calculate the nonlinear response under dynamic load.

CHAPTER 4. MODEL VALIDATION

4.1 Introduction

The nature of the pseudo nail model is a nonlinear spring. With a viscous damper, an SDOF system can be constructed to simulate the dynamic behaviour under earthquake load. Compared to other simple nonlinear spring models, the pseudo nail model has some important features. Firstly, the pseudo nail model simulates the hysteresis loops through finite element procedures which usually give very smooth curves of results under continuous unloading and reloading. The continuity of the first order derivative of the resulting curves is important for the convergence of other gradient-based applications, such as the reliability analysis with FORM. Secondly, the process of identifying the parameters is conducted by the computer, which is independent of the potential variation introduced by human decision.

As a simple nonlinear spring model, the parameters of the pseudo nail model are first established from a half loop of reversed cyclic test results. Then it can be validated with the test results under reversed cyclic load or dynamic load. To study the robustness of this model, verification should be conducted for as many configurations of walls as possible. Typical configurations to verify the model include different nail spacing, resistant types and loading conditions.

The University of British Columbia has conducted many experimental studies on the performance of wood structures. Recent work consists of the performance of shear walls sheathed with oversize OSB panels (Lam et al. 1997, He et al. 1999 and Durham et al. 2001), the shake table tests of full-scale wood frame residential houses (Ventura et al.

2002) and the performance of Japanese shear walls (Stefanescu 2000 and Jossen 2003) and the performance of Japanese post and beam houses (Lam 2005). The test results of these works provide useful information to verify the pseudo nail model.

4.2 Validation of Panel-Sheathed Shear Walls

Durham et al. (2001) reported an experimental study on the earthquake resistance of 2.4 m x 2.4 m shear walls sheathed with regular or oversized OSB panels. This work extends a previous study on walls subjected to reversed cyclic loading regimes to investigating the dynamic behaviour of the shear walls on a shake table. Monotonic, reversed cyclic and dynamic loading tests were performed on shear walls with standard (1.22 m x 2.44 m) and oversize (2.44 m x 2.44 m) OSB panels. In total, 14 walls were tested. This work resulted in a master thesis (Durham 1998).

The test walls were built with No. 2 and better grade of 38 x 89 mm Spruce-Pine-Fir dimension lumber. The end studs and top plates were double members and the bottom plates and interior studs were single members. Studs were spaced at 400 mm on centre. The fasteners connecting the sheathing panels to the frames were pneumatically driven 50 mm spiral nails. Conventional hold downs were installed to prevent uplift. OSB panels (9.5 mm thick) were used as the sheathing panels which were configured into three types with different edge nail spacing (Durham 1998). Two of the configurations were used in this thesis: Type A and Type C. Type A had three regular-size panels, one of which was a single 2.4 x 1.2 m panel horizontally oriented at the bottom and two were 1.2 x 1.2 m panels at the top. Type C had a single 2.4 x 2.4 m panel. Interior nail spacing for all walls was 300 mm. The edge nail spacing was 150 mm for panel configuration Type A

and 75 mm for Type C, respectively. The difference of nail spacing and panel layout of the two configurations can verify the robustness of the proposed pseudo nail model.

The monotonic and reversed cyclic tests were carried out on the same test apparatus as used for the long shear wall tests (Lam et al. 1997). A vertical load of approximately 9 kN/m was applied to the top of walls to represent the weight of one storey. The test protocol for cyclic tests was developed by He et al. (1999). The test results were used by He (2002) to validate a FEM program for wood frame structures, LightFrame3D.

The shake table tests were performed with a testing frame specially designed for 2.4 m x 2.4 m wood walls (Dolan 1989). The earthquake record was chosen as the east-west component of the 1992 Landers, California earthquake recorded at Joshua Tree Station. An inertia mass of 4545 kg was placed on the top of the testing frame which applied the inertia force to the shear wall in testing. The visco-damping ratio is assumed to be 1% of the critical damping with respect to the initial tangential stiffness.

4.2.1 Interpreting Test Data

In the monotonic and cyclic tests, the vertical loads were applied directly to the top plates of the tested shear walls. In shake table tests, the mass was placed on the frame above the top plates of shear walls. Figure 4.1 presents schematic drawings of the testing apparatus on the shake table. The vertical dark line represents the stiff sway frame with the height of L_1. The rotational angle of the frame is noted as θ. The frame has an inertia mass, M, on its top. The shear wall is connected to the sway frame at a distance of L_2 from the bottom. The displacement of the shear wall relative to the ground, or the drift, is x, which equals to θL_2. The behaviour of shear wall is represented by a pair of nonlinear spring, F(x), and damper, c. When the ground is experienced the ground motion of

acceleration, $\ddot{y}$, the dynamic equation can be established from the equilibrium of the mass, as following

$$M[\ddot{y} + L_1\ddot{\theta}] + [F(x) + c\dot{x}]\frac{L_2}{L_1} = 0 \tag{4.1}$$

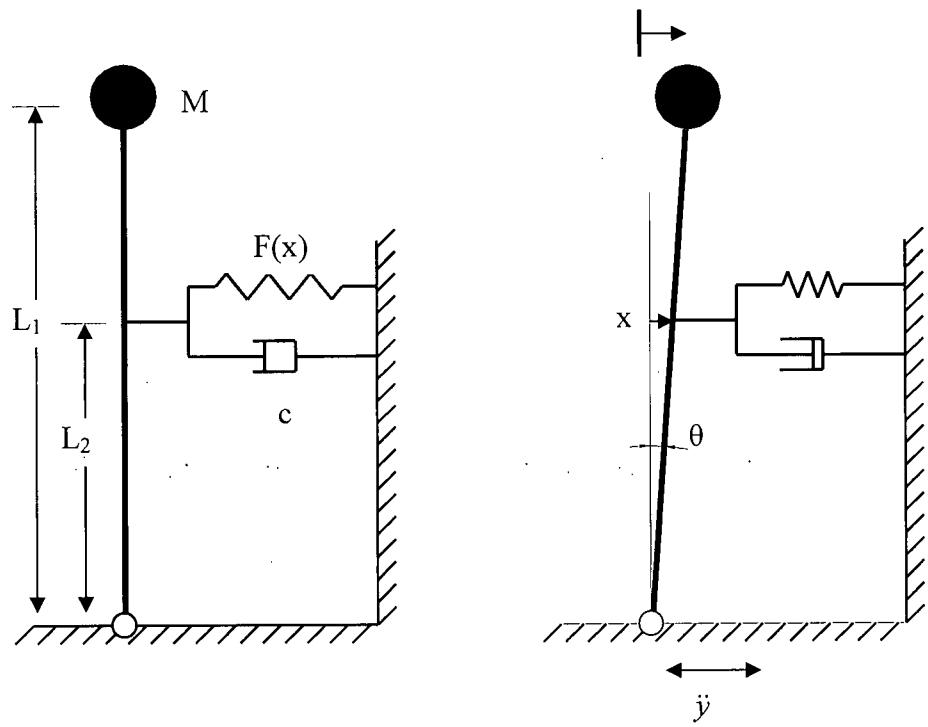

Figure 4.1 Schematic drawing of Dolan's dynamic testing frame

From the relationship of $x = \theta L_2$, Equation 4.1 can be rewritten as

$$(\frac{L_1}{L_2})^2 M\ddot{x} + F(x) + c\dot{x} = -(\frac{L_1}{L_2})M\ddot{y} \tag{4.2}$$

It should be noted that this system is not equivalent to that where a mass of $(\frac{L_1}{L_2})M$ is directly applied to the top plate of the shear wall, which may lead to a wrong equation as

$$(\frac{L_1}{L_2})M\ddot{x} + F(x) + c\dot{x} = -M\ddot{y} \tag{4.3}$$

In Durham's tests, $L_1 = 3043$ mm, $L_2 = 2545$ mm, M=4545 kg. $F(x)$ is defined by the pseudo nail model.

The recorded drift data shown in Figure 5.20 of Durham's work (Durham 1998) were processed with both a low-pass filter and a high-pass filter in frequency domain (Durham 1999). So there is no residual drift shown in the graph in Durham's work. To keep the residual deformation of shear walls, this thesis only filtered high frequency components from the original test results of Durham's work.

The input of each calculation was the recorded shake table acceleration from the individual tests. The calculated drift was then compared with test results. From trial calculation, it was found that the numerical prediction did not match the test results well. Good agreement between test results and numerical prediction was only seen after the measured shear wall drift was phase-shifted for a period of time varying from 0.09s to 0.28s. Durham's thesis attachment (Durham 1999) and Dolan's work (Dolan 1989) showed that two computers were involved to collect the data of the wood shear wall tests in the UBC Civil Engineering laboratory. Obviously there was no electronic device to synchronize the two computers. The manual operation of the computers and corresponding programs created the time lag for some recorded data in Durham's work. After tests, discrete Fourier transformation was implemented to merge the data together. So the discrepancy of phase angle between test results and predicted results can be explained by a possible time lag between the two computers that recorded the table acceleration and shear wall drift. A personal communication with Durham suggested the same explanation. Unfortunately no more detail was found to confirm this explanation.

4.2.2 Pseudo Nail Calibration of Type A Shear Walls

Durham (1998) tested four shear wall specimens of Type A configuration. Test 4 was subject to monotonic loading. Test 8 was subject to reversed cyclic loading. Tests 11 and 14 were conducted under dynamic loading. The reversed cyclic test, Test 8, should be used for the input of the pseudo nail model. But this test did not give the unloading curve after peak load. In Figure 4.2, the unloading part of the input curve was estimated from the cyclic test results. The input curve was fitted with different search methods as discussed in Chapter 3. The fitted results are given in Figure 4.2. Table 4.1 presents the parameters for different search methods.

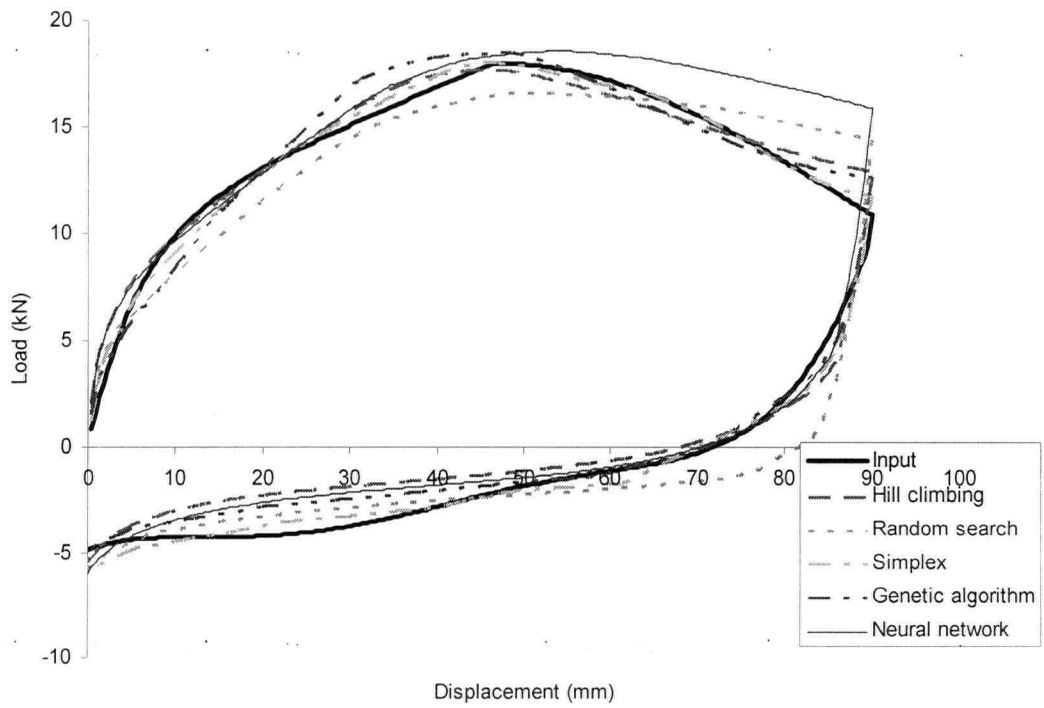

Figure 4.2 Input and fitted curves for Type A walls

Table 4.1 Parameters for Type A shear walls

	Q_0 (kN/mm)	Q_1 (kN/mm^2)	K (kN/mm^2)	D_{max} (mm)	Q_3	D_i (mm)	L (mm)
Hill climbing	0.7389	0.05830	0.2866	30.606	1.3677	9.6000	135.00
Random search	0.0807	0.05113	0.1908	27.697	1.7772	11.605	264.61
Simplex	0.7707	0.02781	0.1100	38.652	1.1867	11.122	455.64
Genetic algorithm	0.0491	0.09211	0.1903	28.093	1.3583	9.8225	397.52
Neural network	0.4847	0.05980	0.2456	30.017	1.3836	10.244	130.88

4.2.3 Validation of Type A Shear Walls

With these sets of parameters in Table 4.1, the load-displacement behaviour of the walls under cyclic and dynamic load was predicted. Figure 4.3 demonstrates the comparison between the model prediction and the cyclic test results (Test 8 of Durham's work).

Two duplicates were tested under dynamic load for Type A shear walls in Durham's work: Test 11 and Test 14. Ideally, they should yield the same results. Due to the variation of material properties and the realization of loading condition, the results from the two specimens are slightly different. In Figure 4.4, the predicted drift of the shear wall is compared with that of experimental results of Test 11. Figure 4.5 shows the comparison between the predicted drift and the experimental results of Test 14. In each case, the recorded shake table acceleration, rather than the input earthquake record exciting the shake table, was fed as the ground motion for numerical calculation. This is to minimize the error of prediction since there was some deviation between the realized shake table acceleration and the input record.

The calculated response in Figure 4.4 was phase shifted forward by 0.09 seconds to match the measured response while the calculated response in Figure 4.5 is shifted backward by 0.08 seconds. Both figures were truncated along the abscissa to show only the significant portion of the results. Figures 4.6 and 4.7 present the correlation between the tested and predicted drift data. The correlation coefficients (or the cross-covariance coefficients with zero time lag) between the data of Test 11 and the predicted drift with the four search methods are presented in Table 4.3. The correlation coefficients between the data of Test 14 and the prediction are tabulated in Table 4.4. The data in Figures 4.6 and 4.7 can be regressed with straight lines intersecting at the origin of the coordinate system. The angle between the regressed straight line and the 45° line (y=x) indicates the deviation of the prediction. Table 4.3 and Table 4.4 also show the angles between the regression and the ideal 45° line in Figures 4.6 and 4.7, respectively.

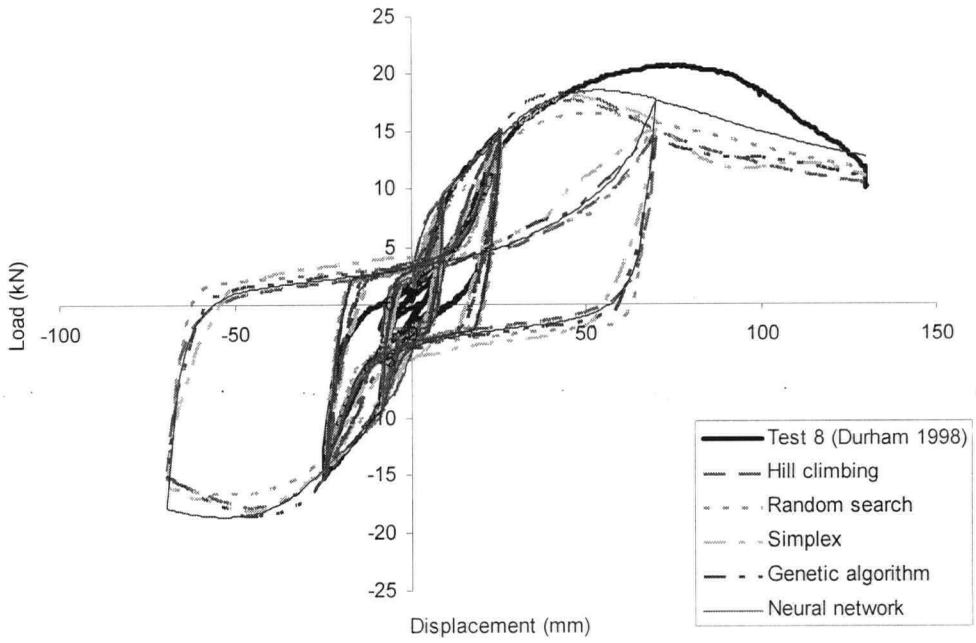

Figure 4.3 Comparison of Type A walls under cyclic load

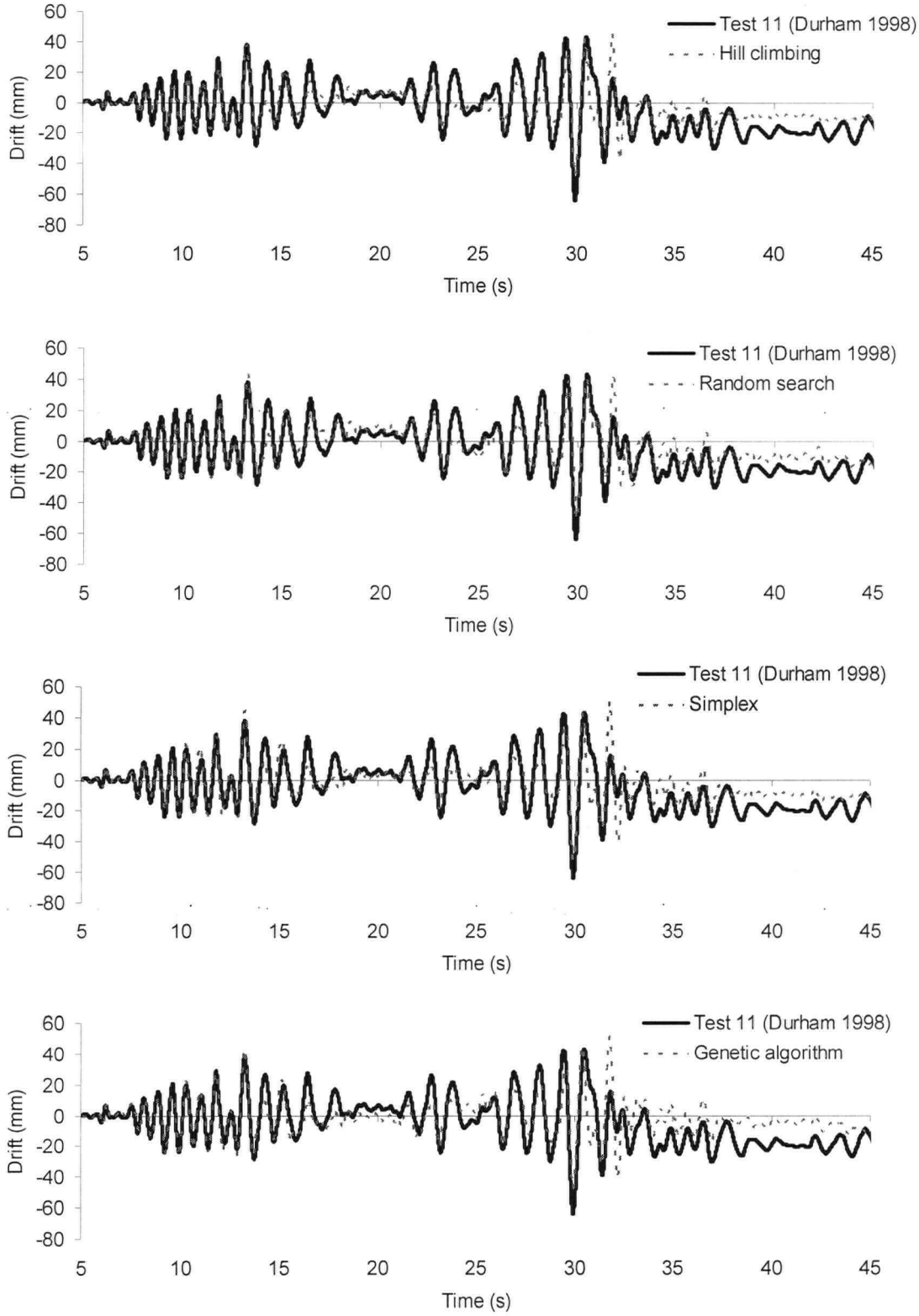

Figure 4.4 Comparison of Type A walls under dynamic load (Test 11)

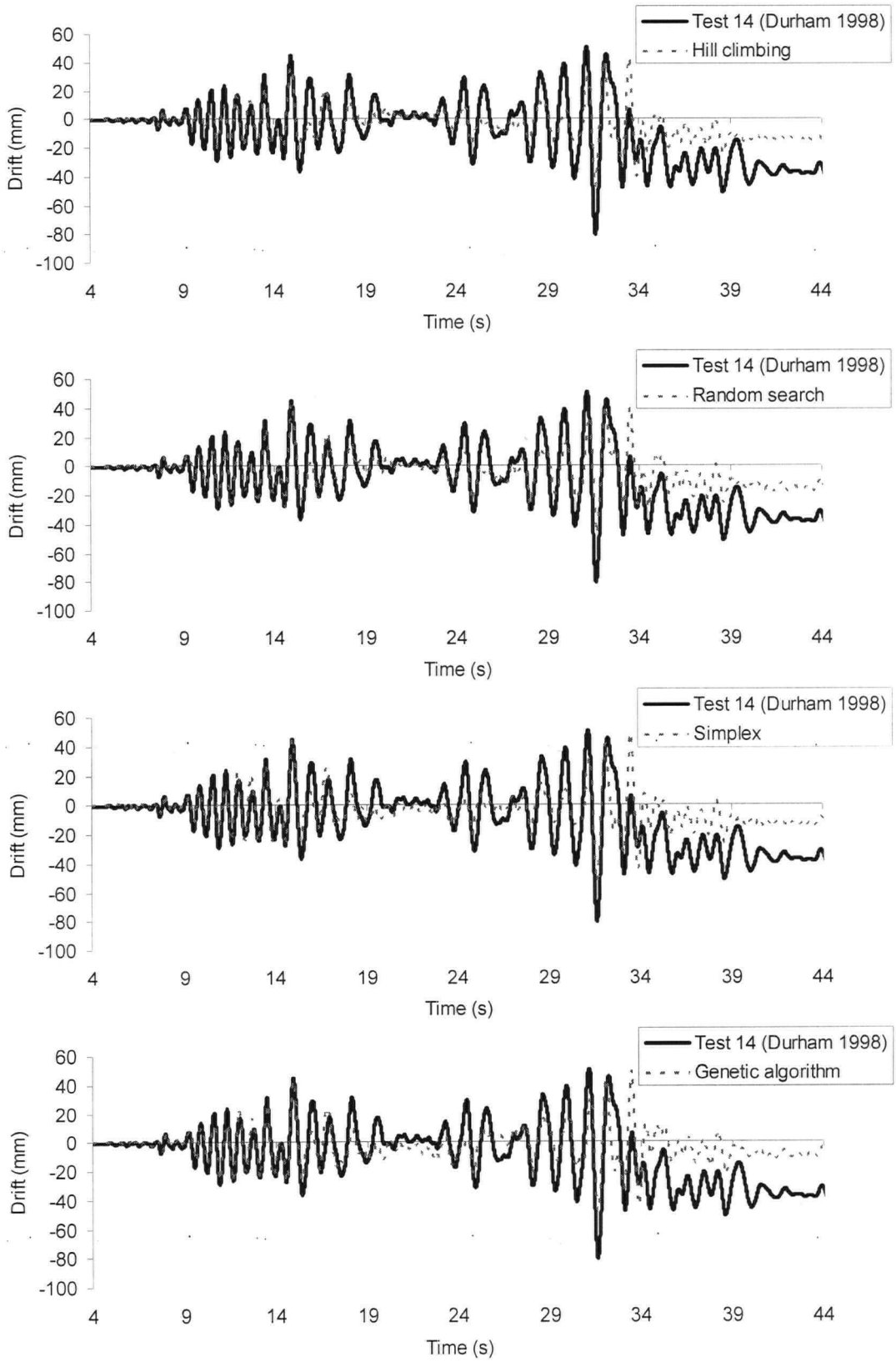

Figure 4.5 Comparison of Type A walls under dynamic load (Test 14)

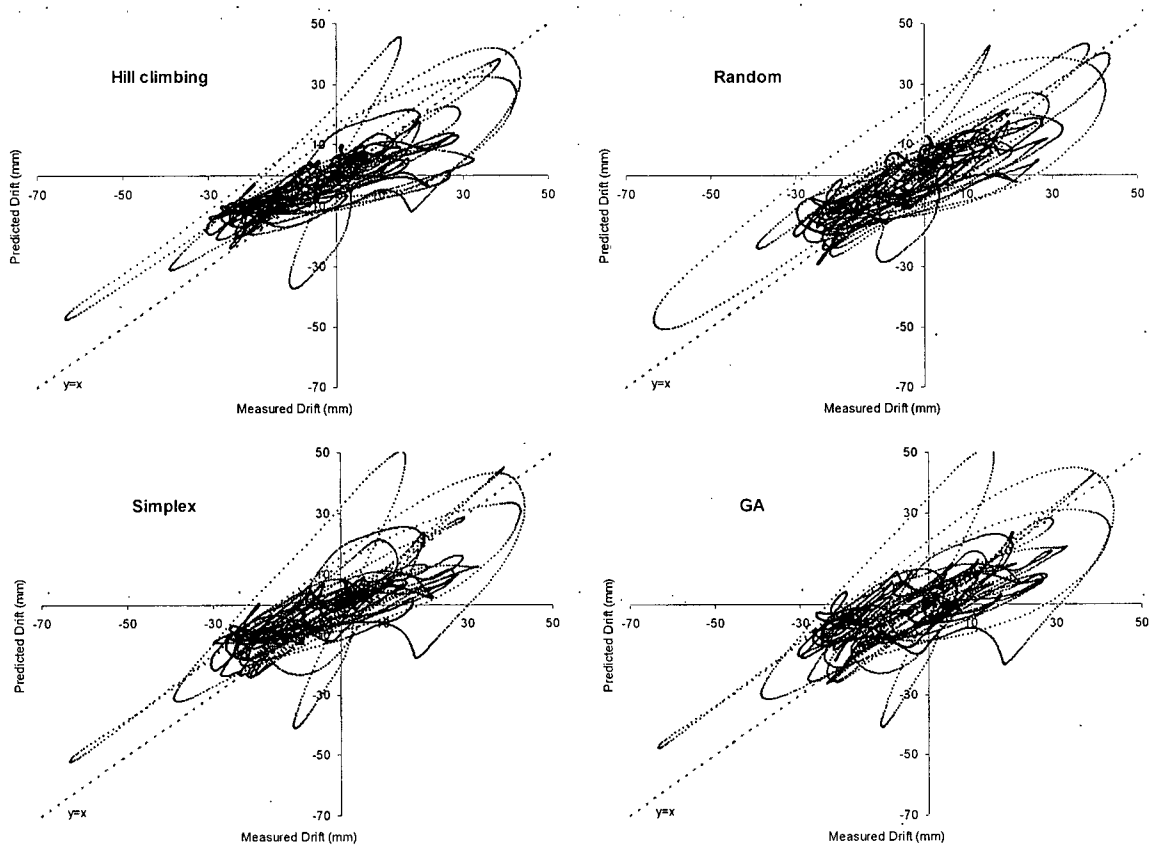

Figure 4.6 Correlation between test and prediction for Type A walls (Test 11)

Table 4.2 Summary of comparison between test and prediction (Test 11)

	Correlation coefficient	Angle to 45° line (°)
Hill climbing	0.8078	15.19
Random	0.8442	11.90
Simplex	0.7967	14.16
Genetic algorithm	0.7259	17.29

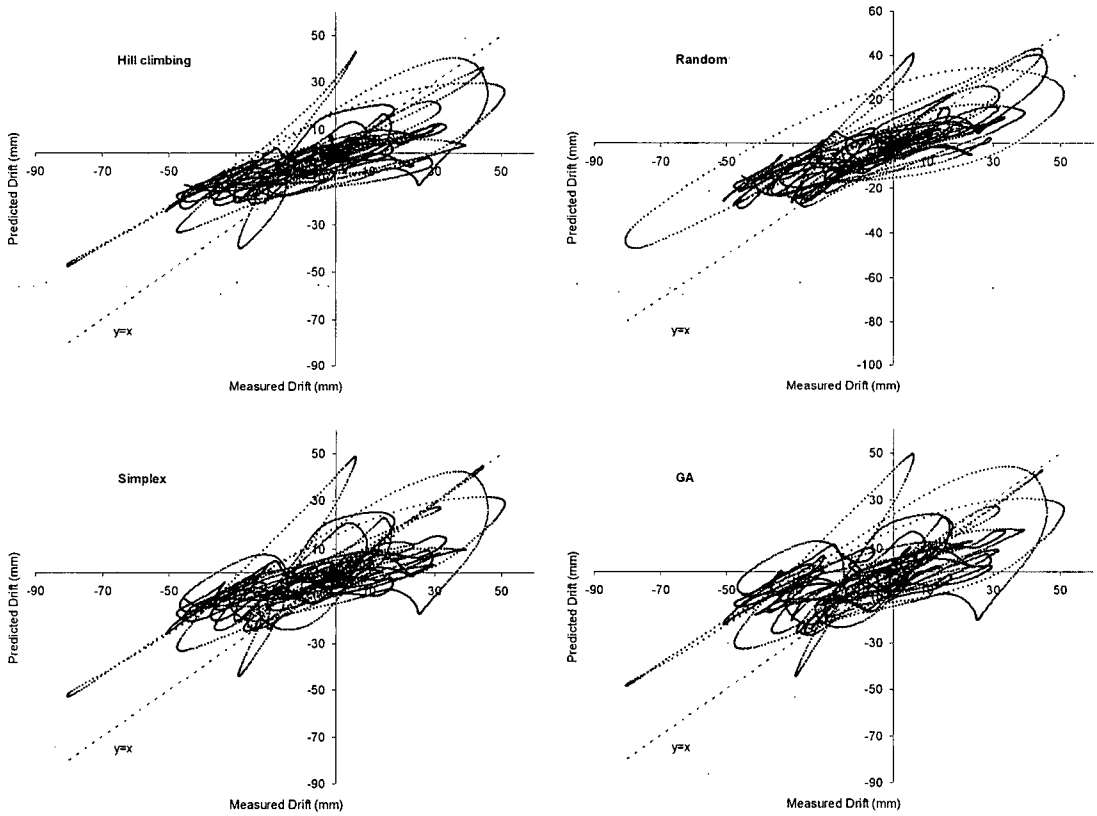

Figure 4.7 Correlation between test and prediction for Type A walls (Test 14)

Table 4.3 Summary of comparison between test and prediction (Test 14)

	Correlation coefficient	Angle to 45° line (°)
Hill climbing	0.7734	23.53
Random	0.7845	19.19
Simplex	0.7307	21.19
Genetic algorithm	0.6630	21.71

4.2.4 Pseudo Nail Calibration of Type C Shear Walls

Three specimen of Type C shear walls of Durham's work (Durham 1998) were compared here: Test 6, Test 10a and Test 15. The results of Test 6 did not have the unloading curve after peak load. So the input curve was obtained through LightFrame3D (Figure 9.18 of He 2002), shown in Figure 4.8. The fitted results from four search methods are presented in the same figure. Table 4.4 outlines the parameters of the pseudo nail model for different methods.

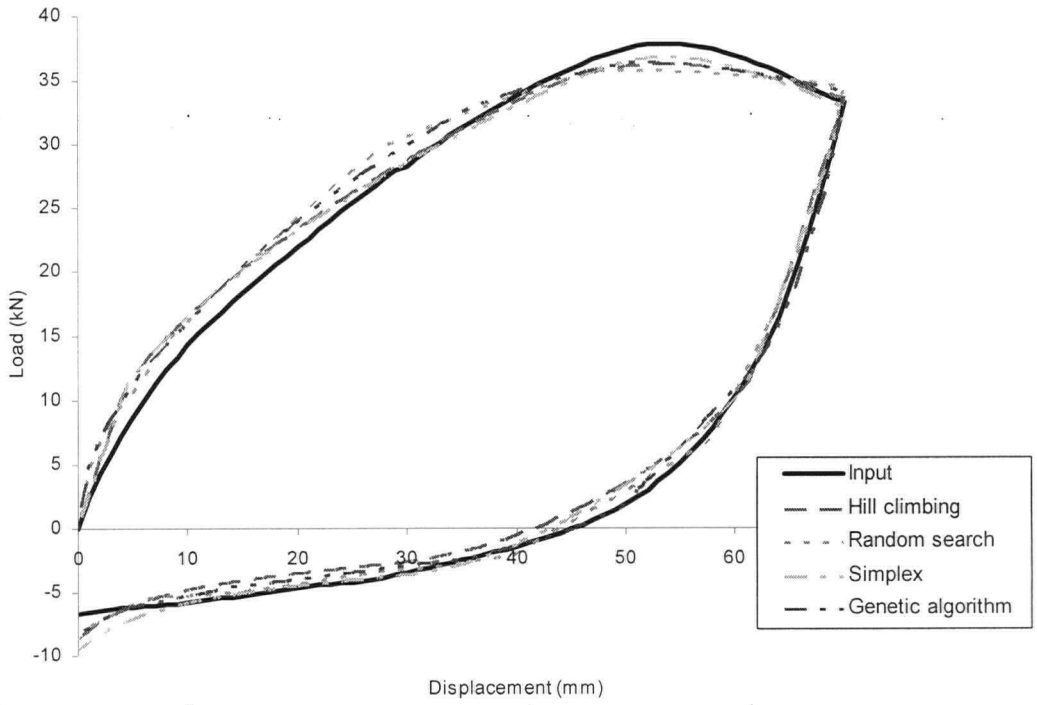

Figure 4.8 Input and fitted curves for Type C walls

Table 4.4 Parameters for Type C shear walls

	Q_0 (kN/mm)	Q_1 (kN/mm^2)	K (kN/mm^2)	D_{max} (mm)	Q_3	D_i (mm)	L (mm)
Hill climbing	8.6214	0.02924	0.1733	32.216	1.438	12.131	412.23
Random	8.2248	0.03400	0.2191	25.211	1.963	11.627	463.87
Simplex	4.8978	0.00977	0.1926	44.537	1.835	12.988	55.84
Genetic algorithm	4.1853	0.04481	0.2582	32.741	1.469	11.513	313.46

4.2.5 Validation of Type C Shear Walls

The cyclic behaviour of this type of shear walls was predicted with these sets of parameters. Figure 4.9 provides the comparison between the prediction and the results of Durham's Test 6. It is clear that the predictions of the various methods agree well with the cyclic test results.

Durham (1998) tested several Type C specimens on the shake table using the Joshua Tree station ground motion record as input. In Test 10a and Test 15, the Type C shear wall specimens were newly built before testing. In Durham's Test 10a, the excitation ground motion was scaled to a peak ground acceleration level of 0.35 g. In Test 15, the ground motion was scaled to an acceleration level of 0.52 g. With the parameters shown in Table 4.4, the dynamic behaviour of the Type C shear wall was predicted. Figure 4.10 shows the comparison between the predicted drift and the experimental results of Test 10a. In this figure, the calculated response curve is flipped and phase shifted forward by 0.28 seconds in order to fit the experimental results. Figure 4.11 presents the case for Test 15. In this figure, no phase angle shift is applied. Both Figures 4.10 and 4.11 are truncated along the abscissa to show the significant portion. Figures 4.12 and 4.13 present the correlation between the tested and predicted drift data. The correlation

coefficients between the data of Test 10a and the predicted drift with the four search methods are presented in Table 4.5. The correlation coefficients between the data of Test 15 and the prediction are tabulated in Table 4.6. The angles between the regression and the ideal 45° line in Figures 4.12 and 4.13 are shown in Tables 4.5 and 4.6, respectively.

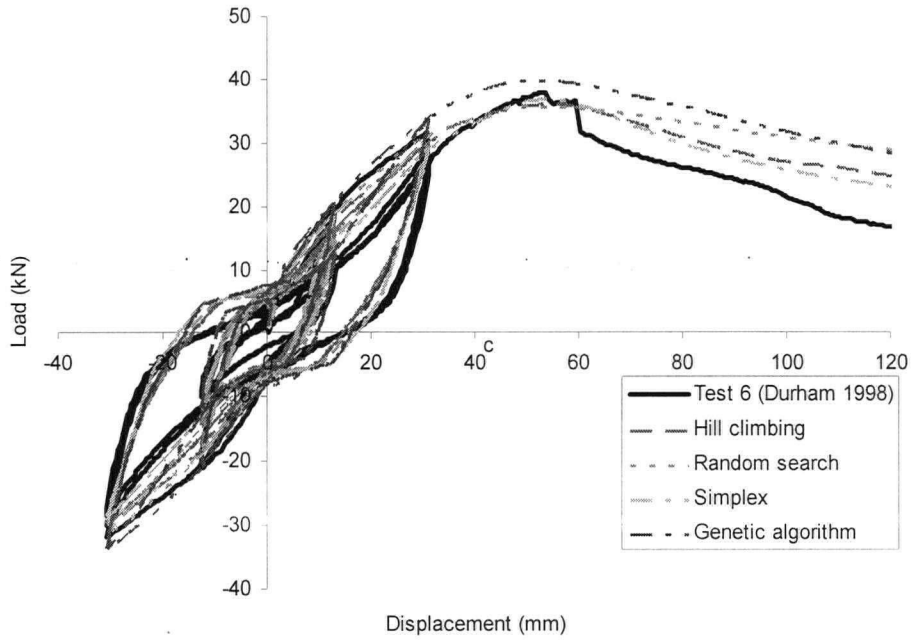

Figure 4.9 Comparison of Type C walls under cyclic load

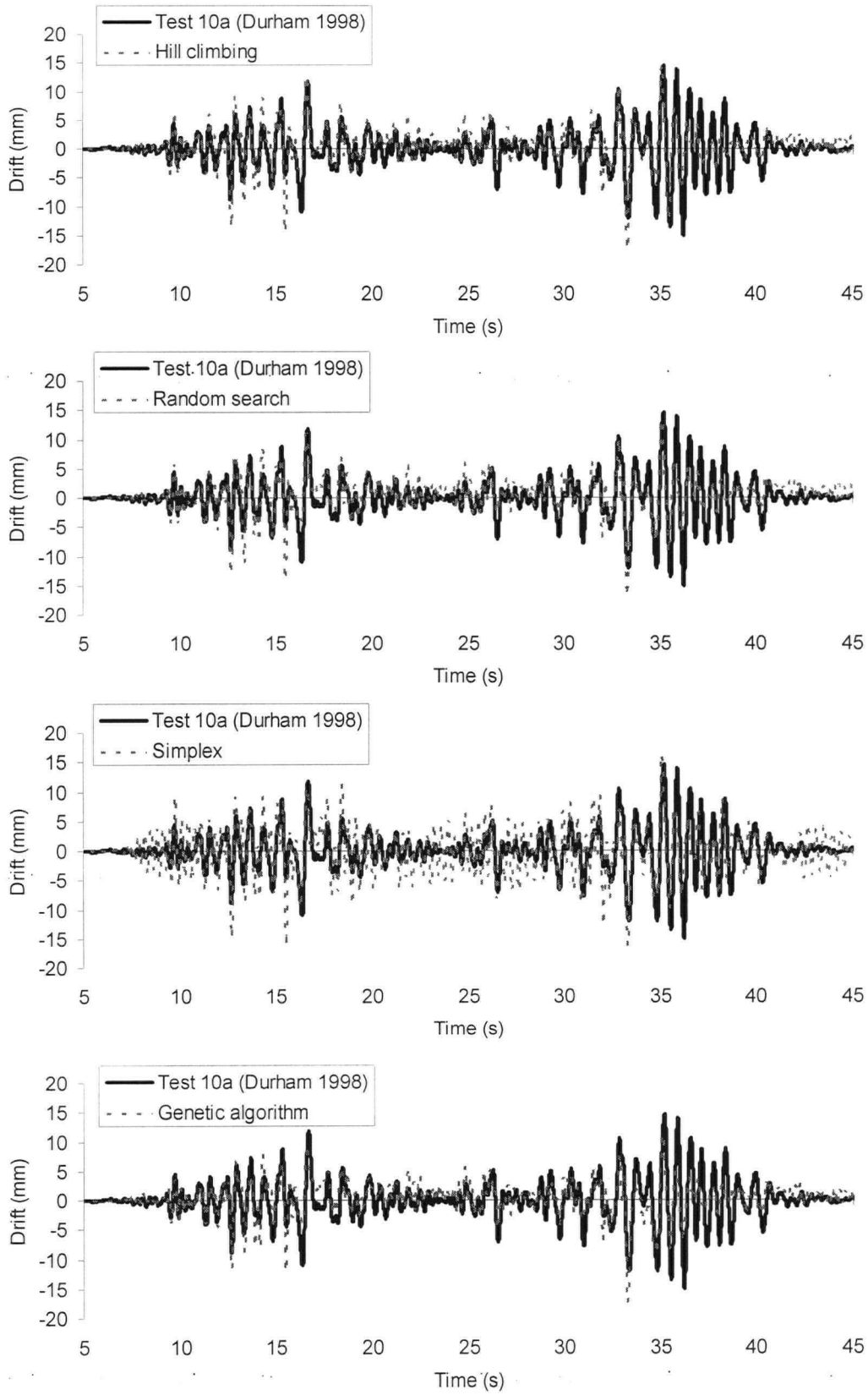

Figure 4.10 Comparison of Type C walls under dynamic load (Test 10a)

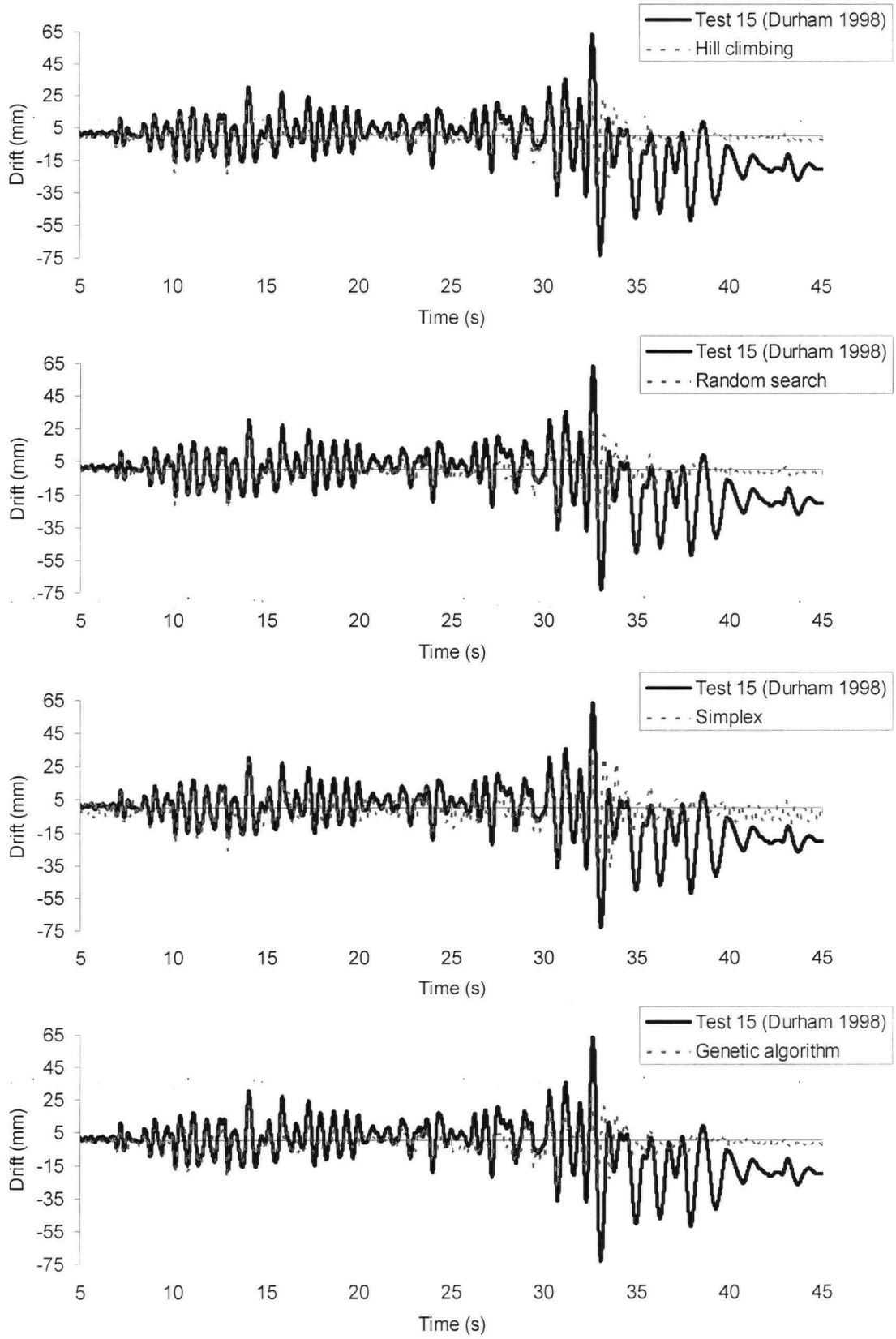

Figure 4.11 Comparison of Type C walls under dynamic load (Test 15)

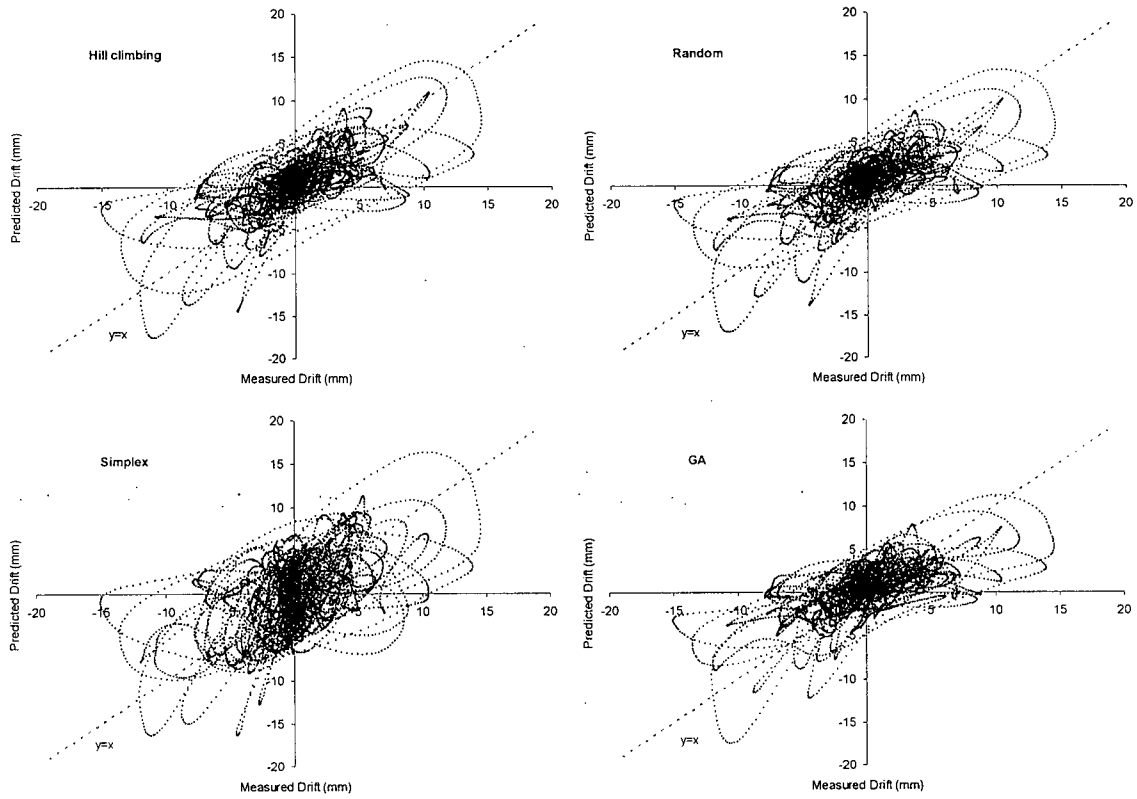

Figure 4.12 Correlation between test and prediction for Type C walls (Test 10a)

Table 4.5 Summary of comparison between test and prediction (Test 10a)

	Correlation coefficient	Angle to 45° line (°)
Hill climbing	0.6727	14.55
Random	0.6597	16.76
Simplex	0.5312	14.38
Genetic algorithm	0.6511	19.29

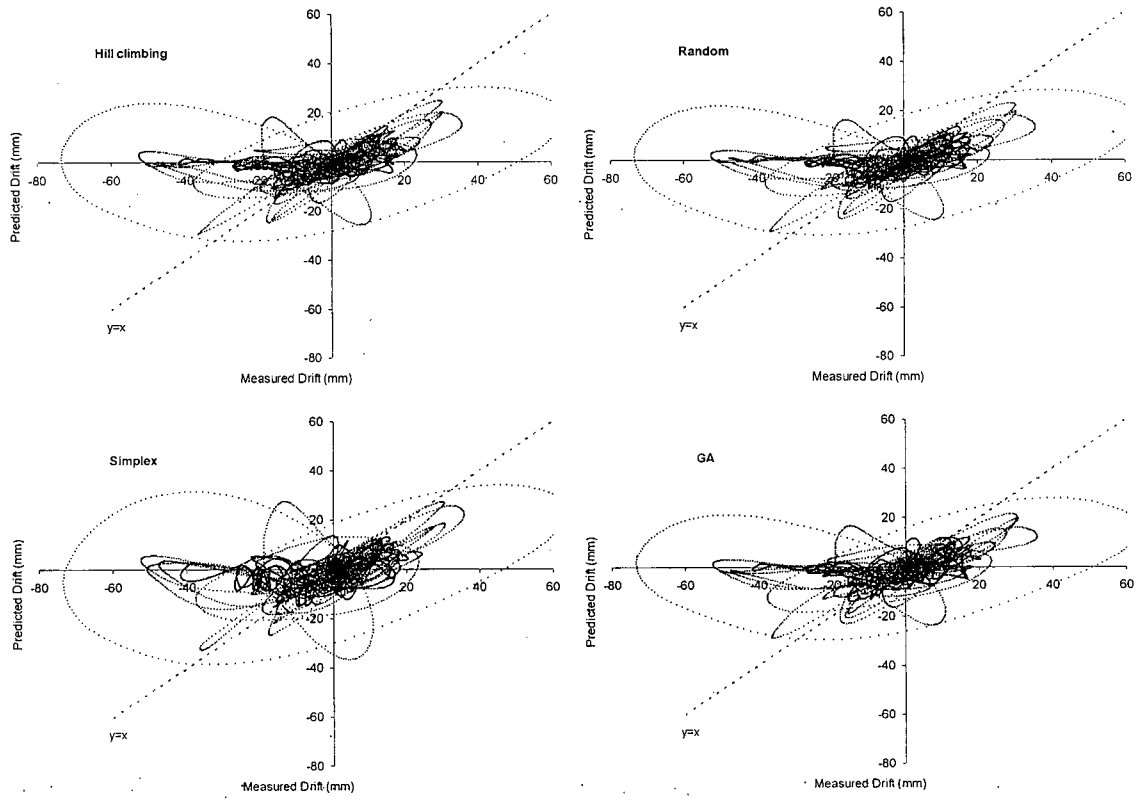

Figure 4.13 Correlation between test and prediction for Type C walls (Test 15)

Table 4.6 Summary of comparison between test and prediction (Test 15)

	Correlation coefficient	Angle to 45° line (°)
Hill climbing	0.3844	35.62
Random	0.3673	36.36
Simplex	0.3836	33.06
Genetic algorithm	0.3813	35.81

4.3 Results Comparison and Comments

4.3.1 Comparing Search Methods

For the artificial neural network, the minimum number of layers and neurons are determined by the type and the number of training data. Generally, its results have a relatively large error compared with other methods. The best results from the neural network are shown in Figures 4.2 and 4.3. Even in this case, the results are worse than the best solution in the training data. This is understandable since the neural network does not evaluate the value of function after prediction.

For all other methods, the accuracy and convergence speed of optimization are heavily dependent on the initial values or boundaries and the problem itself. The hill climbing method and simplex method need a fairly good estimation of initial values while the random method and genetic algorithm have to be given the upper and lower boundaries. The comparison from all shear walls reveals that all methods give relatively good results (Figures 4.4, 4.5, 4.10 and 4.11).

4.3.2 Comments of Model Verification

The pseudo nail model utilizes the information from reversed cyclic tests to predict the behaviour under dynamic load. The validation of the examples in this chapter shows that the pseudo nail model generally provides good accuracy for prediction. In the comparison with Test 15, however, the error between the prediction and the test results is relatively large (Figures 4.11 and 4.13, Table 4.6). This may be partially be attributed to the variation of shear wall behaviour rather than the model itself. It is noticed that the

peak drift in Test 15 (73.36 mm) is 4.87 times of that in Test 10a (15.06 mm) while the excited PGA level in Test 15 (0.52g) is only 1.44 time of that in Test 10a (0.35g).

The input data used to calibrate the model is essential for the accuracy of the pseudo nail model. To capture the characteristics of both loading and unloading paths, the pseudo nail model requires calibration with the response subjected to a half cycle static load. The maximum displacement should be higher than that at the peak load. In Figure 4.2, the maximum displacement of the data used to calibrate the model for Type A walls is 90 mm. So the accuracy of prediction within this range with this model is very good. This is confirmed by the model prediction under dynamic load (Figures 4.4 and 4.5). 90 mm displacement is deemed to be big enough compared with the typical collapse-prevention criterion, 73.2 mm or 3% of the wall height. The accuracy of prediction beyond 90 mm is acceptable; however, it is not as good as that from the lower deformation level (Figure 4.3). Similar phenomenon can be seen in the calibration and validation of Type C walls (Figures 4.8, 4.10 and 4.11).

Since the pseudo nail model fits the results from reversed cyclic tests, it cannot predict the information that does not exist in the cyclic test results. The comparison under the dynamic load in Figures 4.4, 4.5 and 4.11 shows that the predicted residual drift (near the end of time in all figures) does not match the test results well. It is suspected that the difference between the test results and the model prediction are partially attributable to the broken nails or withdrawn of nails that occurs in the shake table tests, which effect was not shown in the results of reversed cyclic tests. The discrepancy could also result from the test facility or the displacement measuring devices. The wall drift was calculated from the difference of the measured displacements of the shake table and

of the shear walls. Any problem of the displacement transducers occurred in the process of motion may cause this type of difference.

CHAPTER 5. SEISMIC RELIABILITY ANALYSIS OF STRUCTURES

Performance-based earthquake engineering and design aim to provide for target performance levels under different hazard levels. The uncertainty of seismic hazard and structural resistance requires reliability based analysis to achieve this goal. Reliability-based performance analysis is typically conducted with validated analytical tools. The seismic reliability evaluation of components or structures typically requires significant computational efforts with many repetitive calculations. Computational efficiency with reasonable accuracy is essential for the analytical tools to perform the numerical calculation. The pseudo nail model provides such an analytical tool for reliability-based analysis of wood shear walls and structures.

5.1 Earthquake Hazard in Reliability Analysis

Earthquakes commonly occur in many parts of the world. For instance the December 24th Sumatra-Andaman earthquake caused a catastrophic tsunami hazard that ravaged many coastal regions of south Asia. Earthquakes can cause other hazards, such as soil liquefaction and ground displacement that keenly interest seismologists. For structural engineering analysis, the most important earthquake hazard is the influence of the shaking of ground on the behaviour of the buildings. The shaking of ground in turn shakes the buildings, which can cause objects to fall and structures to partially or totally collapse with the potential to cause significant loss of life.

The shaking of ground at a specific site relates to many factors, such as the distance to the epicenter, the depth of the focus and the soil condition at the site. The effect of the shaking is particularly important for structural analysis of the buildings at the site. The ground shaking is generally characterized by two variables: frequency components of the earthquakes that could be experienced at this site and the intensity measure of the earthquakes.

The frequency components are typically represented by the frequency content of a set of past earthquake records. These records were recorded by accelerometers at monitor stations. Some earthquake prone zones have many earthquake records. Sometimes the available earthquake records are more than enough for analysis. Some of the records may exhibit similar shape in both time and frequency domains, which cannot be considered as independent samples of frequency components at the observed site. This phenomenon is common for multiple records from same earthquake at different stations. For reliability analysis, the selection of these records has to consider the criteria of coherence function of any two earthquake records, such that the set of the selected records does not contain similar frequency components. With this method, every selected record is an independent (or nearly independent) specimen from the unknown frequency range of earthquakes at the observed site.

The definition of "intensity measure" was adopted from Vamvatsikos and Cornell (2002). Two commonly-used intensity measures are the peak ground acceleration and the spectra acceleration. Using the peak ground acceleration as the intensity measure directly scales the original earthquake records to the prescribed peak ground acceleration levels. Foschi (2003) employed this measure in his reliability study. Using the spectra

acceleration as the intensity measure relies on the elastic design spectra of the records. Each earthquake record is scaled with a non-negative factor that is determined from the original and prescribed levels of earthquake spectra. Many researchers used spectra acceleration as the intensity measure for probabilistic analysis (Cornell et al. 2002, Ellingwood et al. 2004).

When using spectral acceleration as the intensity measure, the scale factor has to be determined from the earthquake spectra at a given value of natural frequency or period. However, wood structures exhibit inelastic response over the entire range of lateral deformation (Foliente et al. 2000, Filiatrault and Folz 2002). It does not show a definite yield point and cannot be characterized by a single-value variable, such as the system frequency or period. Although there are some definitions for the linear stage of load-displacement curves of wood structures, the resulting linear stage or the system frequency varies from protocol to protocol. Peak ground acceleration, rather than spectral acceleration, is used as the intensity measure in this thesis.

5.2 Performance Measure and Criteria

Performance measure refers to a particular designated value that characterizes the performance of structures. For panel sheathed shear walls, the rigidity of the sheathing panels is transferred to the frame members by the nail joints. The nail joints are the weakest element within the load transfer path and they affect the structural behaviour of the shear wall. Benefiting from the ductile nail connection as well as structural redundancy, the load-deformation relationship of shear walls exhibits good ductility. The shear walls tested in the laboratory typically failed after large deformation. No nailed panel sheathed shear wall has been reported to exhibit brittle failure. Based on this fact,

deformation control is naturally selected as the performance measure to conduct performance-based seismic engineering and design. The deformation criteria provided by FEMA 273 (FEMA 1997) can be the basis of engineering practice.

Compared with panel sheathed shear walls, braced walls have less redundancy and less ductility. The full-scale braced wall tests conducted at UBC and the Center for Better Living Japan (CBL) show that some specimens failed with broken brace members near the connection. Splitting of girders and sills caused by the tension perpendicular to grain stress is another common phenomenon of braced walls. Brittle failure mode can also be observed from the load-displacement curves of test results. Since this type of failure is governed by the capacity of strength of wood members, force criterion may be an extra choice for performance-based design for braced walls although it is not considered in this thesis.

5.3 Drift Demand and Its Distribution

Peak drift of a specific structure can be calculated from nonlinear time-history analysis under a given earthquake record scaled to a certain level of peak ground acceleration. The value of peak drift varies with earthquake records and peak ground acceleration levels. The peak drift can be expressed as a function of the earthquake records and the peak ground acceleration, shown as

$$d = d(r, a_G) \tag{5.1}$$

where

d is the peak drift;

$r(.)$ is the earthquake ground motion representing the frequency component of the ground shaking;

a_G is the scaled peak ground acceleration representing the intensity of the ground shaking.

For each earthquake record, performing dynamic analysis with varied peak ground acceleration obtains a relationship between peak drift and peak acceleration. This process was named as Dynamic Pushover Test by analogy with the pushover test under static load. The dynamic pushover tests for all selected earthquake records constitute the drift function as stated in Equation 5.1.

The ground motion records and the earthquake intensity are generally related. For the feasibility of reliability assessment, they are assumed to be independent variables. The selected earthquake records, or their frequency components, are discrete and implicitly assumed to be distributed uniformly over the range of all possible earthquakes. Therefore it is important to verify that there is no (or little) similarity between the frequency components of any two earthquake records. The distribution of earthquake intensity is a subject of interest for engineers and seismologists and generally cannot be determined prior to application. The peak drift follows a two-dimensional distribution of the random variables for the earthquake records and the intensity measure. The probability density function of the peak drift is illustrated in Figure 5.1.

In this figure, the dotted lines are equally spaced and they divide the virtual range of frequency component of the earthquake records. Each curve within every two adjacent dotted lines represents the density distribution of scaled acceleration levels for one record. All curves are same in shape and parallel in the direction of frequency component

because all records are scaled to have the same distribution of peak ground acceleration levels. Given any peak acceleration level, the probability density at all curves is same, which indicates that all earthquake records have the same occurrence probability.

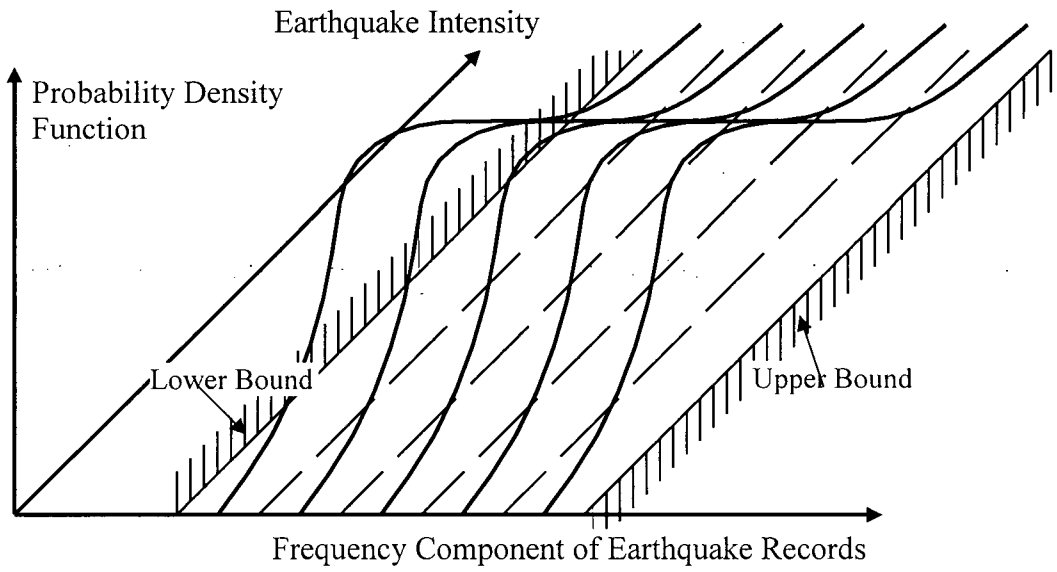

Figure 5.1 Probability density function of drift demand

5.4 Traditional Format For Seismic Reliability Analysis

The probability of structural failure can be expressed as

$$P_f = P(C \leq D) \tag{5.2}$$

where

C is the drift capacity of the system;

D is the drift demand of the system.

When the region of non-performance is integrable and the drift demand and capacity are uncorrelated, Equation 5.2 can be further expressed by the integration of probability density function of the capacity and demand, shown as

$$P_f = \iint_{C \leq D} f_{C,D}(x,y)dS \tag{5.3}$$

$$= \iint_{C \le D} f_C(x) f_D(y) dS \tag{5.4}$$

$$= \int_0^{+\infty} f_C(x)[\int_{x \le y} f_D(y) dy] dx] \tag{5.5}$$

$$= \int_0^{+\infty} f_C(x)[1 - F_D(x)] dx \tag{5.6}$$

where

$f_{C,D}(x, y)$ is the joint probability density function of drift capacity, C, and drift demand, D;

S is the integration variable representing a region;

$f_C(.)$ is the probability density function of drift capacity C;

$f_D(.)$ is the probability density function of drift demand D;

$F_D(.)$ is the cumulative probability function of drift demand D;

x, and y are the integration variables;

An alternative format of Equation 5.6 is:

$$P_f = \int_0^{+\infty} f_D(y)[\int_{x \le y} f_C(x) dx] dy] \tag{5.7}$$

$$= \int_0^{+\infty} f_D(x) F_C(x) dx \tag{5.8}$$

where

$F_C(.)$ is the cumulative probability function of drift capacity D;

The drift demand is a function of ground motion records and earthquake intensity (Equation 5.1). The probability density function of drift demand is illustrated in Figure 5.1. Therefore, three random variables are involved in the calculation of Equations 5.6 or

5.8: drift capacity, ground motion records and earthquake intensity. Ideally, Equations 5.6 and 5.8 can be further expressed as the integration of the frequency component of ground motion and the intensity, if all the three elements are assumed to be uncorrelated and integrable. Noting Equation 5.1, Equation 5.6 (or 5.5) can be expressed as

$$P_f = \int_0^{+\infty} f_C(x)[1 - \iint_{d(r,a_G)<x} f_{r,a_G} dS]dx \tag{5.9}$$

$$= \int_0^{+\infty} f_C(x)[1 - \iint_{d(r,a_G)<x} f_r f_{a_G} dS]dx \tag{5.10}$$

where

f_{r,a_G} is the joint probability density function of earthquake records and intensity;

$f_r(.)$ is the probability density function of frequency component of the earthquake records, r;

$f_{a_G}(.)$ is the probability density function of peak ground acceleration levels to be scaled, a_G.

A closed form of expression of $d(r,a_G)$ is necessary to symbolically solve Equation 5.10. Assume that the drift demand $d(r,a_G)$ can be graphically shown as the curved surface in Figure 5.2; the plane $d = x$, which is parallel to $r - a_G$ plane, intersects the demand surface, S, as a curve of m, which is an inverse form of $x = d(r,a_G)$ about r. If the curve m is monotonic (or segmental monotonic) with respect to the intensity a_G, one can further express Equation 5.10 as

$$P_f = \int_0^{+\infty} f_C(x)[1 - \int_0^{+\infty}\{\int_0^{m(a_G)|d=x} f_r dr\} f_{a_G}(y)dy]dx \tag{5.11}$$

where

$m(a_G)|d = x$ is the curve intersected by the plane $d = x$.

The curve m in Figure 5.2 is analogous to a shoreline of the integration which emerges into the water. The integration process of Equation 5.1 can be imagined as the increasing level of sea water which pushes the "shoreline" upward step by step until the whole surface emerges into the water.

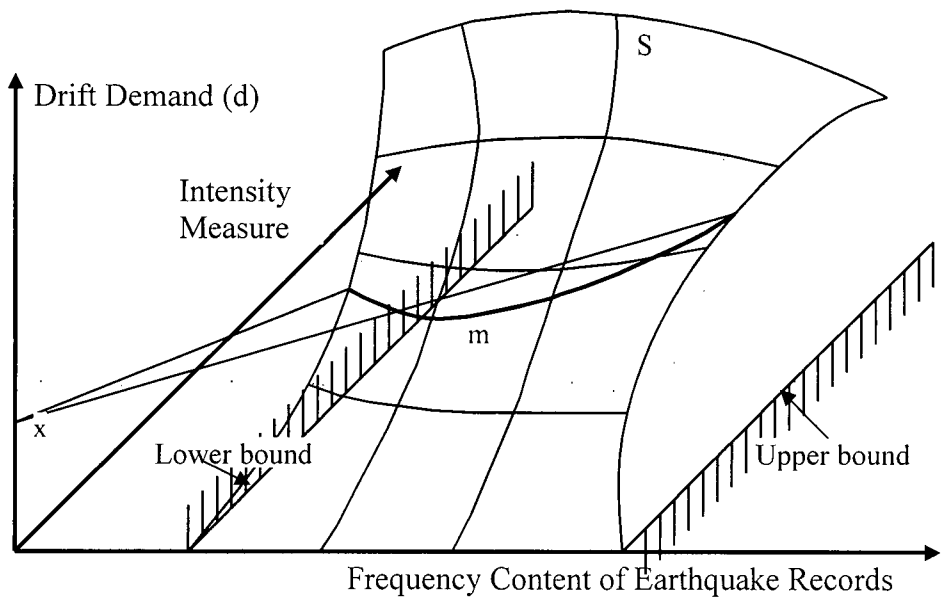

Figure 5.2 Surface of drift demand and integration range

Typically the demand surface is not as smooth as that shown in the example. It could have some caves or hills due to the nature of different records. The closed form of the curve m may not exist or may not be continuous, which leads to the difficulty to further express Equation 5.11 in closed form. To facilitate the problem, some researchers (Cornell et al. 2002, Li and Ellingwood 2004) adopted a procedure which estimates the probability of failure with the conditional distributions for a given earthquake intensity measure:

$$F_D(x) = P(X \le x) \tag{5.12}$$

$$= \int_0^{+\infty} \{ \int_0^{m(a_G)|d=x} f_r dr \} f_{a_G}(y) dy \tag{5.13}$$

$$\approx \int_0^{+\infty} P(D \le x | a_G = y) f_{a_G}(y) dy \tag{5.14}$$

With this concept, Equation 5.11 can be written as:

$$P_f \approx \int_0^{+\infty} f_C(x)[1 - \int_0^{+\infty} P(D \le x | a_G = y) f_{a_G}(y) dy] dx \tag{5.15}$$

$$= \int_0^{+\infty} f_C(x)\{1 - \int_0^{+\infty} [\int_0^{x} f_{D|a_G=y}(z) dz] f_{a_G}(y) dy\} dx \tag{5.16}$$

where

$P(D \le x | a_G = y)$ is the probability of drift demand not exceeding value x given the intensity level of $a_G = y$;

$f_{D|a_G=y}(.)$ is the probability density function of drift demand, D, given the intensity level of $a_G = y$.

To evaluate Equation 5.15 numerically, the exceeding probability, $P(D \le x | a_G = y)$, can be evaluated by ranking the drift demand values at the given intensity level of $a_G = y$. The integration also involves infinite upper bound of earthquake intensity measure. To evaluate the integration with limited samples, an integration strategy is used here. Assume N points are sampled from the range of earthquake intensity measure. They are numbered in an ascending order of their cumulative probability (Figure 5.3). The

incremental cumulative probability [discrete form of $f_{a_G}(y)dy$] can be calculated from the cumulative probability of adjacent two samples, shown as

$$\Delta P_i = f_{a_G}(y_i)\Delta y_i \tag{5.17}$$

$$= (P_{i+1} - P_{i-1})/2 \tag{5.18}$$

where

i is the ith sample ($1 \le i \le N+1$);

P_i is the cumulative probability at the ith sample.

The (N+1)th point is set to the upper bound, where the cumulative probability equals to 1 ($P_{i+1} = 1$). The conditional exceeding probability at each of N discrete samples in Equation 5.15 can be evaluated. However, the N samples divide the cumulative probability range (between 0 and 1) into N+1 division (Figure 5.3). Consequently, the summation of all $\Delta P_i (i = 1...N)$ is less than 1. The portion of the first half interval ($\Delta P_1/2$) and the last half interval ($\Delta P_N/2$) is missed. The conditional exceeding probability corresponding to half ΔP_1 is declared to 1 and the conditional exceeding probability corresponding to half ΔP_N is declared to 0. When the sample number N is big enough, the error introduced by the assumption is minor and the result of the numerical integration will close to the real one.

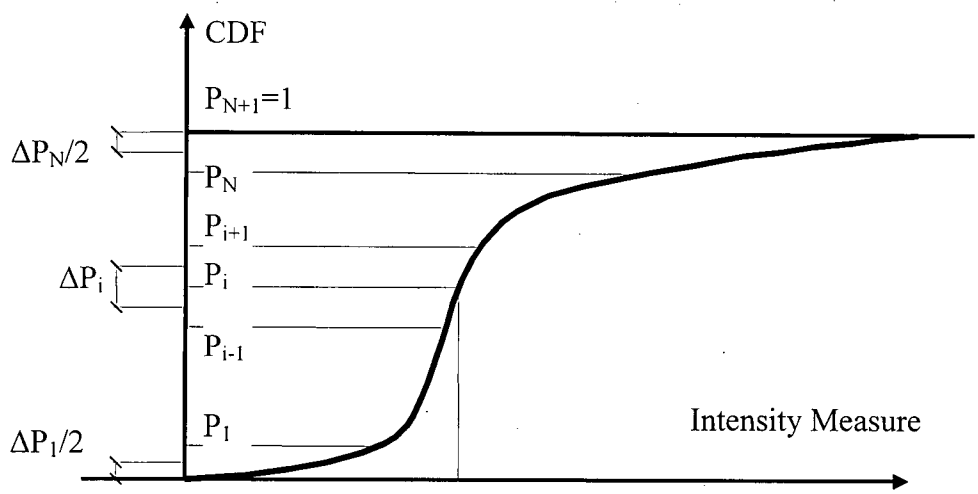

Figure 5.3 Sampling of intensity measure

5.5 A Procedure Based on Conditional Distribution of Given Records

In the traditional procedure (Equation 5.15), the conditional distribution is constructed at given levels of earthquake intensity measure. The total demand function is the summation of the conditional distribution weighted by the incremental cumulative probability. A similar formula can be deduced if the conditional distribution is established at given earthquake records, shown as

$$P_f \approx \int_0^{+\infty} f_C(x)[1 - \int_{y \in r} P(D \le x | r = y) f_r(y) dy] dx \qquad (5.19)$$

where

$P(D \le x | r = y)$ is the probability of drift demand not exceeding the value x given the earthquake record of $r = y$;

$f_r(.)$ is the probability density function of the earthquake record, r.

Since the earthquake records are always discrete, the variable r does not have a form for integration. The discrete form of Equation 5.19 is

$$P_f \approx \int_0^{+\infty} f_C(x)[1-\sum_i P(D \le x|r_i = y) f_{r_i} \Delta y_i]dx \tag{5.20}$$

where

$P(D \le x|r_i)$ is the probability of drift demand not exceeding value x given the earthquake record of $r_i = y$

$f_{r_i}(.)$ is the probability density function of the earthquake record of r_i;

Δy_i is the ith interval representing the distance of adjacent earthquake records;

i is the ith earthquake record.

Because the earthquake records are assumed to be uniformly distributed, the value of probability density function, f_{r_i}, and the interval, Δy_i are the same for all records (Figure 5.1). Noting the relationship that

$$\sum_{i=1}^{N} f_{r_i} \Delta y_i = 1 \tag{5.21}$$

where

N is the total number of earthquake records to be analyzed.

One has

$$f_{r_i} \Delta y_i \approx \frac{1}{N} \qquad (i = 1 \sim N) \tag{5.22}$$

Equation 5.20 can be written as

$$P_f \approx \int_0^{+\infty} f_C(x)[1-\frac{1}{N}\sum_{i=1}^{N} P(D \le x|r_i)]dx \tag{5.23}$$

$$= \int_0^{+\infty} f_C(x)[1 - \frac{1}{N}\sum_{i=1}^{N}(\int_0^x f_{D|r_i} dy)]dx \tag{5.24}$$

$$= \int_0^{+\infty} f_C(x)[1 - \frac{1}{N}\sum_{i=1}^{N}\{\int_0^x f_{a_G}[d^{-1}(y,r_i)]\left|\frac{\partial d^{-1}(y,r_i)}{\partial y}\right| dy\}]dx \tag{5.25}$$

where

$f_{D|r_i}(.)$ is the probability density function of drift demand given the ith earthquake record of r_i;

$d^{-1}(y,r_i)$ is the inverse function of drift demand, $d(r,a_G)$ as stated in Equation 5.1, about intensity measure, a_G for the ith earthquake record.

Equation 5.23 indicates that the probability of drift demand is calculated from the weighted average of probability failure with the conditional distributions over all earthquake records. As a format parallel to the traditional format (Equation 5.15), the difficulty to implement Equation 5.25 is to identify the inverse function of drift demand. But for approximate numerical calculation, it is not necessary to obtain the closed form to express the probability density function in Equation 5.25. The exceeding probability at a given drift capacity in Equation 5.23 can be interpolated directly from the values of drift demand.

The general procedure to evaluate the probability of failure with Equation 5.25 is summarized as following:

1) Conduct dynamic push-over tests for all earthquake records;
2) For each push-over curve, find the relationship of $a_G = d^{-1}(y,r_i)$ for each earthquake record;

3) Find the conditional density function of drift demand for each earthquake record, $f_{a_G}[d^{-1}(y,r_i)]\left|\frac{\partial d^{-1}(y,r_i)}{\partial y}\right|$;

4) Calculate the average of cumulative probability function of demand and evaluate the exceeding probability.

5.6 Construction of Confidence Curves

Riddell and Newmark (1979) used 84.1% cumulative probability curves over an ensemble of earthquake records (one standard deviation above the mean curve) to construct a linear design spectra. For nonlinear problems, similar confidence curves can be constructed to estimate the randomness of the selected earthquake records. At any peak ground acceleration level, the resulting peak drift data from the nonlinear time history analysis for all records can be ranked to establish a conditional probability distribution. Figure 5.4 shows an example. In this figure, four earthquake records were scaled to five levels of ground acceleration. Peak drift can be obtained from nonlinear time history analysis. Ranking the peak drift at a selected level of earthquake ground acceleration gives a probability distribution, typically in a cumulative form. For illustration, Figure 5.4 expresses that in the form of probability density function.

This distribution can be used to determine a point representing a certain magnitude of probability of exceedance, for instance, 15.9% (Figure 5.5). Linking the points at different acceleration levels establishes a curve which represents 15.9% of exceeding probability at any peak ground acceleration level over all records. This curve has a relationship between peak ground acceleration and drift demand with a confidence level

of 84.1% over all earthquake records. This kind of confidence curves is noted as PGA-based Curves.

Alternatively, at a given peak drift level, a distribution of peak ground acceleration can be established over all records. With this distribution, a point can be determined at some magnitude of exceeding probability. The points at different peak drift levels can be linked together to construct a design curve representing this level of confidence. This kind of confidence curves is noted as Drift-based Curves (Figure 5.6).

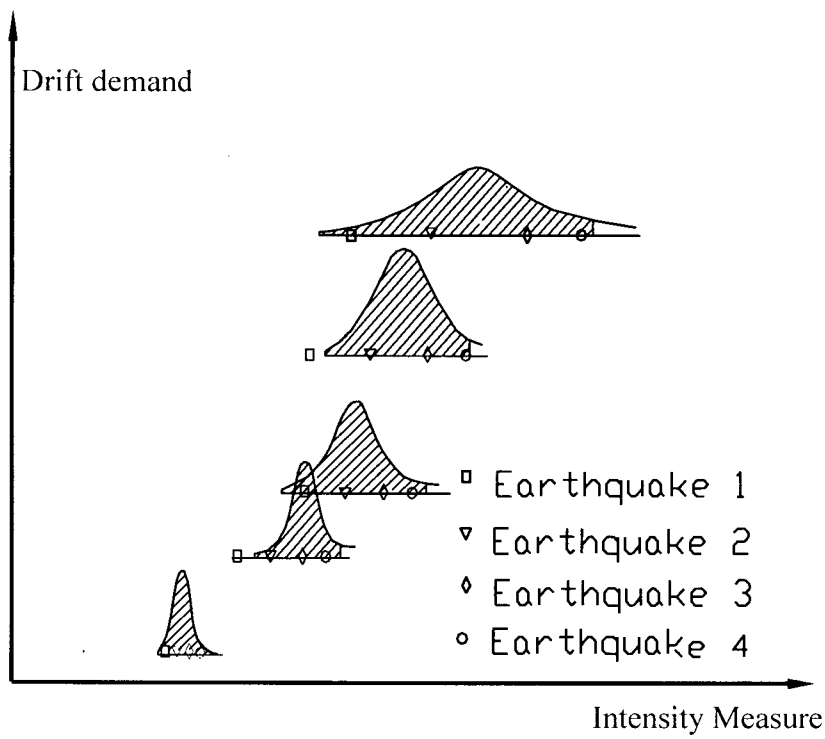

Figure 5.4 Drift demand at different intensity levels and its distribution

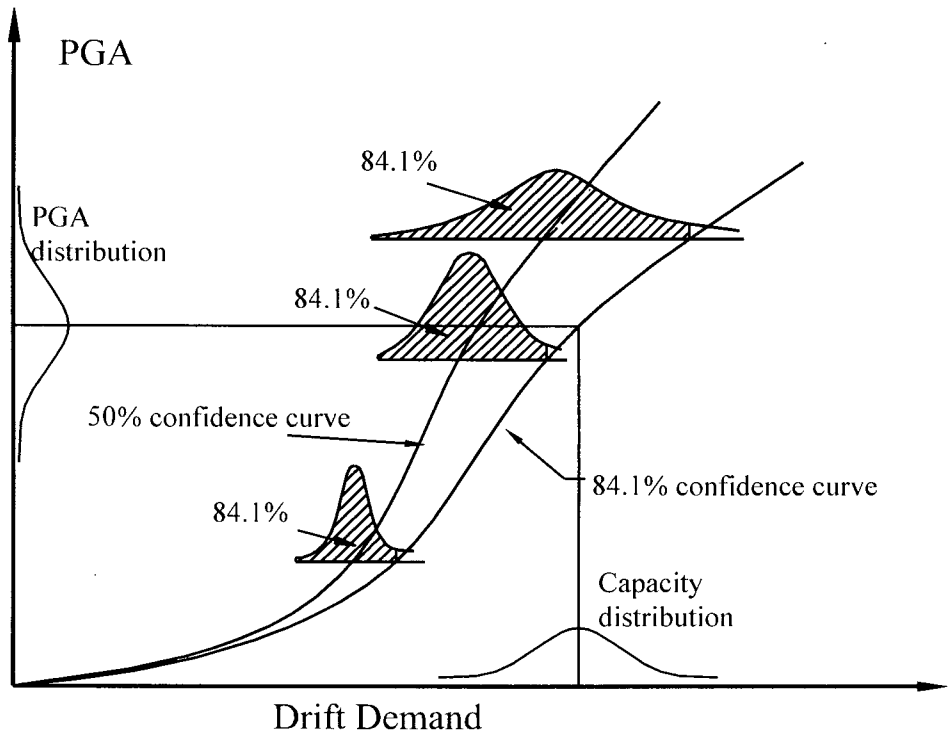

Figure 5.5 Confidence curves constructed from design PGA levels

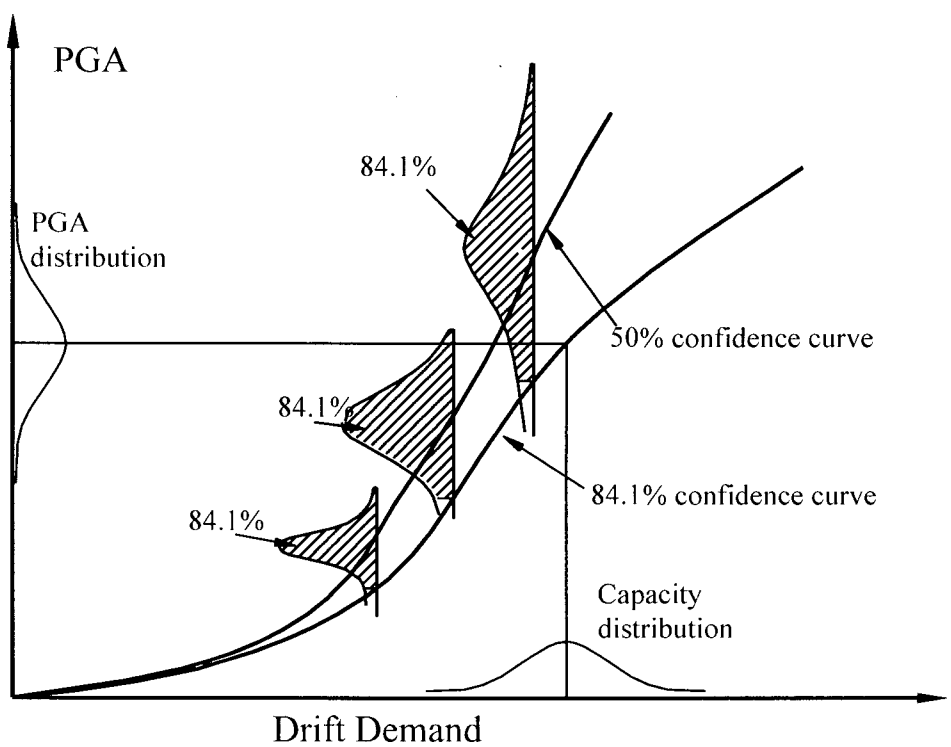

Figure 5.6 Confidence curves constructed from design drift levels

Confidence curves simplify the relationship between drift demand and its variables, including scaled earthquake intensity and records. These curves present the structural behaviour under earthquake load. They can be used to compare the seismic behaviour of different structures and materials.

5.7 Assessing Seismic Reliability with Monte Carlo Method

5.7.1 Original Monte Carlo Method

The discrete form of distribution of drift function is written as following

$$P(D < x) = \sum_{d(r,a_G)<x} f_r f_{a_G} \Delta_r \Delta_{a_G} \tag{5.26}$$

Imagine using a traditional Monte Carlo simulation process to generate the distribution of drift demand. An earthquake record is randomly picked from the selected set of records that representive of the frequency content at the site. A level of earthquake intensity is also randomly determined from its distribution. With the pair of the earthquake record and the level of intensity, nonlinear dynamic analysis is conducted in order to obtain the peak drift. Repeating this process with enough times will obtain many sets of data. Then the values of drift demand can be ranked to give a cumulative distribution curve. This process is very time-consuming to obtain accurate results, especially for the tail portion of the distribution.

Ranking the values of drift demand with the original Monte Carlo simulation implies two assumptions:

1) The sampling of random variables have followed their own distributions;
2) Each set of samples equally contributes to the formation of cumulative distribution of drift demand.

Successful realization of the simulation requires sufficient number of samples, especially for the reliability assessment that concentrates on the tail of the distribution. For earthquake reliability analysis, the number of earthquake records is limited by the observation of earthquakes. Even with enough earthquake records, the requirement of time (or cost) in performing nonlinear time history analysis limits the number of samples for drift demand computation.

It is noted from Equation 5.26 that each set of samples is associated with a certain value of "incremental" probability. For example, for the ith earthquake record scaled to the jth level of intensity, the drift demand, d_{ij}, is (Equation 5.1)

$$d_{ij} = d(r_i, a_{Gj}) \tag{5.27}$$

The incremental probability associating to drift demand, d_{ij}, is

$$\Delta P_{ij} = (f_r \Delta_r)_i (f_{a_G} \Delta_{a_G})_j \tag{5.28}$$

With Equation 5.22, one has

$$\Delta P_{ij} = \frac{1}{N} (f_{a_G} \Delta_{a_G})_j \tag{5.29}$$

Equation 5.29 states that the associated incremental probability of each sample of drift demand equals to that of the corresponding sample of earthquake intensity measure divided by the number of earthquake records. If intensity measure is sampled from its distribution, the cumulative distribution of drift demand can be constructed from ranking their values directly as stated by the Monte Carlo simulation method. To minimize the number of samples of earthquake intensity, a Quasi Monte Carlo method was used in which the intensities were sample at constant cumulative probability intervals.

It is obvious that

$$\sum_j \sum_i \Delta P_{ij} = \sum_{j=1}^{M} \sum_{i=1}^{N} \frac{1}{N} (f_{a_G} \Delta_{a_G})_j \tag{5.30}$$

$$= \sum_{j=1}^{M} (f_{a_G} \Delta_{a_G})_j \tag{5.31}$$

$$= 1 \tag{5.32}$$

where

M is the total number of division to sample the range of intensity measure.

5.7.2 Monte Carlo Method Considering Weighted Ranking

Equation 5.29 indicates that each value of drift demand, d_{ij}, has an incremental probability of ΔP_{ij}. The values of the incremental probability may vary from one sample to another. For the original Monte Carlo simulation, these values of incremental probability are the same for all samples of drift demand. It requires that the sampling of intensity measure follow its distribution.

Sometimes, the sampling of intensity has been pre-determined (for example, in this study, the data of drift demand are ready for use based on a range of earthquake intensities of 0.0243g ~ 1.19 g) and does not follow the rules as required by the Quasi Monte Carlo method. In this study a few extra sampling points were added to enrich the sampling around the upper tail of the distribution. The weighted ranking Monte Carlo method intends to improve the efficiency of the Monte Carlo method used, especially when the time-consuming process to establish the database of drift demand has been completed before the distribution of intensity measure is known. With this method, the generation of random numbers does not have to be same as that of the Quasi Monte Carlo method. After obtaining the data combination $(d_{ij}, \Delta P_{ij})$ $(i = 1 \sim N, j = 1 \sim M)$, ranking

the drift demand d_{ij} in an ascending order gives a set of sorted data noted as $(d_k^{'}, \Delta P_k^{'})$ ($k = 1 \sim NM$), where $d_1^{'} \le d_2^{'} \le \cdots \le d_k^{'} \le \cdots \le d_{NM-1}^{'} \le d_{NM}^{'}$. During the sorting process, ΔP_{ij} is always associated with the corresponding d_{ij} which is noted as $\Delta P_k^{'}$. $\Delta P_k^{'}$ is just a different arrangement of ΔP_{ij}. Here k is corresponding to the original combination of i and j. Accumulating $\Delta P_k^{'}$ produces the cumulative distribution $P_k^{'}$ corresponding each value of $d_k^{'}$, shown as:

$$P_k^{'} = \sum_{j=1}^{k} \Delta P_j^{'} \tag{5.33}$$

With the cumulative distribution of drift demand of $d_k^{'}$, the probability of failure can be evaluated with Equation 5.6 or 5.8. For the determined drift capacity C, the probability of failure can be obtained directly from the distribution of $d_k^{'}$.

The whole procedure to analyze the seismic reliability with the weighted ranking Monte Carlo method is summarized as follow:

1) Prepare a set of ground motion records; scale the earthquake intensity to multiples levels (their cumulative probability levels does not have to be uniformly distributed);
2) Perform dynamic analysis and obtain the peak drift d_{ij} for the ith earthquake record scaled to the jth level of intensity;
3) For a specific design requirement, determine the probability distribution of intensity measure and calculate the incremental probability ΔP_{ij} with Equation 5.29;

4) Sort the data set ($d_{ij}, \Delta P_{ij}$) by d_{ij} and note the sorted set as ($d_k^{'}, \Delta P_k^{'}$); evaluate the accumulative probability with Equation 5.33;

5) Calculate the structural reliability with Equation 5.6 or 5.8.

The accuracy of the method heavily depends on that of the incremental probability, ΔP_{ij}. The incremental probability can be calculated from the difference of cumulative probability or from the integration of probability density function. If the incremental cumulative probability is calculated from the integration of density function, different formats of Newton-Cotes method for numerical integration can be implemented.

Using the ranking method for Monte Carlo simulation requires that the calculated maximum drift demand should be greater enough to evaluate the exceeding probability. If the maximum of drift demand is found to be not great enough after calculation or the distribution of intensity measure is changed, all samples of intensity measure have be changed accordingly and all values of drift demand have to be re-calculated. With the weighted ranking technique, only the extra samples are needed to calculate their drift demand.

5.8 An Example of Shear Wall Analysis

An example of a 2.4 m x 2.4 m shear wall is presented here, which has the configuration of Type C of Durham (Durham 1998) as introduced in Chapter 4. The dynamic behaviour of the shear wall is simulated with a SDOF system using the pseudo nail model. The visco-damping ratio is 1% of the critical damping about the initial tangential stiffness. The supported load is 5400 kg. The set of 20 ordinary CUREE Woodframe Project records (Krawinkler 2001) were used as the input for the dynamic

pushover analysis. The drift demand data from the calculation are shown in Figure 5.7. Three confidence curves (84.1%, 50% and 15.9%) were established (Figure 5.8). Linear interpolation was applied to create points while generating these curves.

Assume that the peak ground acceleration follows a lognormal distribution with a mean of 0.3g and a coefficient of variation of 0.55. According to Foschi's mapping method (Foschi 2003, Zhang and Foschi 2003), the statistics are consistent with a site design acceleration of 0.86 g (corresponding to a return period of 475 years) and a mean arrival rate of earthquakes of 0.2 (average of one every five years). The drift capacity is assumed to be 73.2 mm or 3% of wall height. The reliability index of this type of walls with the load of 5400 kg was calculated with three methods: the traditional method (Equation 5.15), the method based on conditional distribution given earthquake record (Equation 5.23) and the Monte Carlo simulation with weighted ranking technique. The calculated reliability indices with the three methods are 2.178, 2.062 and 2.181, respectively.

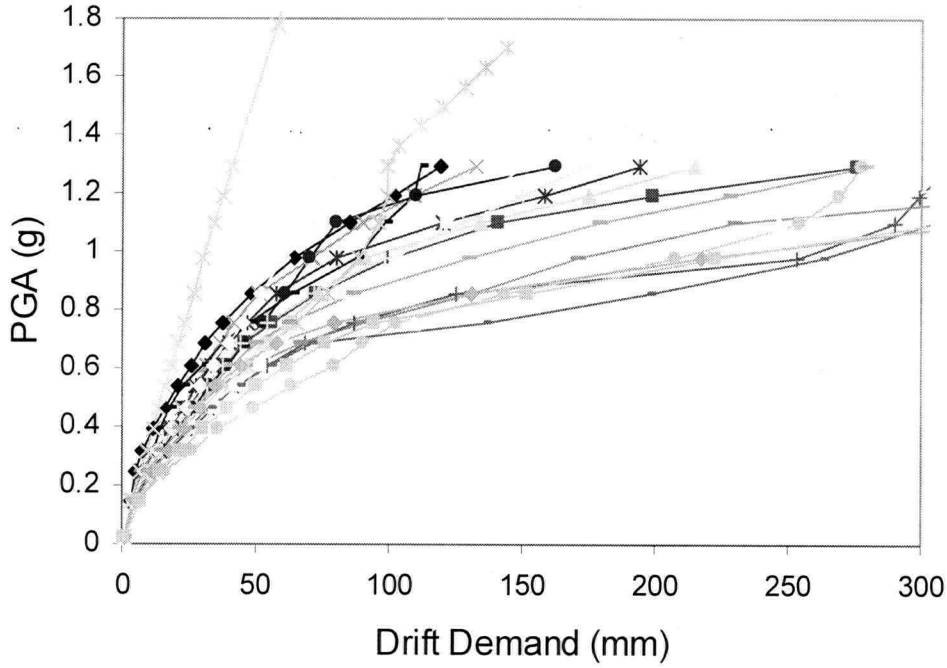

Figure 5.7 Peak drift demand at different ground acceleration levels

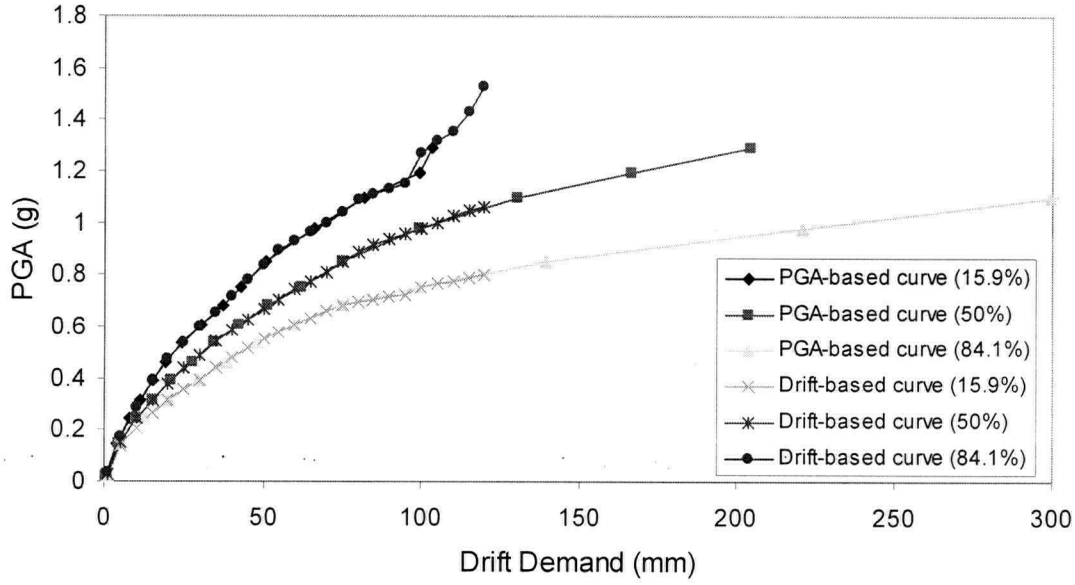

Figure 5.8 Confidence curves determined from both methods

5.9 Summary

Reliability methods considering the randomness of earthquake ground motion records and intensity measure are discussed here. To perform displacement–based reliability analysis under earthquake load, the dynamic push-over "test", or Incremental Dynamic Analysis, has to be conducted. During this process, drift demand for all ground motion records at different levels of intensity measure is calculated.

The traditional method calculates the structural probability of failure from conditional distribution of drift demand at given intensity level. Two new methods are developed. The first method is similar to the traditional one, which evaluates the probability of failure from conditional distribution of drift demand at given ground motion record. The second new method is a modified Monte Carlo simulation procedure. It is based on the fact that every earthquake ground motion record is a sample representing a realization of unknown distribution of the possible ground motion characteristics. Recognizing that all ground motion records are uniformly distributed in the range of their representing random variable, Quasi Monte Carlo method is used to conduct seismic reliability analysis. To increase the efficiency of calculation, weighted ranking technique is implemented into this calculation.

CHAPTER 6. PERFORMANCE EVALUATION OF JAPANESE WALLS

6.1 Introduction

Japan has a strong tradition to build wooden post-and-beam housing. Over the years, much effort has been made to improve the performance of this type of buildings, especially under seismic loads since Japan is an earthquake-prone country. Besides the use of traditional mortise-and-tenon connections, metal hardware, hold down devices, braces and sheathed shear walls are used to improve the lateral resistance of these structures. Although many species of wood are available in the Japan market for the construction of such buildings, the design values for wood shear walls are typically developed on the basis of Japanese Sugi (*Cryptomeria japonica*).

As a part of an international research project between Canada and Japan, the Centre for Better Living Japan conducted a series of shear wall tests supported by Canadian forest industry. The primary objective of the tests was to identify and compare the structural behaviour of Japanese shear walls made with three wood species: Japanese Sugi, Canadian Tsuga (Hemlock) and European Whitewood glulam. Both two-brace walls and panel sheathed walls were tested. The test results from the Center for Better Living Japan (Center For Better Living 2001, Okabe et al. 2004) were used as the input to calibrate the model parameters of the pseudo nail model for simulation. The calibrated models were used in nonlinear dynamic time step analysis to obtain the peak drifts of different walls subject to seismic ground motions as input. A set of confidence curves

was constructed for each type of walls. Reliability indices were computed with the methods introduced in Chapter 5.

6.2 Description of Specimen and Testing

All the walls had the width of 1.82 m and the height of 2.73 m. The girders (top beam) of the tested walls had cross-section of 105 mm x 180 mm. The sills and posts had cross-section of 105 mm x 105 mm. The studs were 30 mm x 105 mm or 45 mm x 105 mm. They were placed 450 mm on centre. Mortise-and-tenon connections were used between posts and girders or sills. For the braced walls, the braces were 45 mm x 90mm in cross-section. In all tests, S-HD20 hold down devices were installed between post and sill or girder connections to prevent uplift. Each hold down was connected to posts with four M12 bolts.

Three types of configuration were tested: two-brace walls (Figure 6.1), plywood panel-sheathed shear walls and OSB panel-sheathed shear walls (Figure 6.2). In braced walls, the ends of brace were connected to the post and sill or girder with "Z' marked "BP2" steel plates. Five ZS 50 nails connected the end "BP2" plate to the post, sill or girder. The "BP2" plate and brace were jointed with seven ZS 50 nails and one M12 bolt. In plywood shear walls, JAS grade two vertically oriented larch plywood panels with 9.5 mm thickness were used in the tests. JAS grade 4 OSB panels made by Ainsworth Lumber Co. with thickness of 9 mm were used for the OSB walls. The dimensions of all panels is 1.82 mm x 0.91 mm. These panels were connected to the frames with JIS A5508 N50 nails at a spacing of 150 mm and the edge distance of 15 mm.

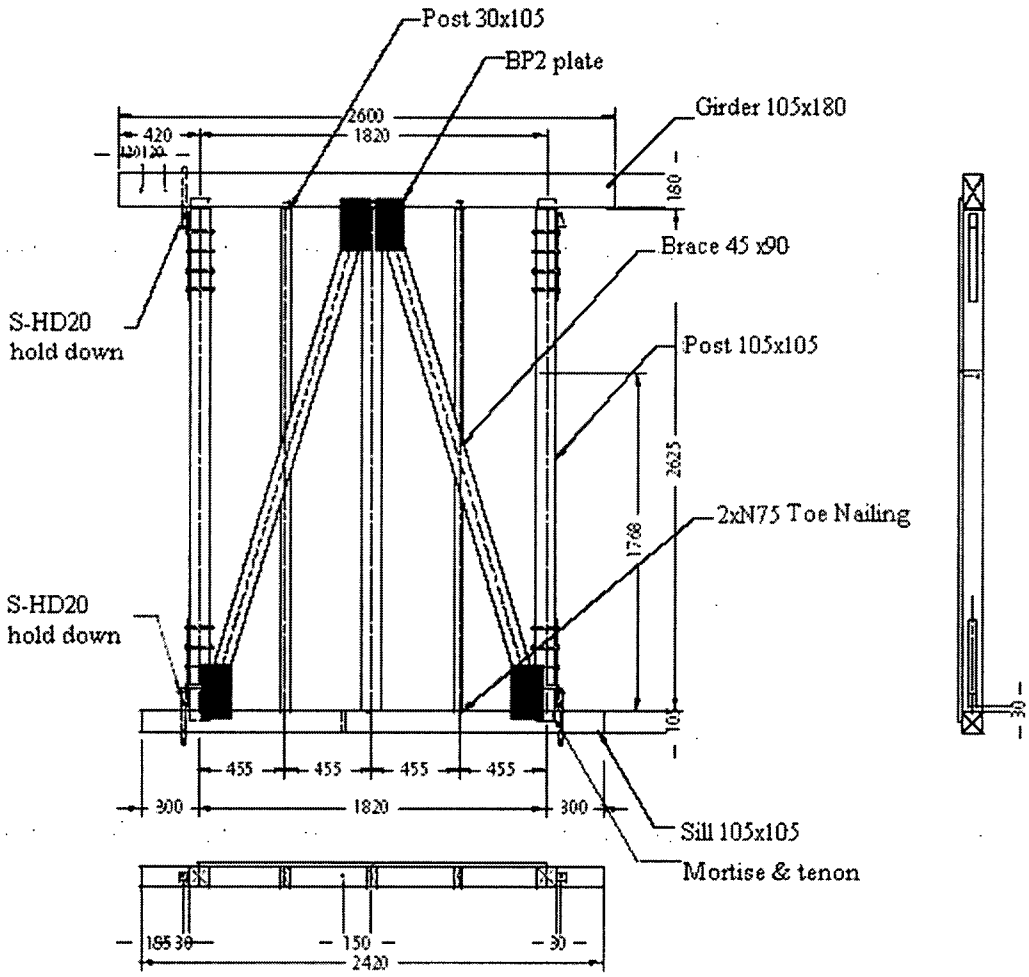

Figure 6.1 Configuration of two-brace shear walls (Center For Better Living 2001)

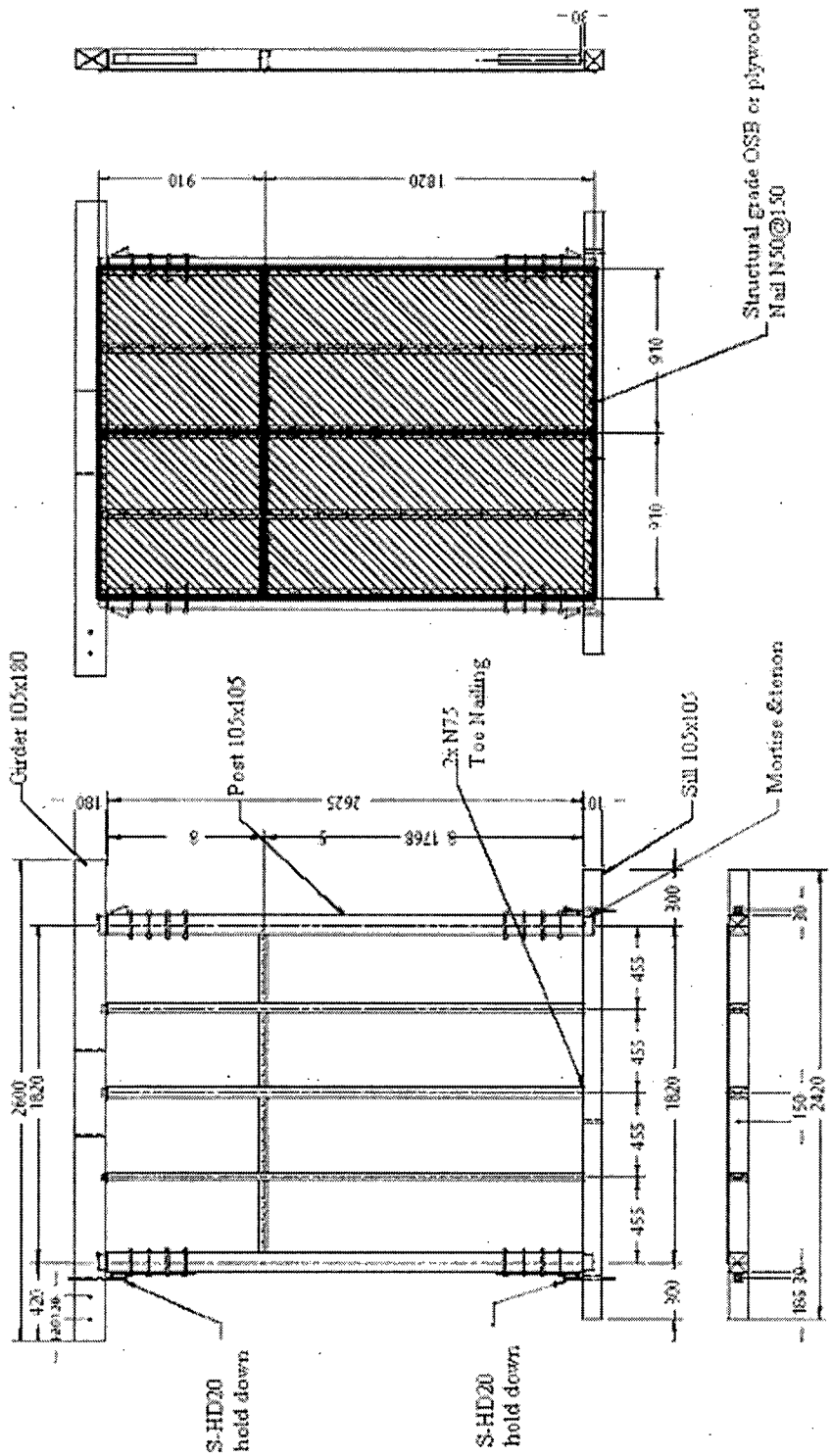

Figure 6.2 Configuration of OSB/plywood sheathed shear walls (Center For Better Living 2001)

In all the tests, the girders were constructed with Douglas fir lumber. The posts, sills, studs and braces were made from three different species: Canadian Tsuga (Hemlock), Japanese Sugi and European Whitewood glulam. Canadian Tsuga and Japanese Sugi were used in the tests of all three types of configurations. They were not graded in JAS standard. The grade of Whitewood glulam was E85-F300. Whitewood was only used in the tests of two-brace walls and plywood sheathed shear walls. The test matrix is presented in Table 6.1. Three replications for each type were tested. All materials are in dry condition.

Table 6.1 Replication of test specimens of different configurations and species

Species	Two-brace walls	Plywood shear walls	OSB shear walls
Sugi	3	3	3
Tsuga	3	3	3
Whitewood	3	3	-
Subtotal	9	9	6

The walls were tested under reversed cyclic loading controlled by the shear deformation angle of the walls. The amplitudes of shear deformation angles of the cycles were 1/600, 1/450, 1/300, 1/200, 1/150, 1/100, 1/75, 1/50, 1/30, 1/24, 1/20, 1/15 radians. Each of the amplitude was repeated for three cycles. No dead load or vertical load was applied to the top of the beam.

6.3 Cyclic Test Results

In all figures, "SG", "TG" and "WW" refer to the abbreviation of "Sugi", "Tsuga" (Hemlock) and "Whitewood", respectively. "BR", "PL" and "OS" are the abbreviation of "Brace", "Plywood sheathing" and "OSB sheathing", respectively. The number, "1", "2" or "3" of the legend is the number of replication of the tests for that configuration from the report of the Center for Better Living Japan (2001). For example, "WW-PL-2" means the second specimen of the plywood sheathing shear walls with European Whitewood glulam as framing members.

In each type of walls, the test results from all three replications were consistent, especially for those walls sheathed with plywood or OSB panels. From three replications of each type, the specimen with the moderate envelope curve of test results was selected as the input of data fitting of the pseudo nail model. The obtained parameters for each type of walls are listed in Table 6.2. With these sets of parameters, the predicted load-displacement behaviour is compared with test results in Figures 6.3 to 6.10. It can be seen that the level of displacement of the validation in all figures are more than 100 mm, which exceeds the performance level considered in this thesis, 68.3 mm.

Table 6.2 Parameters of the pseudo nail model for each type of walls

Wall type	Q_0 (kN/mm)	Q_1 (kN/mm^2)	K (kN/mm^2)	D_{max} (mm)	Q_3	D_i (mm)	L (mm)
SG-BR	4.09257	0.106469	0.518693	30.2831	1.958082	3.62639	72.4866
SG-PL	0.337608	0.0275855	0.0834557	45.2553	1.80881	9.27850	426.697
SG-OS	0.675727	0.0343936	0.0835077	29.4405	1.98132	8.36695	412.964
TG-BR	0.0121494	0.0583440	0.0587390	54.6693	1.25350	9.41585	461.161
TG-PL	0.80209	0.029098	0.19012	75.720	1.1145	10.771	41.552
TG-OS	0.22109	0.028795	0.061880	54.520	1.2947	10.830	207.88
WW-BR	0.152276	0.0675076	0.384076	68.8104	1.08092	7.67615	47.6601
WW-PL	0.87649	0.045017	0.099672	22.129	2.9286	8.8215	410.20

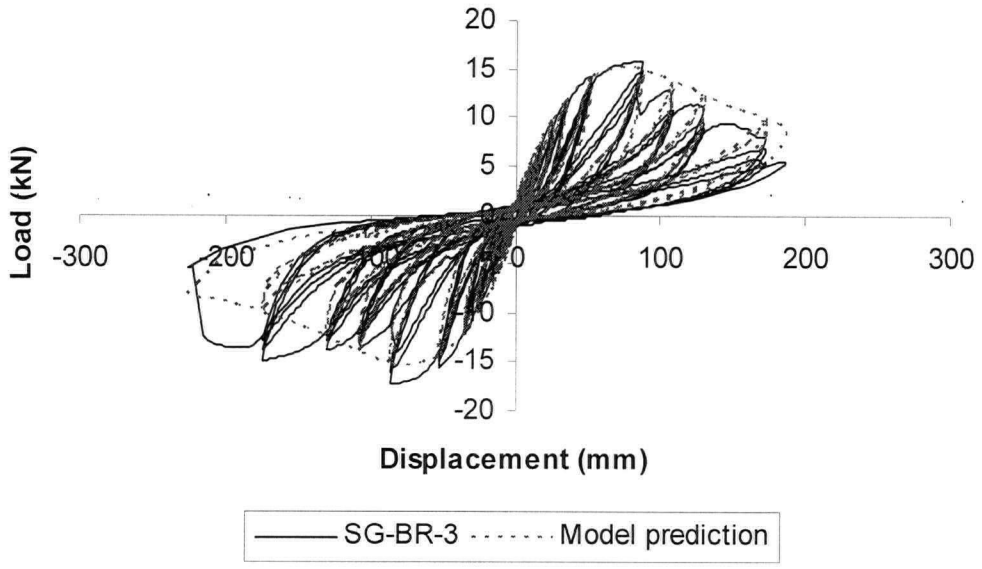

Figure 6.3 Comparison of Sugi braced walls under cyclic load

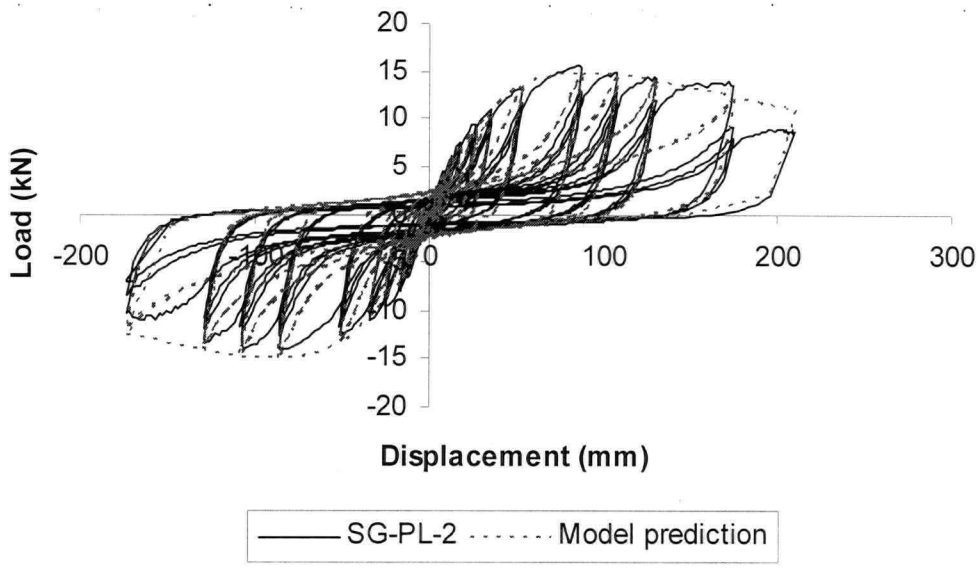

Figure 6.4 Comparison of Sugi plywood walls under cyclic load

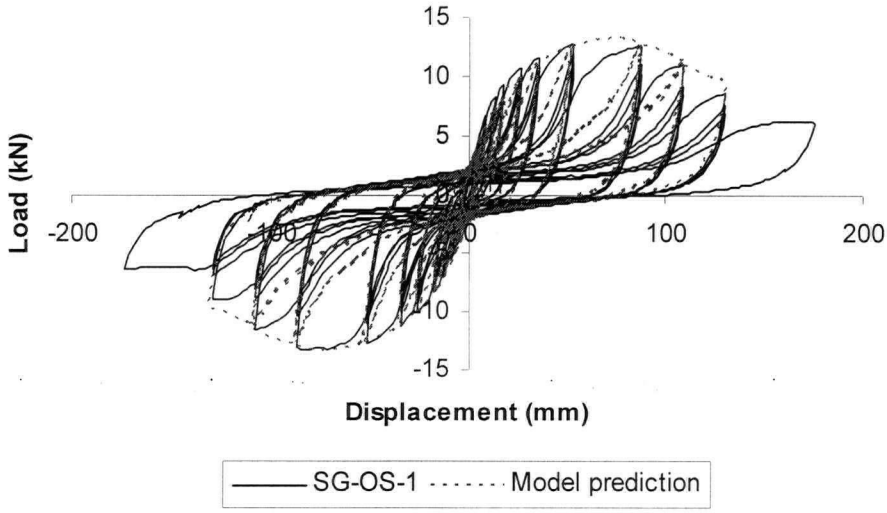

Figure 6.5 Comparison of Sugi OSB walls under cyclic load

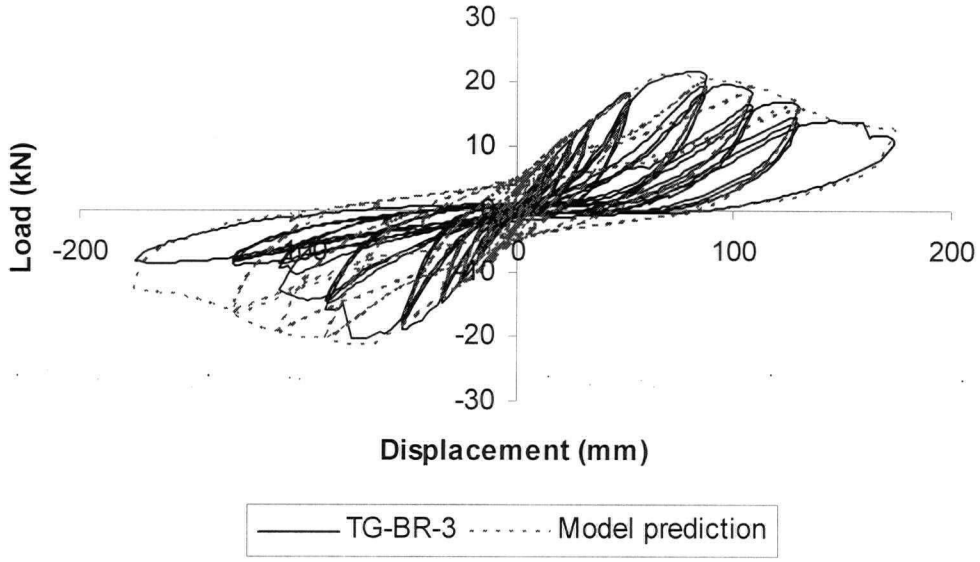

Figure 6.6 Comparison of Tsuga braced walls under cyclic load

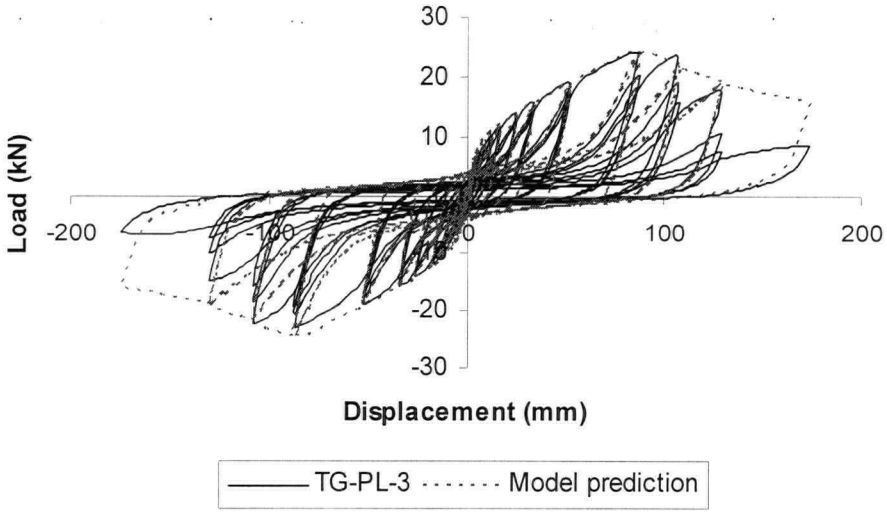

Figure 6.7 Comparison of Tsuga plywood walls under cyclic load

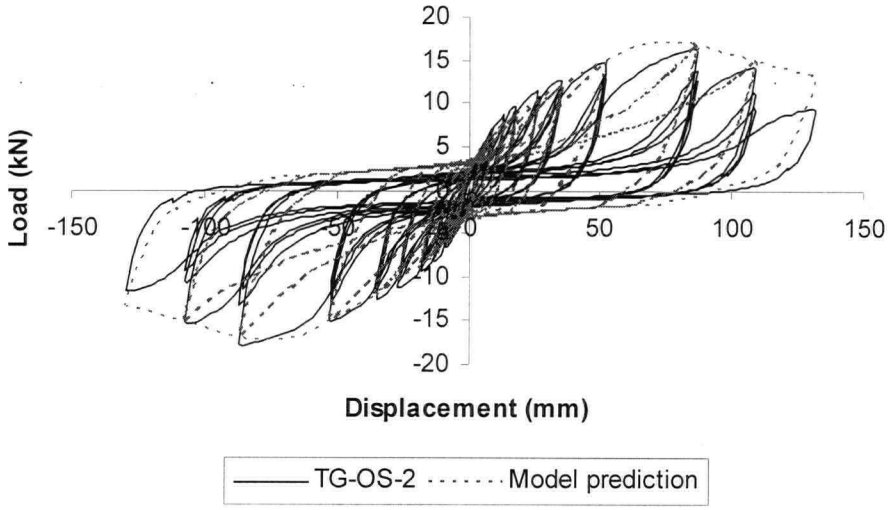

Figure 6.8 Comparison of Tsuga OSB walls under cyclic load

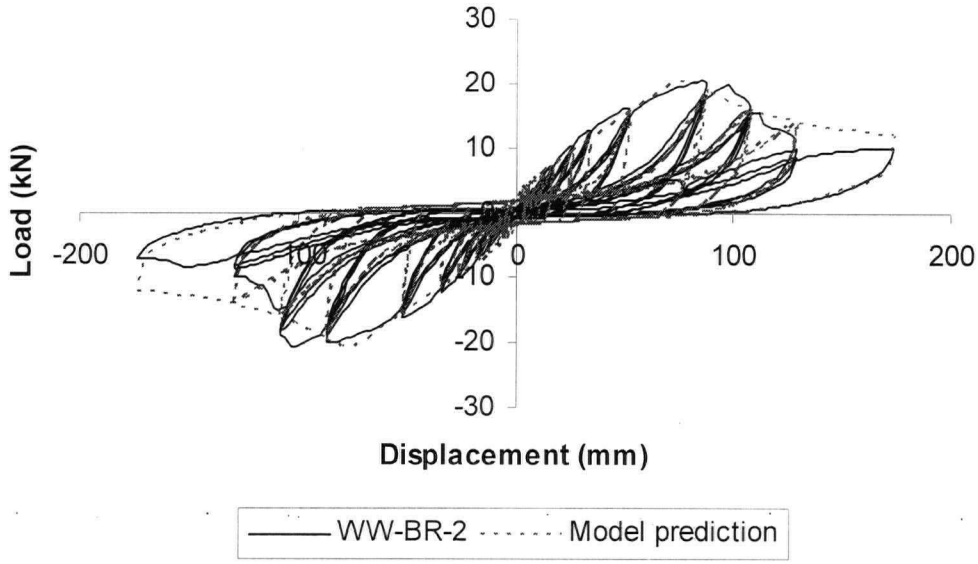

Figure 6.9 Comparison of Whitewood braced walls under cyclic load

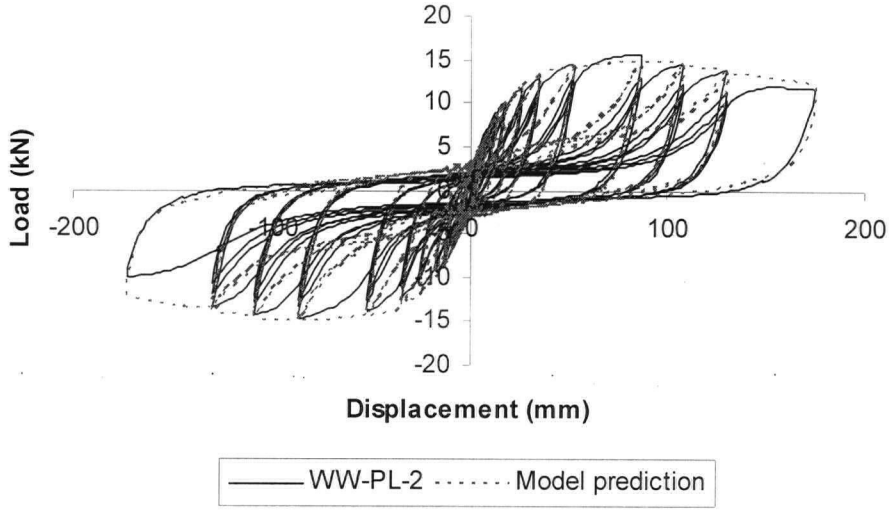

Figure 6.10 Comparison of Whitewood plywood walls under cyclic load

6.4 Seismic Performance Analysis of Japanese Walls

A set of 10 earthquake ground motion records were selected to conduct the seismic performance analysis (Table 6.3). The first seven records in Table 6.3 were recommended by the Building Center of Japan. Five of the seven records were recorded from representative earthquakes that occurred in Japan in the past. Other two records were recorded from the 1952 Kern County Earthquake and the 1940 Imperial Valley Earthquake in California. The Building Center of Japan published the set of records in 1994. Another three records was added in the analysis: the north-south component of the 1994 Northridge Earthquake recorded at Beverly Hills Station, the east-west component of the 1992 Lander Earthquake at Joshua Tree Station and the north-south component of the 1995 Kobe Earthquake recorded at Shin-Osaka Station.

Table 6.3 Ground motion records for performance analysis of Japanese walls

Event name	Year	Direction	PGA (g)	Station
Headland of Echizen	1963	EW	0.02551	Nihon Itagarasu (Osaka 205)
Northern Miyagi Prefecture	1962	EW	0.04847	Tohokudaigaku Kogakubu (Sendai 501)
-	1956	NS	0.07551	Todai Jishinkenkyujo (Tokyo 101)
Tokati	1968	EW	0.1866	Hachinohe
Kern County	1952	EW	0.1795	Taft Lincoln School Tunnel
Tohoku	1978	NS	0.2634	-
Imperial Valley	1940	EW	0.2144	El Centro Site Imperial Valley
Northridge	1994	NS	0.416	Beverly Hills- 14145 Mulhol
Lander	1992	EW	0.284	Joshua Tree Station
Kobe	1995	NS	0.243	Shin-Osaka

Nonlinear time history analysis was conducted to obtain the peak drift using the pseudo nail model with parameters given in Table 6.2. Fifteen levels of earthquake intensity (or 15 scale factors for each record) were used in the analysis. In some calculations, the nonlinear time history analysis did not converge at some high levels of intensity measure. In these cases, only 10 to 14 levels of earthquake intensity were used. The visco-damping ratio is assumed to be 1% of the critical damping with respect to the initial tangential stiffness. Three levels, 15.9%, 50% and 84.1%, of confidence curves were established from the results of peak drift demand. Three fixed gravity/dead load levels were considered: 20 kN, 30 kN and 40 kN. The results for each type of walls under three load levels are presented from Figures 6.11 to 6.34.

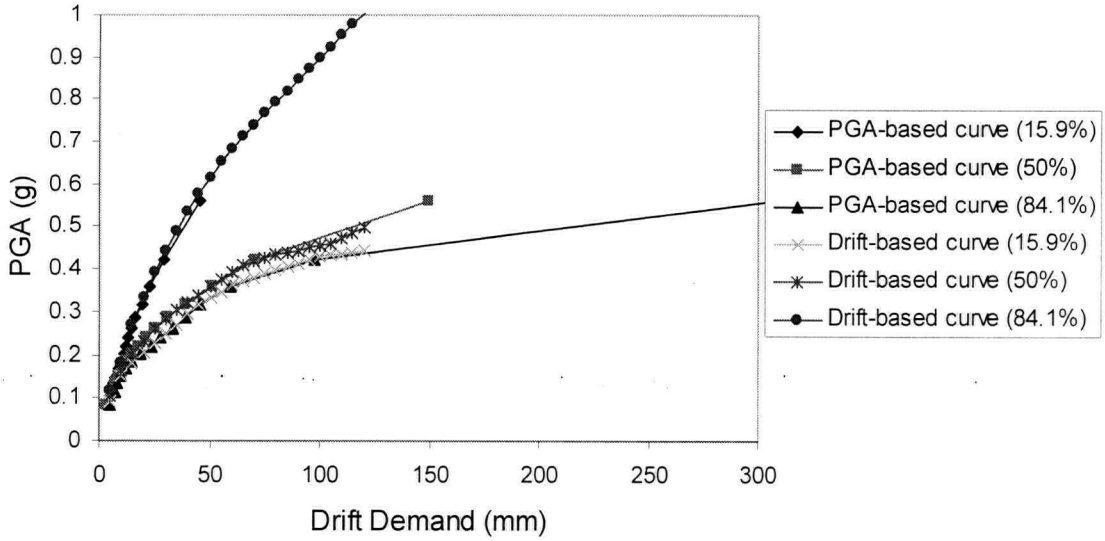

Figure 6.11 Confidence curves for Sugi braced walls (20 kN load)

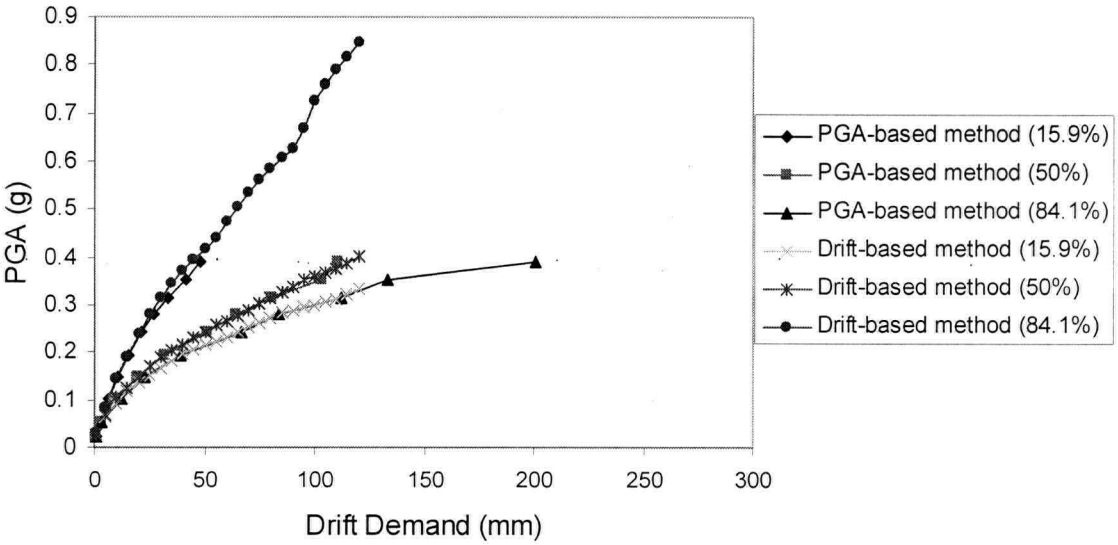

Figure 6.12 Confidence curves for Sugi braced walls (30 kN load)

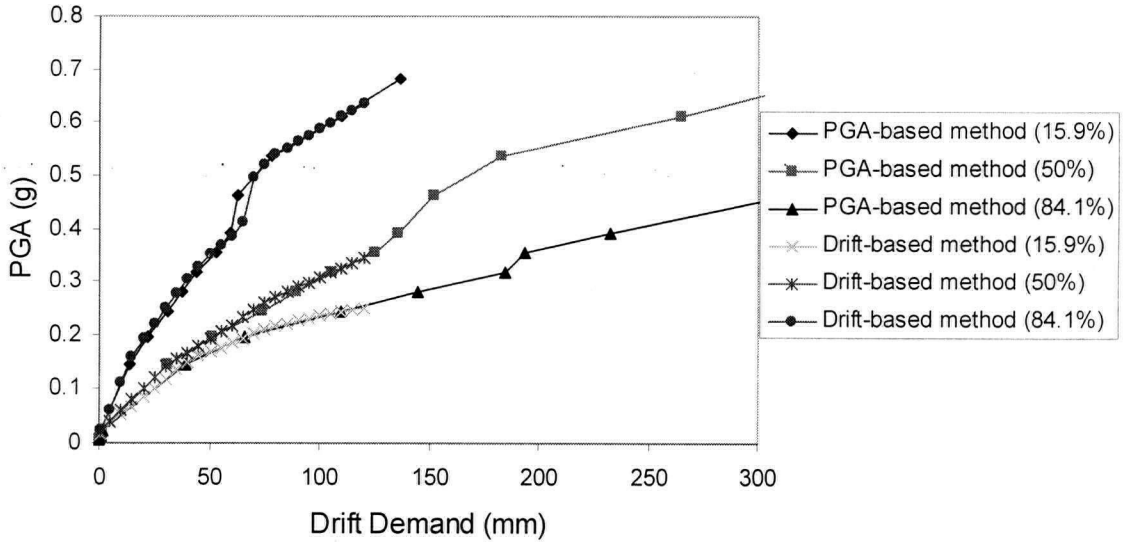

Figure 6.13 Confidence curves for Sugi braced walls (40 kN load)

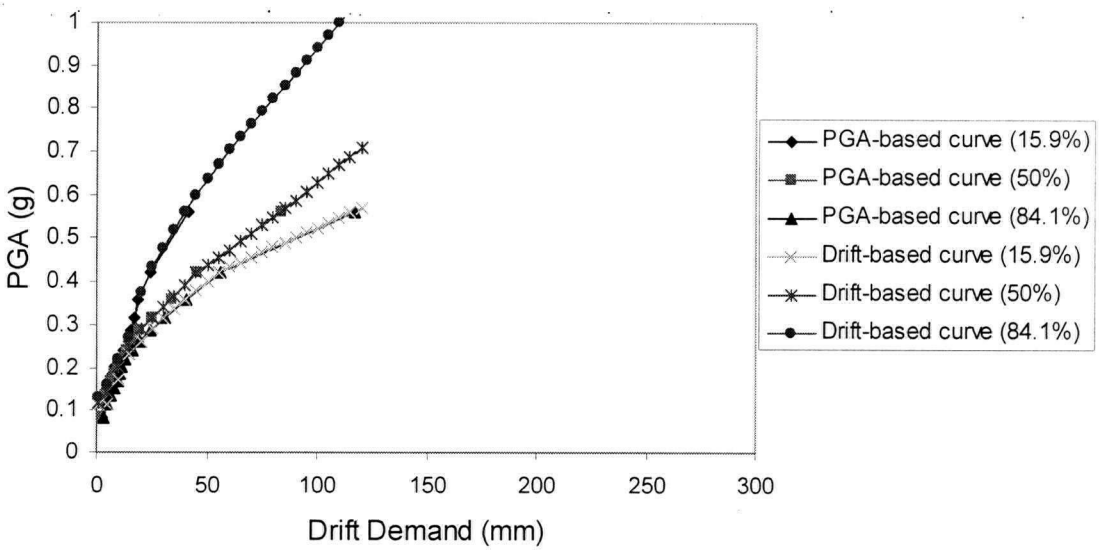

Figure 6.14 Confidence curves for Sugi plywood walls (20 kN load)

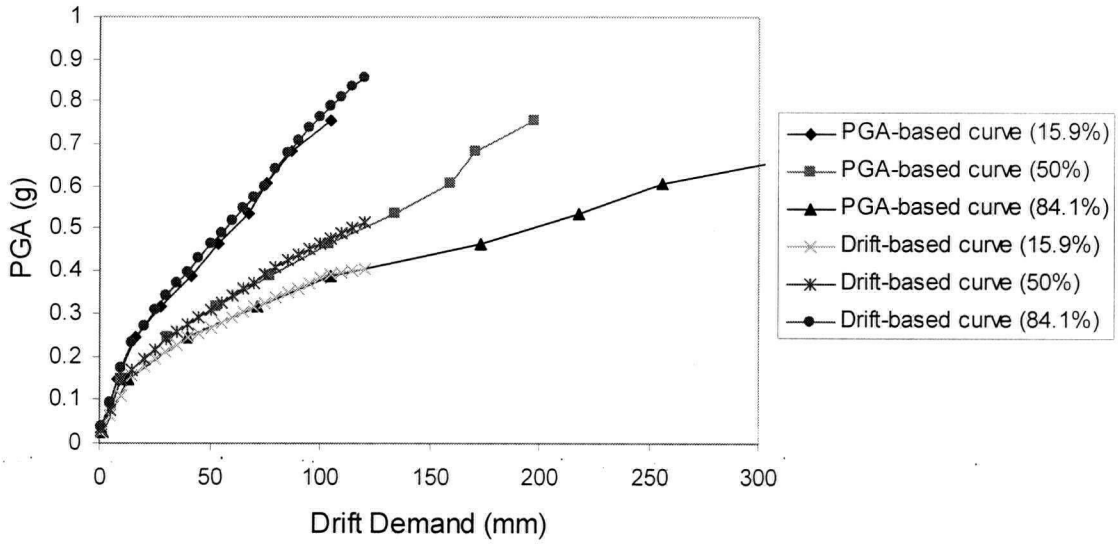

Figure 6.15 Confidence curves for Sugi plywood walls (30 kN load)

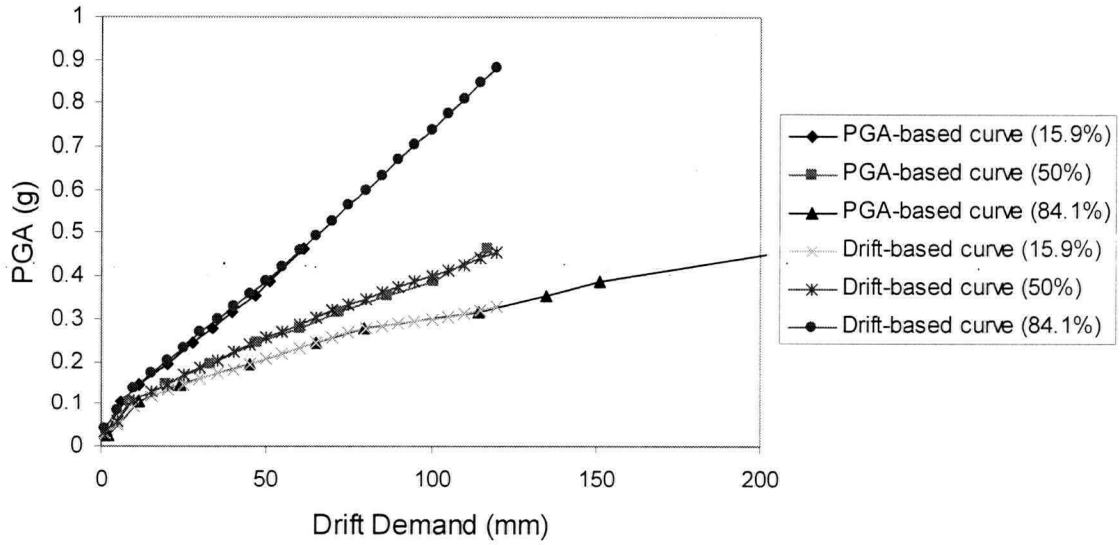

Figure 6.16 Confidence curves for Sugi plywood walls (40 kN load)

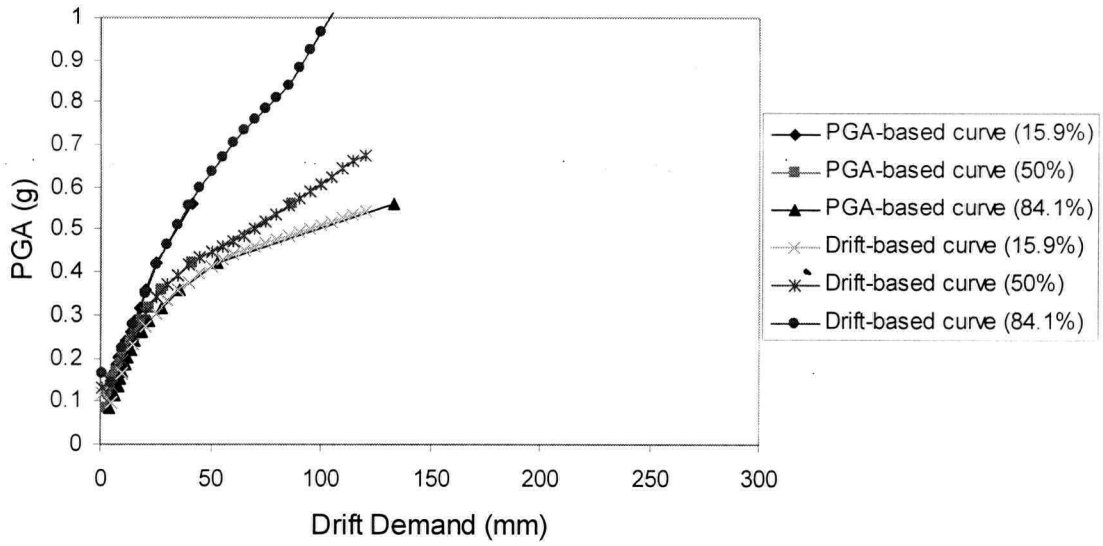

Figure 6.17 Confidence curves for Sugi OSB walls (20 kN load)

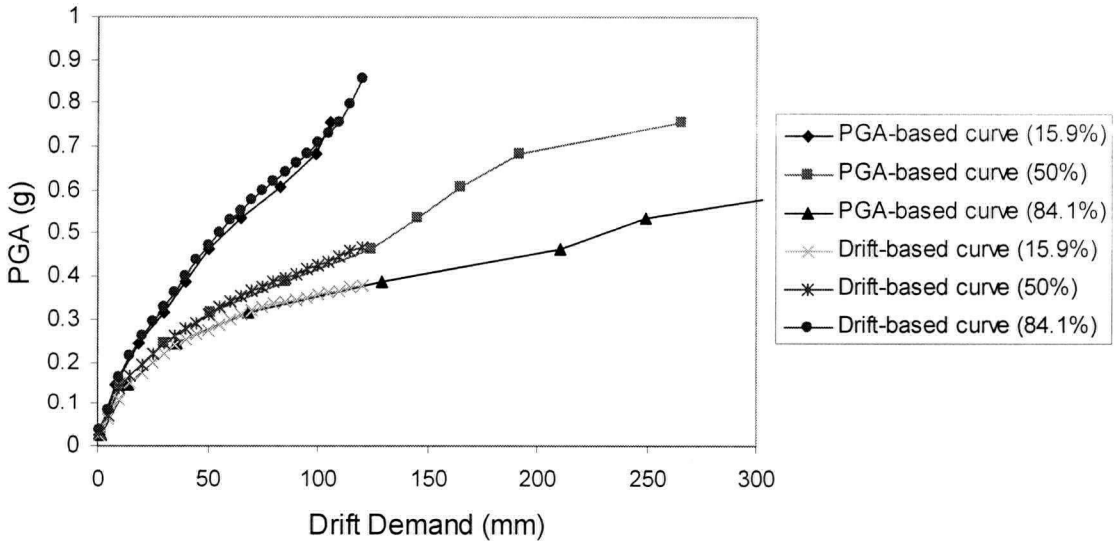

Figure 6.18 Confidence curves for Sugi OSB walls (30 kN load)

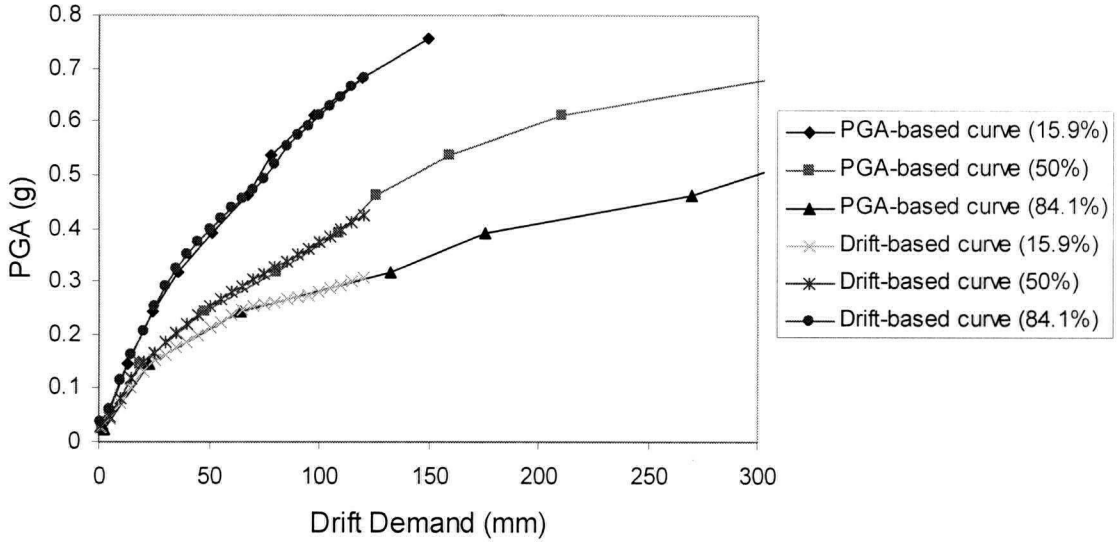

Figure 6.19 Confidence curves for Sugi OSB walls (40 kN load)

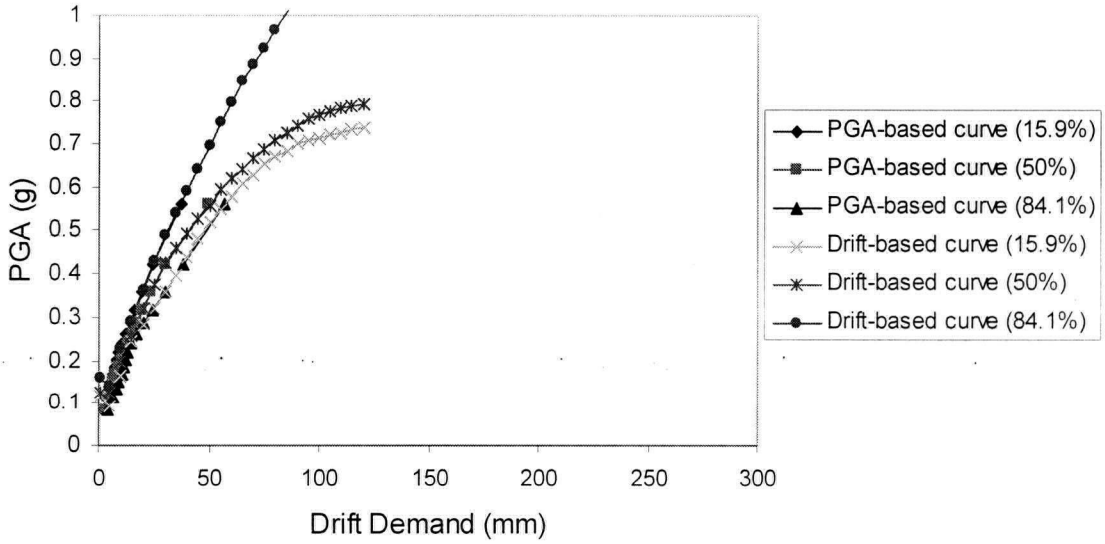

Figure 6.20 Confidence curves for Tsuga braced walls (20 kN load)

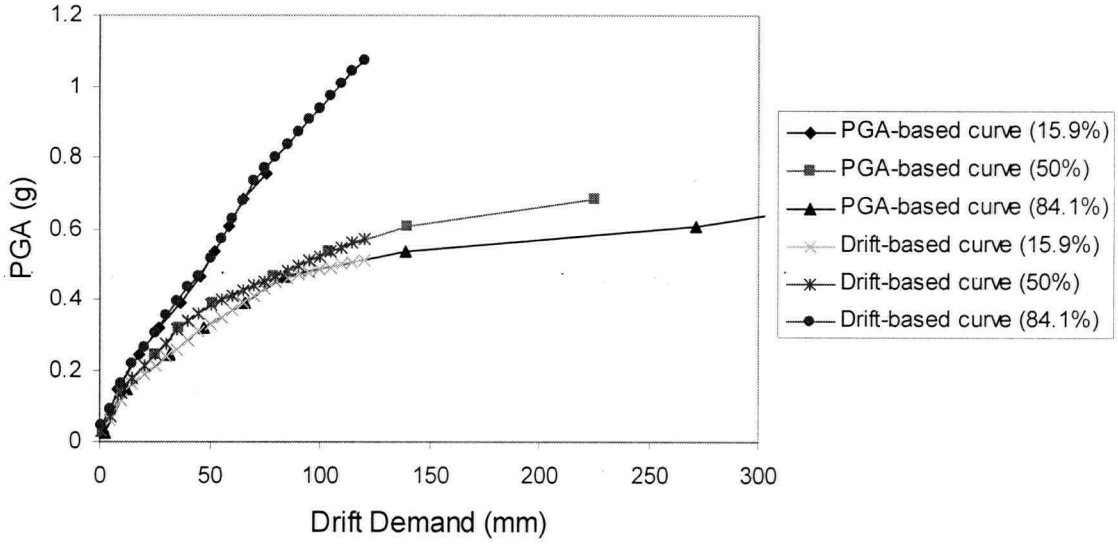

Figure 6.21 Confidence curves for Tsuga braced walls (30 kN load)

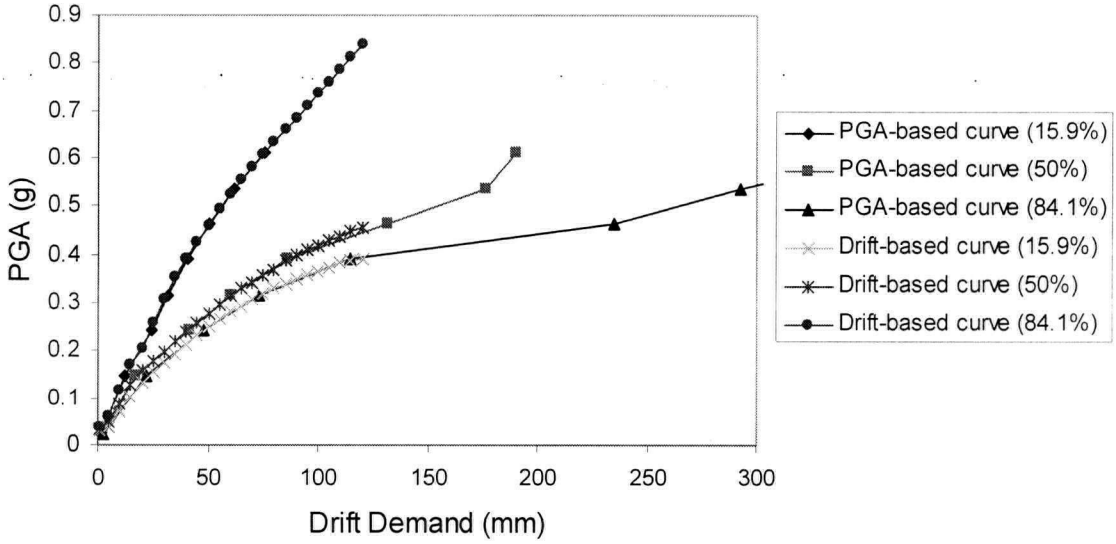

Figure 6.22 Confidence curves for Tsuga braced walls (40 kN load)

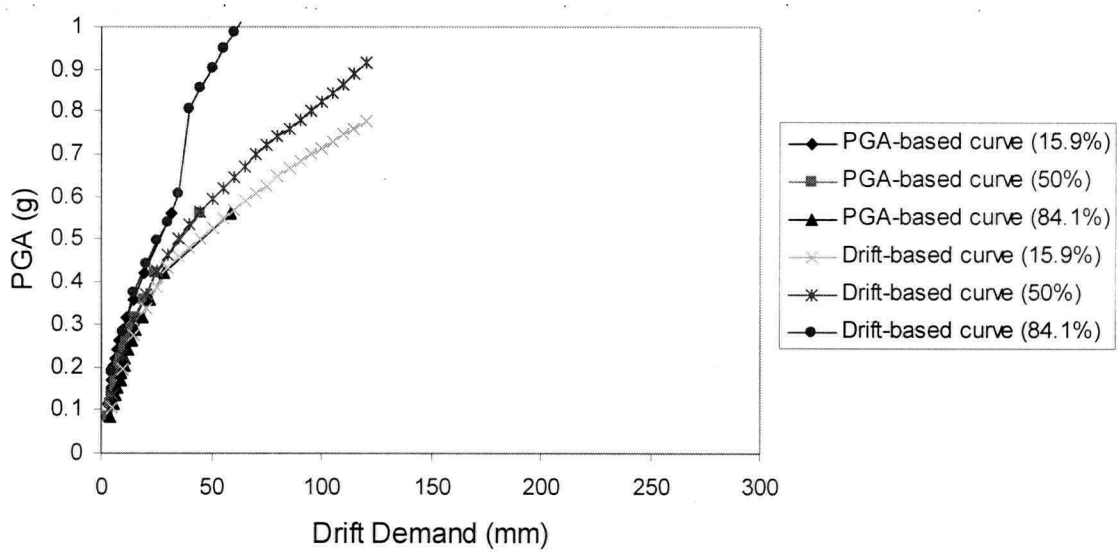

Figure 6.23 Confidence curves for Tsuga plywood walls (20 kN load)

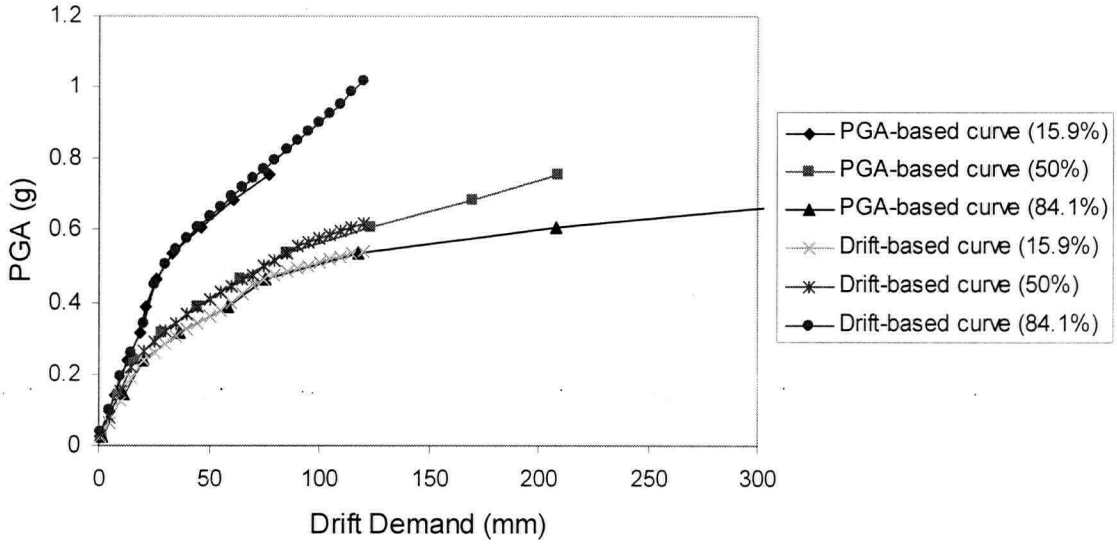

Figure 6.24 Confidence curves for Tsuga plywood walls (30 kN load)

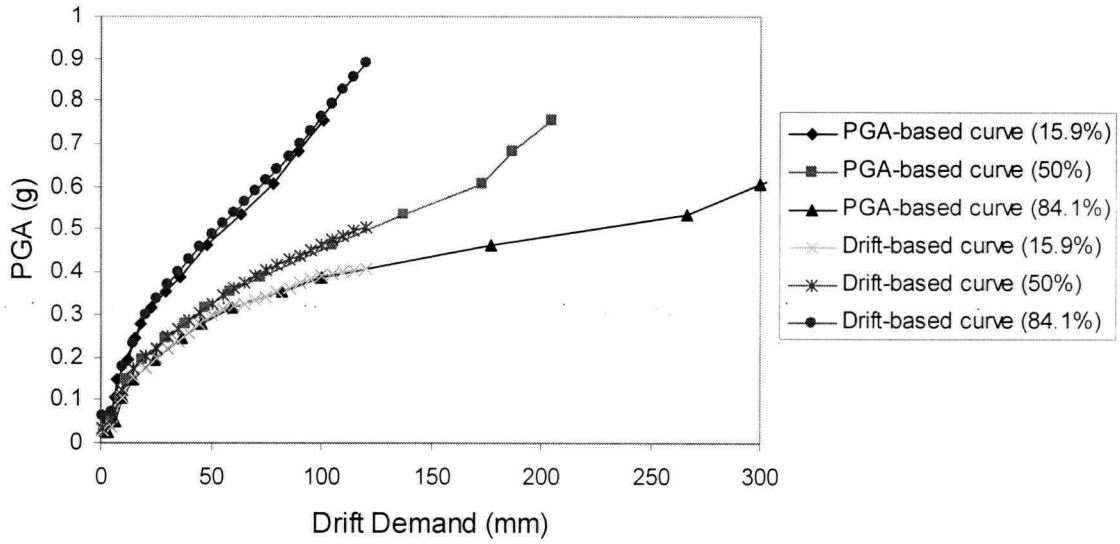

Figure 6.25 Confidence curves for Tsuga plywood walls (40 kN load)

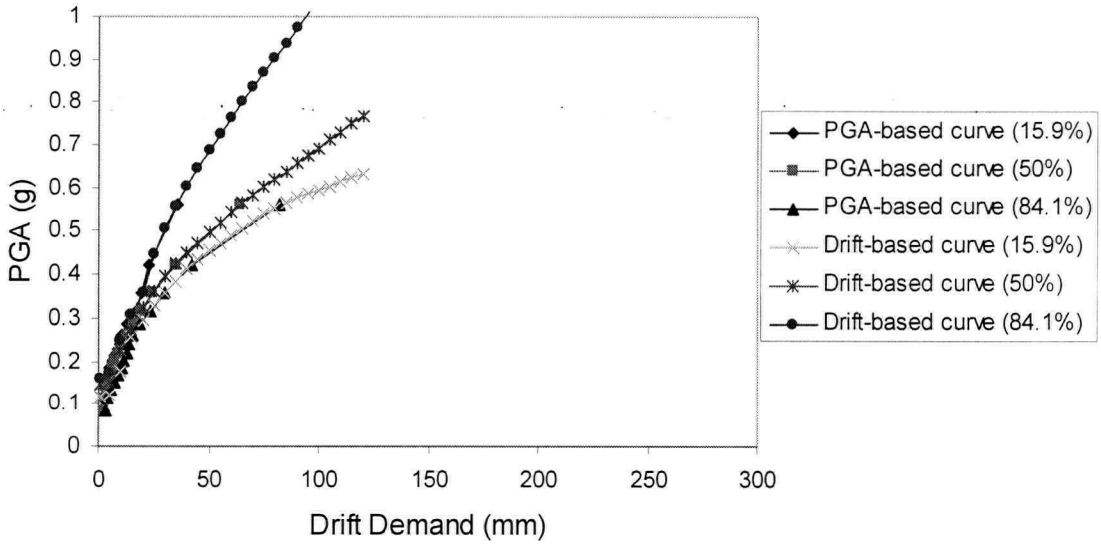

Figure 6.26 Confidence curves for Tsuga OSB walls (20 kN load)

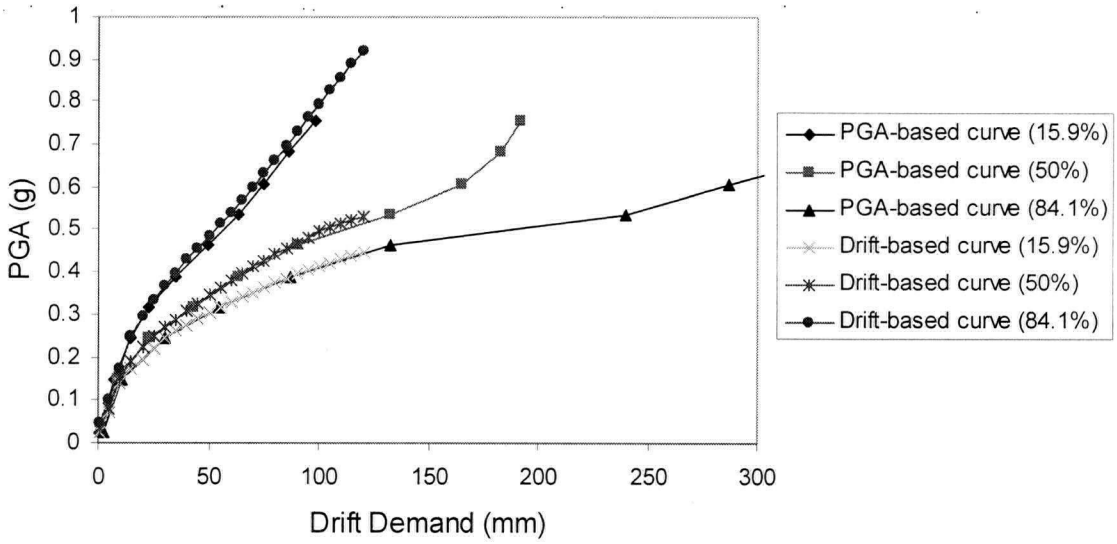

Figure 6.27 Confidence curves for Tsuga OSB walls (30 kN load)

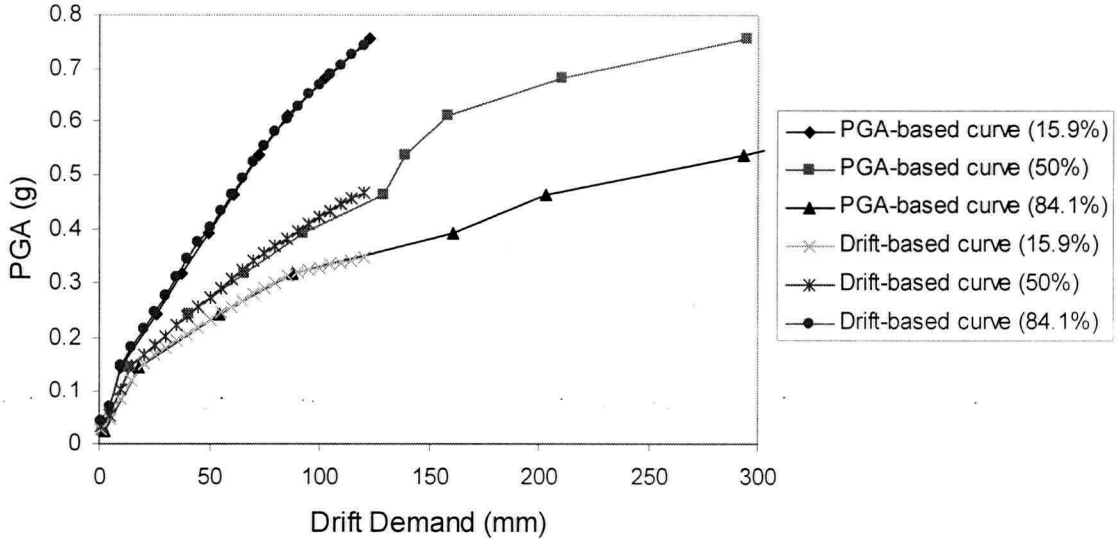

Figure 6.28 Confidence curves for Tsuga OSB walls (40 kN load)

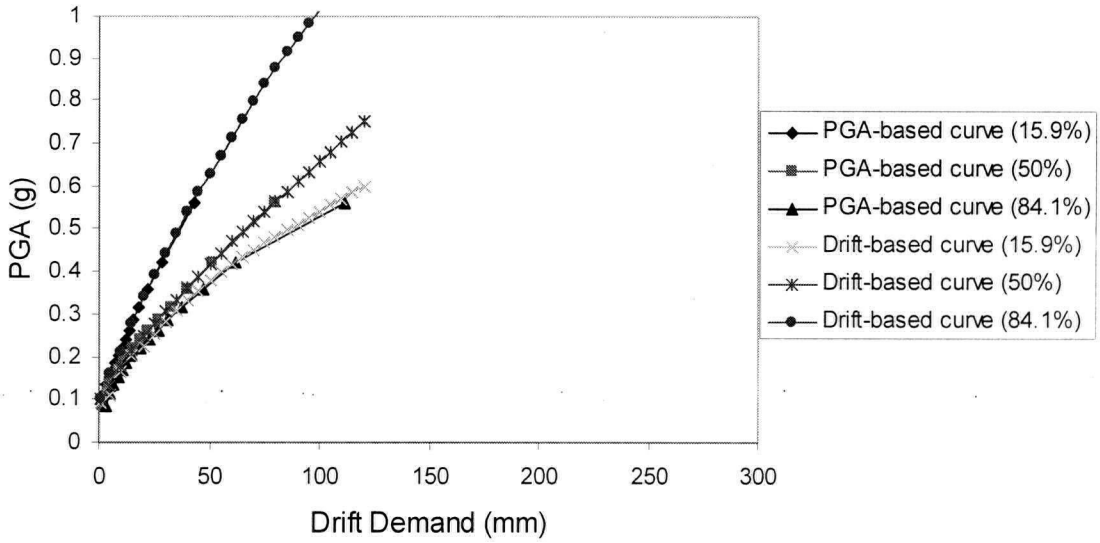

Figure 6.29 Confidence curves for Whitewood braced walls (20 kN load)

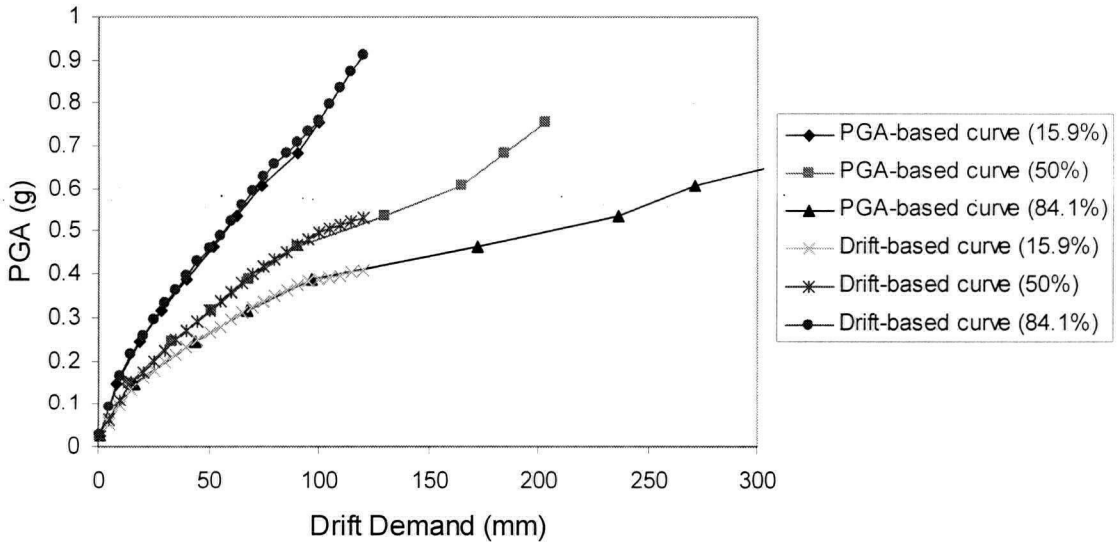

Figure 6.30 Confidence curves for Whitewood braced walls (30 kN load)

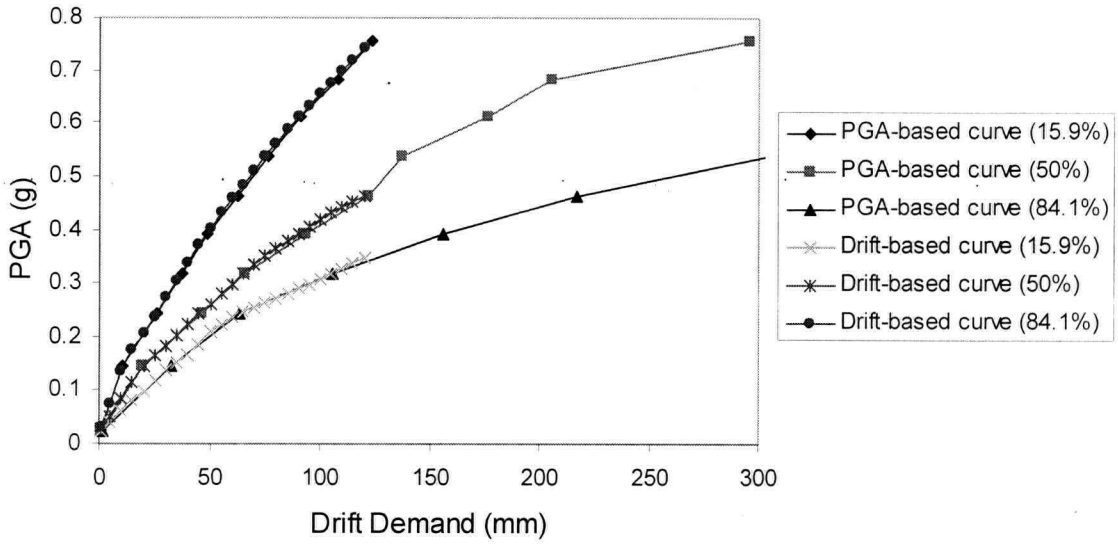

Figure 6.31 Confidence curves for Whitewood braced walls (40 kN load)

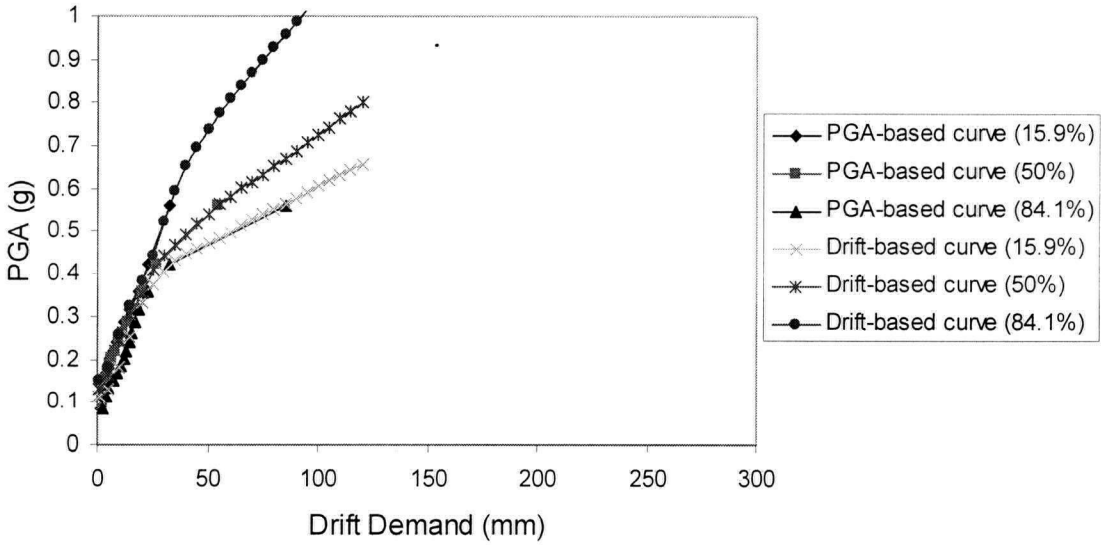

Figure 6.32 Confidence curves for Whitewood plywood walls (20 kN load)

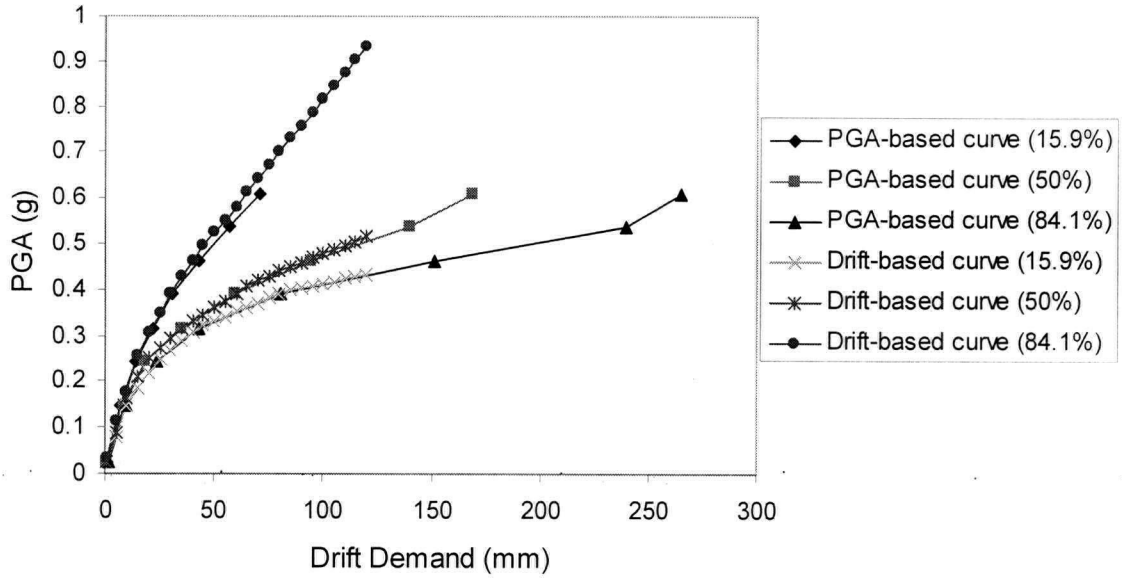

Figure 6.33 Confidence curves for Whitewood plywood walls (30 kN load)

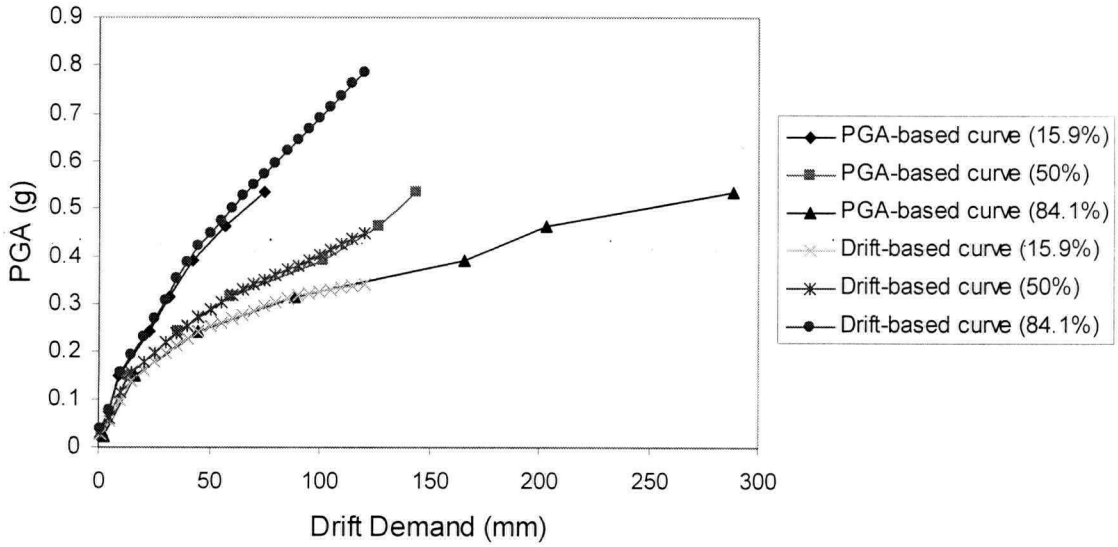

Figure 6.34 Confidence curves for Whitewood plywood walls (40 kN load)

Three methods were implemented to calculate the reliability indices of the walls. In Tables 6.4 to 6.6, "Method 1" refers to the traditional procedure (Equation 5.15). "Method 2" refers to the method based on the conditional distribution for given earthquake records (Equation 5.23) and "Method 3" refers to the Monte Carlo simulation improved by weighted ranking technique. The scaled peak ground acceleration level is assumed to follow a lognormal distribution with a mean of 0.25 g and a coefficient of variation of 0.55. According to Foschi's mapping method (Foschi 2003, Zhang and Foschi 2003), the statistics are consistent with a site design acceleration of 0.717 g (corresponding to a return period of 475 years) and a mean arrival rate of earthquakes of 0.2 (average of one every five years). This level of ground acceleration is relatively high. The drift capacity is a fixed level with a value of 68.3 mm (2.5% of wall height). The calculated reliability indices of the walls are tabulated in Table 6.4, 6.5 and 6.6 for the gravity/dead load levels of 20 kN, 30 kN and 40 kN, respectively.

Table 6.4 Reliability indices of the Japanese walls (20 kN)

Wall Type	Method 1	Method 2	Method 3
SG-BR	1.407	1.326	1.592
SG-PL	1.848	1.808	1.818
SG-OS	1.592	1.612	1.928
TG-BR	2.221	2.200	2.258
TG-PL	2.240	2.196	2.477
TG-OS	1.967	1.859	2.029
WW-BR	1.624	1.595	1.855
WW-PL	2.070	1.972	2.304

Table 6.5 Reliability indices of the Japanese walls (30 kN)

Wall Type	Method 1	Method 2	Method 3
SG-BR	0.743	0.648	0.690
SG-PL	1.088	1.040	1.129
SG-OS	1.046	1.017	1.124
TG-BR	1.464	1.410	1.545
TG-PL	1.627	1.566	1.691
TG-OS	1.264	1.219	1.629
WW-BR	1.144	1.068	1.209
WW-PL	1.326	1.305	1.474

Table 6.6 Reliability indices of the Japanese walls (40 kN)

Wall Type	Method 1	Method 2	Method 3
SG-BR	0.339	0.328	0.541
SG-PL	0.759	0.743	0.903
SG-OS	0.670	0.636	0.798
TG-BR	0.991	0.922	1.105
TG-PL	1.197	1.133	1.239
TG-OS	0.861	0.828	0.922
WW-BR	0.795	0.752	0.915
WW-PL	0.891	0.878	1.039

Table 6.7 Ratios of probability failure of the Japanese walls

Wall Type	Method 1	Method 2	Method 3
SG-BR	6.35	6.65	8.41
SG-PL	2.57	2.54	5.21
SG-OS	4.44	3.85	4.06
TG-BR	1.05	1	1.81
TG-PL	1	1.01	1
TG-OS	2.14	2.27	3.2
WW-BR	4.16	3.98	4.80
WW-PL	1.53	1.75	1.60

6.5 Comparison of Performance of Japanese Walls

The reliability indices in Tables 6.5 and 6.6 are less than 1.7, which is relatively low compared with general requirement of design codes. Higher reliability indices can be achieved through the decreasing of gravity/dead load level or design acceleration level. The 1% viscous damping coefficient used in the nonlinear time history analysis may be lower than that of real structures. Higher value of viscous damping coefficient will yield smaller drift demand and consequently bigger reliability indices. Under the load level of 20 kN, Tsuga braced walls, Tsuga plywood sheathed walls and Whitewood plywood sheathed walls have the reliability indices greater than 2.0. These three types of walls also show higher reliability indices than other types of walls at 30 kN and 40 kN load. Sugi braced walls have the lowest reliability indices.

Table 6.7 presents another format of Table 6.4. This table expresses the probability of failure in ratios relative to the minimum values of each method at the load level of 20 kN. It is clear that the Tsuga plywood sheathed walls has the lowest probability of failure

at the 2.5% drift capacity. The probabilities of failure of Tsuga braced walls, Tsgua OSB sheathed walls and Whitewood plywood sheathed walls are larger than those associated with Tsuga plywood sheathed walls by a factor between 1.0 and 2.0. The probabilities of failure of Sugi plywood sheathed walls, Sugi OSB sheathed walls and Whitewood braced walls are larger than those of Tsuga plywood sheathed walls by a factor between 2.0 and 5.0. The probabilities of failure of Sugi braced walls are larger than five times that of Tsuga plywood sheathed walls.

The reliability indices from the three methods are consistent with each other. The slight difference of the results may be explained by the difference of the three methods. Method 2 generally gives conservative results in most cases while Method 3 gives the highest values of reliability indices. All the three methods can be equally used to evaluate the structural reliability. Method 2 is recommended for future practice since it gives conservative results.

The comparison from Figures 6.10 to 6.33 shows that the results of PGA-based and Drift-based confidence curves are very similar. Only PGA-based confidence curves are used in the following comparison. 90% confidence curves were selected for the comparison although other levels of confidence curves yield similar results. The comparison of confidence curves of braced walls made from different species is given in Figure 6.35. Figures 6.36 and 6.37 illustrate the comparison of the shear walls sheathed with plywood panels and OSB panels, respectively.

The comparison of Tables 6.4, 6.5 and 6.6 and Figures 6.35, 6.36 and 6.37 shows that Canada Tsuga is superior to other two species in any type of walls. The performance of Whitewood is slightly lower than that of Tsuga.

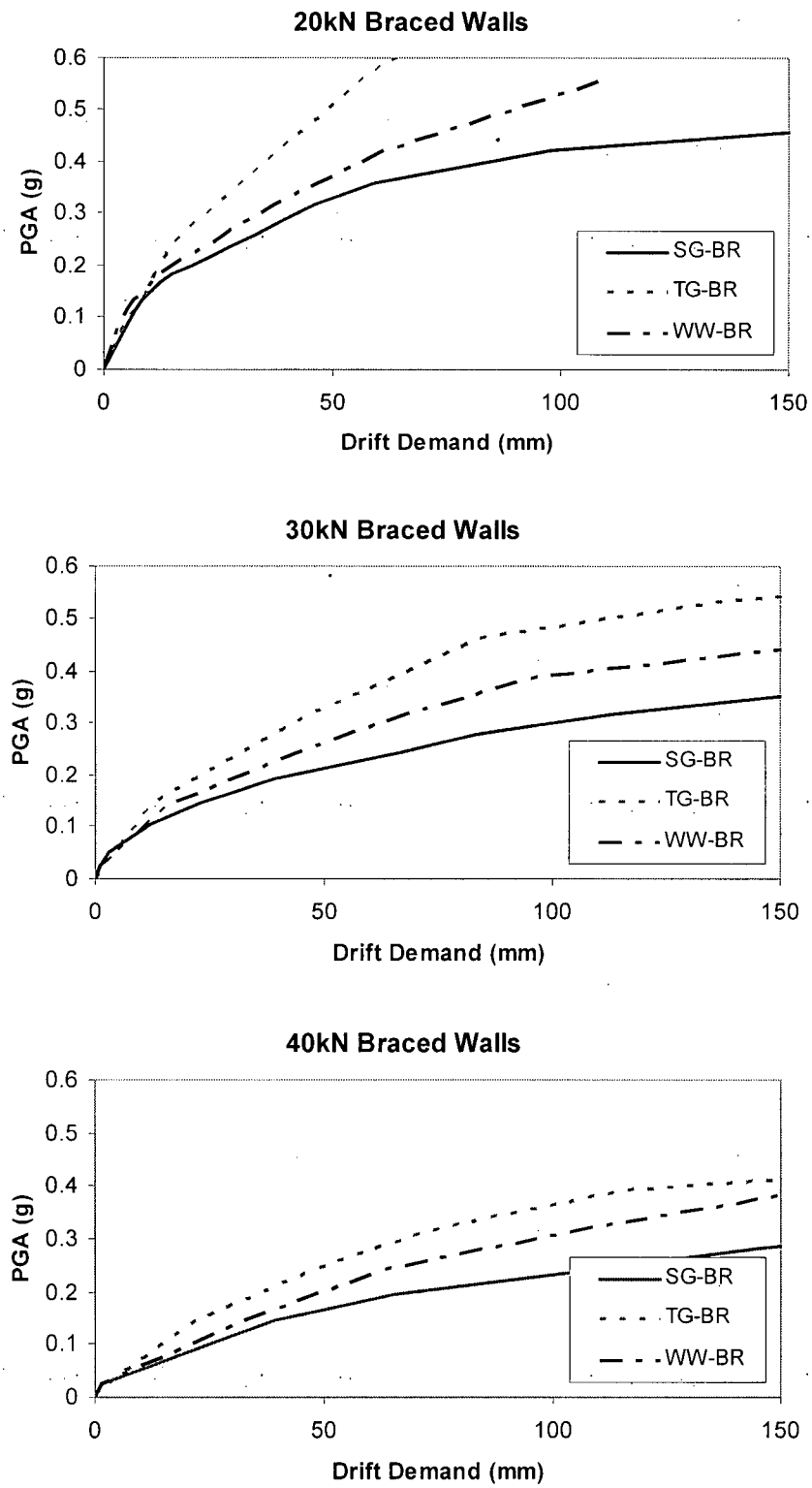

Figure 6.35 Comparison of two-brace walls under three load levels

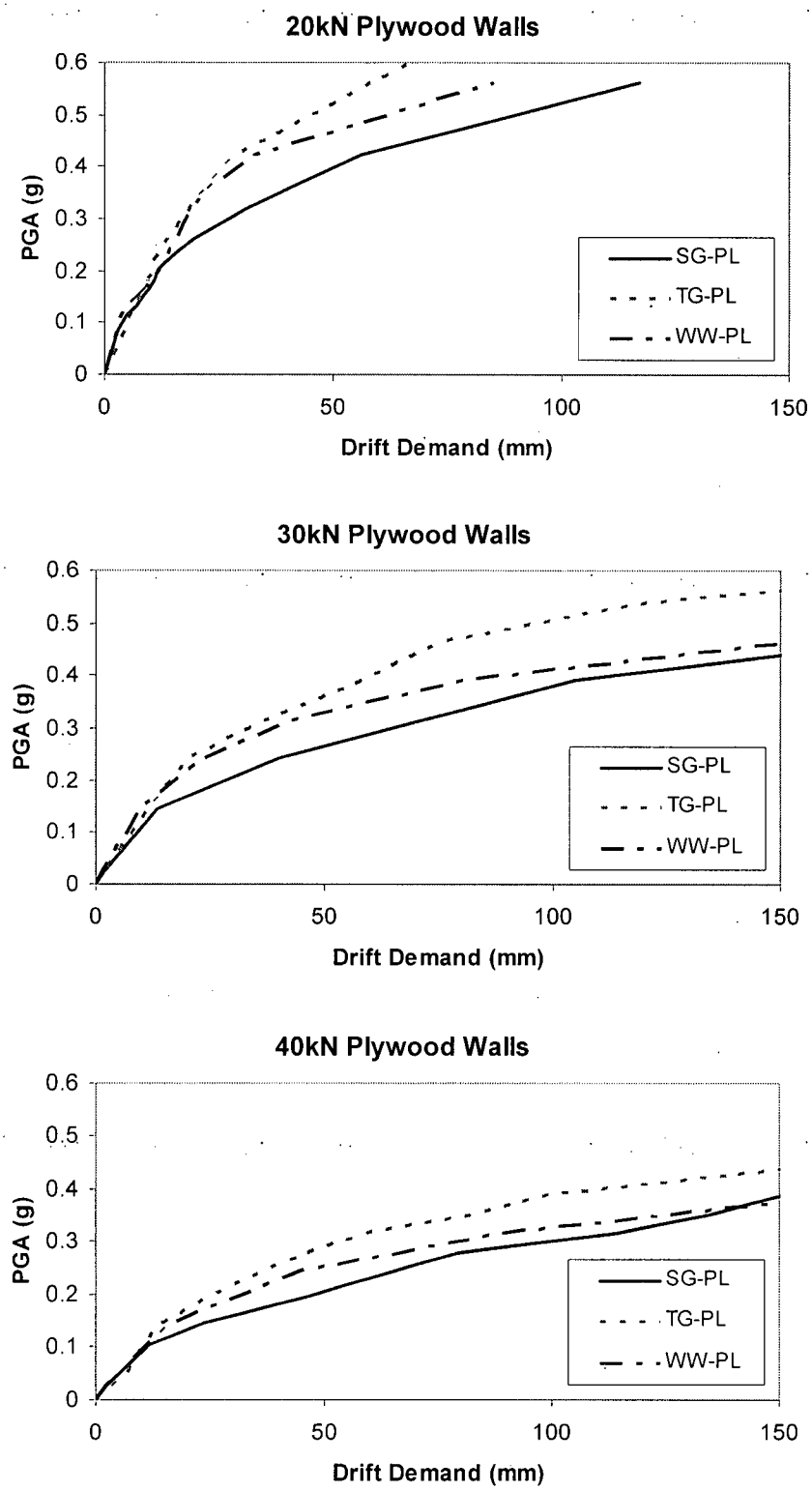

Figure 6.36 Comparison of plywood walls under three load levels

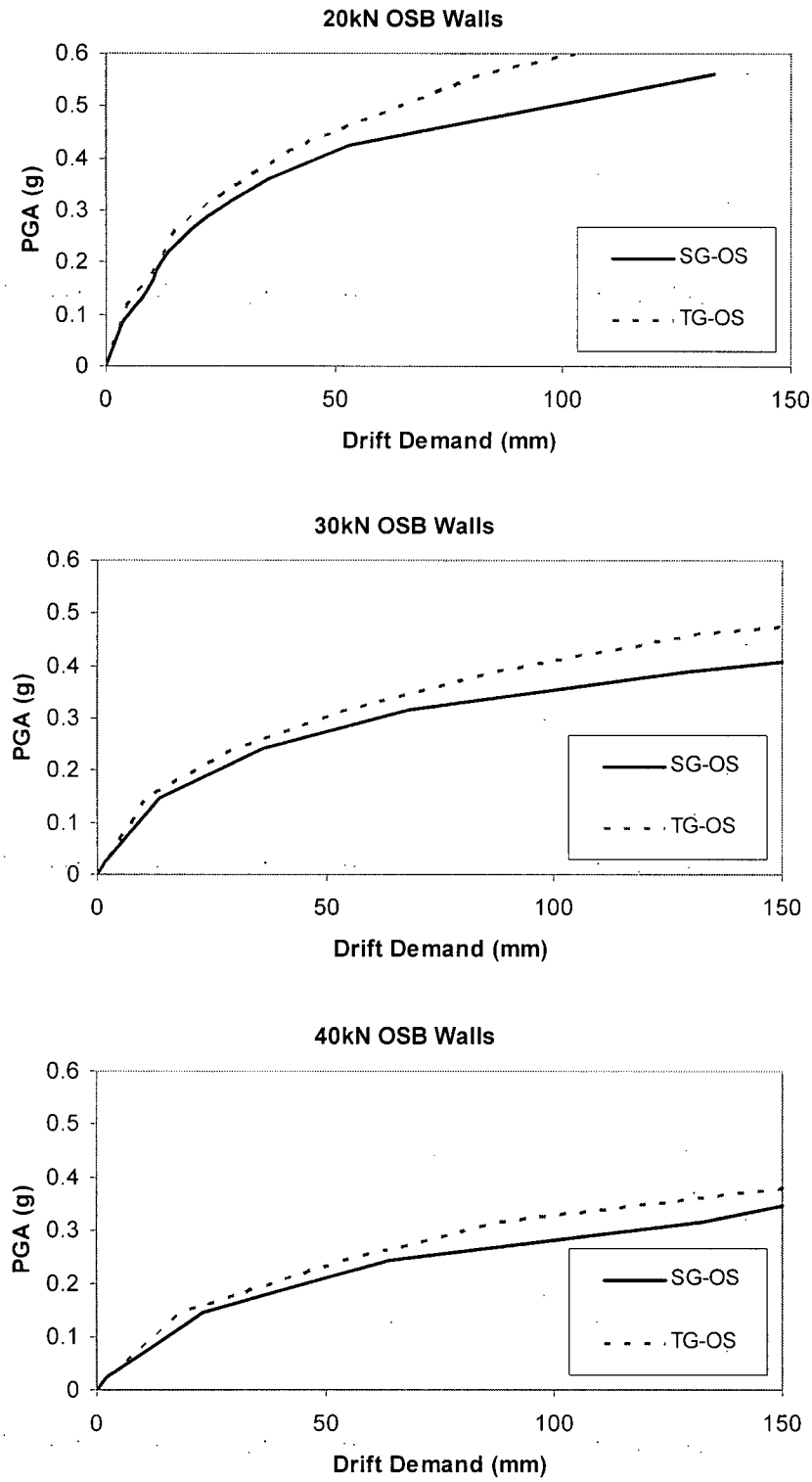

Figure 6.37 Comparison of OSB walls under three load levels

CHAPTER 7. CONCLUSIONS AND RECOMMENDATIONS

7.1 Summary of the thesis work

Seismic performance assessment in a reliability format requires two aspects of knowledge: a model to compute the dynamic response of structures and reliability analysis procedures. This thesis discusses the development of a pseudo nail model for wood shear walls and the reliability analysis procedures. An application of the analysis to Japanese wood walls is introduced.

The process of repetitive computation of nonlinear time-history analysis of wood shear walls is generally time-consuming and may represent a bottleneck to generate dynamic response of shear walls for reliability analysis. A SDOF model was developed with the characteristic load-displacement curve of shear walls simulated by the pseudo nail model. Compared with other SDOF systems, the accuracy of this model is satisfactory with improved computational efficiency over detailed FEM models.

The concept of this model originates from the similarity of the load-displacement curves of individual nail connectors and shear walls. The similarities can be explained by the mechanism of wood frame shear walls. It is well recognized that the lateral response of shear walls is governed by the characteristics of the nails connecting panels to framing members. The combined effect of all nails of a wall is superimposed together to exhibit an overall load-displacement curve for the shear wall.

Since the load-displacement curve of a shear wall is the group effect from all of the nail connectors and its shape is similar to that of the nail connectors, it is possible to represent the shear wall behavior with a pseudo nail. The process to identify the

appropriate parameters from the given load-displacement behaviour can be accomplished by a nonlinear optimization problem which minimizes the summation of square error between predicted and observed data. Five search methods were implemented to solve the optimization problem: hill climbing method, random search method, genetic algorithm, simplex method and artificial neural network. The input of the pseudo nail model requires the test results of half cyclic static loading, in which the peak displacement is recommended to be greater than that at the peak load and the load at the peak displacement should be less than 80% of the peak load.

The pseudo nail model was validated against the laboratory test results of two types of regular panel-sheathed shear walls. Good agreement was obtained between the model prediction and test results. The comparison also shows that, except for the artificial neural network, the other four search methods succeeded in identifying the parameters in the optimization problem.

Seismic reliability analysis involves two types of earthquake ground shaking hazard: earthquake intensity measure and ground motion records. Since the drift demand is a function of earthquake intensity measure and records, the distribution of drift demand relates to both intensity and records. A popular format of reliability procedure based on conditional distribution at given earthquake intensity is discussed. Then a new format based on conditional distribution at given earthquake records is proposed. Another method, the weighted ranking technique, is also proposed to improve the efficiency of the classical Quasi Monte Carlo simulation process. Instead of equal spacing of samples used in the classical Monte Carlo simulation method, this method calculates the incremental cumulative probability as the spacing to rank samples.

Construction of confidence curves is presented to simplify the two-dimensional distribution of drift demand. The confidence curves are established from the conditional distribution of drift demand given intensity or drift demand. They can be employed to compare the performance of structures made with different materials under different earthquake intensity levels.

Eight types of Japanese walls were analyzed with the pseudo nail model. These walls consisted of three species: Japanese Sugi, Canadian Tsuga and European Whitewood, and two structural types: two-brace walls and panel-sheathed walls. From the comparison of confidence curves and reliability indices of the walls, it is shown that the seismic performance of Canadian Tsuga walls is superior to that of other species, and the performance of panel-sheathed walls seems better than that of braced walls.

7.2 Conclusions

The developed pseudo nail model is a SDOF system to simulate the dynamic behaviour of wood shear walls. This model was verified with laboratory tests under cyclic load and dynamic load, which results shows that it can successfully predict the dynamic behaviour under earthquake load. The examples show that this model is computationally efficient and accurate; therefore it is suitable for earthquake reliability analysis.

Two new procedures were developed to perform the earthquake reliability analysis. The first one is established on conditional distribution at given earthquake records. The second one is based on Monte Carlo method with weight ranking technique to improve the efficiency for seismic reliability analysis.

Both the pseudo nail model and the earthquake reliability procedures were used to analyze and compare the reliability indices of Japanese walls under earthquake load. The results can be used for engineering practice and to guide the modification of building codes.

7.3 Recommendations for Future Work

The developed pseudo nail model is a nonlinear spring to calculate the response of a shear wall. To evaluate the response of structures, multiple springs can be placed on all sides of walls to form a one-storey model. Furthermore, multiple-storey models can be established to study the seismic performance of whole structures. A preliminary study of such a model shows encouraging results (Lam 2005).

The computation efficiency of the searching process to identify the parameters of the pseudo nail model is to be further improved. The execution of FEM subroutines is very suitable for parallel computation, especially with the distributed systems through the Internet which connects multiple personal computers together. To achieve that, a set of interface programs following communication protocols, such as TCP/IP, is to be developed.

Over the past years, many dynamic models were developed to analyze seismic performance of wood walls. These models have different computational efficiency and accuracy. Compared with the uncertainties of materials and modeling, the earthquake hazard has high uncertainty. For example, the coefficient of variation of earthquake intensity could be as high as 50%. Whether the accuracy of models is important to the results of reliability analysis is to be studied in the future.

Earthquake ground shaking is not the only source of uncertainty of reliability analysis. The wood and joint properties, geometry miscellaneous, construction error, load condition and other variables contribute significantly to the performance of structures. To improve the efficiency, the reliability of structures under multiple variables can be solved with some other tools, such as RELAN with the implementation of the artificial neural network (Zhang and Foschi 2003).

BIBLIOGRAPHY

Andreasson, S., Yasumura, M., and Daudeville, L. (2002). "Sensitivity study of the finite element model for wood-framed shear walls". Journal of Wood Science, 48(3), 171-178.

Baber, T.T. and Wen, Y.K. (1981). "Random vibration of hysteretic degrading systems." ASCE Journal of Engineering Mechanics Division, 107(EM6), 1069-1089.

Baber, T.T. and Noori, M.N. (1986). "Random vibration of degrading pinching systems" ASCE Journal of Engineering Mechanics, 111(8), 1010-1025.

Bathe, K.J. (1996). Finite Element Procedures. Prentice Hall, NJ.

Bouc, R. (1967). "Forced vibration of mechanical systems with hysteresis", abstract. Proceedings of Fourth Conference on Nonlinear Oscillation, Praque, Czechoslovakis.

Building and Fire Research Laboratory (BFRL). (1998). "A summary of the Structural Performance of Single-Family, wood-Frame Housing." NISTIR 6224, United States Department of Commerce, Sept. Gaithersburg, MD.

Bolc, L. and Cytowaki, J. (1992). Search Methods for Artificial Intelligence. Academic Press Inc. San Diego, CA.

Carney, J. M. (1975). ''Bibliography on wood and plywood diaphragms''. ASCE Journal of Structural Division, 101(11): 2423–2436.

Ceccotti, A. and Foschi, R. O. (1998), "Reliability assessment of wood shear walls under earthquake excitation." Proceedings of Third International Conference on Computational Stochastic Mechanics, Thera-Santorini, Greece, 311-317.

Ceccotti, A. and Karacabeyli, E. (2002). "Validation of seismic design parameters for wood-frame shearwall systems." Canadian Journal of Civil Engineering, National Research Council of Canada, 29(3), 484-498.

Ceccotti, A. and Vignoli, A. (1990). "Engineered timber structures: an evaluation of their seismic behavior." Proceedings of 1990 International Timber Engineering Conference, 946-953, Tokyo, Japan.

Center For Better Living Japan (2001). "In-plane Shear Test of Traditional P&B Load Bearing Walls and Single-plane Shear Test of Nailed Joints". Technical report No.012630, Center for Better Living, Tokyo, Japan.

Charbonneau P. (2003) "Subroutine PIKAIA." http://www.hao.ucar.edu/public/research/si/pikaia/pikaia.html. Université de Montréal. Last updated on April 28, 2003. Visited on September 6, 2003.

Cheung, C.K., Itani, R.Y. and Polensek, A (1988). "Characteristics of wood diaphragms: experimental and parametric studies." Wood and Fiber Science, The Society of Wood Science and Technology, 20(4), 438-456.

Chopra A.K., (2001). Dynamics of Structures: Theory and Applications to Earthquake Engineering, 229, Prentice Hall, NJ.

Cornell, C.A., Jalayer F., Hamburger R.O. and Foutch, D.A. (2002). "Probabilistic basis for 2000 SAC Federal Emergency Management Agency steel moment frame guidelines." ASCE Journal of Structural Engineering, 128 (4): 526-533.

Diekmann, E.F. (1997). "Design and code issues in the design of diaphragms and shearwalls." Earthquake Performance and Safety of Timber Structures, 36-43., Forest Products Society, MA.

Dinehart, D.W. and Shenton III, H.W. (2000). "Model for dynamic analysis of wood frame shear walls." ASCE Journal of Engineering Mechanics, 128(9), 899-908.

Dolan, J.D. (1989). "The dynamic response of timber shear walls." Ph.D thesis, University of British Columbia, Vancouver, BC.

Durham, J. (1998). "Seismic response of wood shearwalls with oversized oriented strand board panels." M.A.Sc thesis, University of British Columbia, Vancouver, BC.

Durham, J. (1999). "Jennifer Durham Masters thesis File Directory". Attachment to master thesis, University of British Columbia. Vancouver, BC.

Durham J., Lam F., Prion H.G.L. (2001). "Seismic resistance of wood shear walls with large OSB panels." ASCE Journal of Structural Engineering, 127(12), 1460-1466

Easley, J.T., Foomani, Mehdi and Dodds, R. H.(1982). "Formulas for wood shear walls.", ASCE Journal of the Structural Division, 108(ST 11), 2460-2478.

Ellingwood, B. R., Rosowsky, D. V., Li, Y. and Kim, J. H. (2004). "Fragility assessment of light-frame wood construction subjected to wind and earthquake hazards". ASCE Journal of Structural Engineering, 130(12): 1921-1930

Ewing, R.D., Healey, T.J. and Agbabian, M.S. (1980). "Seismic analysis of wood diaphragms in masory buildings." Proceedings of the workshop on design of Horizontal Wood Diaphragms, Applied Technology Council, Berkeley, CA: 253-276.

Federal Emergency Management Agency (FEMA). (1997). "NEHRP Guidelines for the seismic rehabilitation of buildings." Federal Emergency Management Agency, No. 273, Washington, DC.

Filiatrault, A. (1990). "Static and dynamic analysis of timber shear walls." Canadian Journal of Civil Engineering, 17(4), 1990: 643-651

Filiatrault, A. and Folz, B. (2002). "Performance-based Seismic Design of Wood Framed Buildings." ASCE Journal of Structural Engineering, 128(1), 39-47.

Foliente, G.C. (1993). "Stochastic Dynamic Response of Wood Structural Systems." Ph.D thesis, Virginia Polytechnic Institute and State University, Blacksburg, VI.

Foliente, G.C. (1997). "Timber structures in seismic regions: General overview and research needs." Earthquake Performance and Safety of Timber Structures. Ed.: Foliente, G.C., Forest Products Society, 3-23, MA.

Foliente, G.C., Phillip, P., Taiki, S. and Naohito, K. (2000). Seismic capacity rating and reliability assessment of wood shear walls. Proceedings of World Conference in Timber Engineering, Whistler, BC.

Folz, B., and Filiatrault, A. (2001). "Cyclic analysis of wood shear walls." ASCE Journal of Structural Engineering, 127(4), 433–441.

Foschi, R. O. (1977). "Analysis of wood diaphragms and trusses. Part I: Diaphragms." Canadian Journal of Civil Engineering. 4(3), 345-352.

Foschi, R. O. (1990). "Diaphragm analysis program-user's manual (Version 1.1)." Univ. of British Columbia, BC.

Foschi, R. O. (2000). "Modeling the hysteretic response of mechanical connections for wood structures." Proceedings of World Conference in Timber Engineering, Whistler, BC.

Foschi, R. O. (2003). "Estimating Reliability and Implementing Performance-Based Design for Shear Walls." ASCE Structures Congress, June, Seattle, WA.

Foschi, R. O. (2004). "Modeling the structural behaviour, reliability and performance of Japanese post and beam walls", research report, University of British Columbia, Vancouver, BC.

Foschi, R. O., Folz, B. and Yao, F. (1988). RELAN-User Manual. Department of Civil Engineering, University of British Columbia, Vancouver, BC.

Foschi, R. O, Li, H. and Zhang, J. (2002). "Reliability and performance-based design: a computational approach and applications." Structural Safety, 24(2-4), 205-218

Goldberd, D., (1989). Genetic Algorithms in Search, Optimization, and Machine Learning. Addison-Wesley Publishing Company, Inc., Don Mills, ON.

Gupta, A.K., Kuo, G.P. (1985). "Behavior of wood-framed shear walls." Journal of Structural Engineering, ASCE, 111(8), 1722-1733.

Gupta, A.K., Kuo, G.P. (1987). "Wood-Framed shear walls with uplifting." Journal of Structural Engineering, ASCE, 113(2), 241-259.

Hagan, M.T., Demuth, H. B. and Beale, M. (1995). Neural Network Design. PWS Publishing Company. Boston. MA.

Hampson, J.A., Prion, H.G.L. and Lam F. (2003). "The effect of end distance on the moment resistance of timber rivet connections". Canadian Journal of Civil engineering, 30(5), 945-948.

Hayashi K. (1988). "Studies on methods to estimate the racking resistance of houses with wooden wall panel sheathing (Part 1 experimental study)". Proceedings of the 1988 International Conference on Timber Engineering. Vol. 1, 774-783. Seattle, WA.

Hirashima, Y. (1988). "Analysis of observed earthquake response of post-and-beam wood structure". Proceedings of the 1988 International Conference on Timber Engineering. 235-242, R. Y. Seattle, WA.

He, M., Magnusson, H., Lam, F. and Prion, H.G.L. (1999). "Cyclic performance of perforated wood shear walls with oversize OSB panels." Journal of Structural Engineering, ASCE, 125(1):10-18.

He, M. (2002). "Numerical modeling of three-dimensional light wood-framed buildings." Ph.D thesis, Univ. of British Columbia, Vancouver, BC.

Houbolt, J. C. (1950). "A recurrence matrix solution for the dynamic response of elastic aircraft". Journal of the Aeronautical Sciences, 17, 540-550.

Itani, R.Y., Tuomi, R.L. and McCutcheon, W.J. (1982). "Methodology to evaluate racking resistance of nailed walls." Forest Product Journal, 32(1), 30-36.

Itani, R.Y. and Cheung, C.L. (1984). "Nonlinear analysis of sheathed wood diaphragms." Journal of Structural Engineering, ASCE, 110(9), 2137-2147.

Japan Housing and Wood Technology Center. (1996). "Design technology of joints of wooden post and beam structures." Japan Housing and Wood technology Center.

Jossen, D. (2003). Earthquake resistant connections for the Japanese post-and-beam wall construction. Master thesis. Swiss University of Applied Science. Biel, Switzerland.

Kakaoka, Y. and Asano, K. (1988). "The lateral behaviour of frame structures stiffened by shear diaphragms". Proceedings of the 1988 International Conference on Timber Engineering. Vol 1, 784-793, Seattle, WA.

Källsner, B. (1984). "Panels as wind-bracing elements in timber-framed walls". Report 56. Swedish Institute for Wood Technology Research, Stockholm, Sweden.

Källsner, B. and Lam, F. (1995). "Diaphragms and shear walls." Holzbauwerke Nach Eurocode 5 Grundlagen Entwichlungen Ergänzungen Step 3, Informationsdientst Holz, Düsseldorf, Germany.

Kamiya, F. (1988). "Nonlinear earthquake response analysis of sheathed wood walls by a computer actuator on-line systems." Proceedings of the 1988 International Conference on Timber Engineering, Vol. 1, 838-847, Seattle, WA.

Karacabeyli, E., and Ceccotti, A. (1996). ''Test results on the lateral resistance of nailed shear walls.'' Proceedings of the International Wood Engineering Conference, Vol. 2, New Orleans, LO. 179–186.

Kasal, B. and Leichti, R.J. (1992a). "Nonlinear finite-element model for light –frame stud walls." Journal of Structural Engineering, 118(11), 3122-3135.

Kasal, B. and Leichti, R.J. (1992b). "Incorporating load sharing in shear wall design of light-frame structures." Journal of Structural Engineering, 118(12), 3350-3361.

Kawai, N. (1998). "Seismic performance testing on wood framed shear wall". Proceedings of International council for building research studies and documentation working commission CIB-W18A Timber structures. Savonlinna, Finland.

Krawinkler, H., Parisi, F., Ibarra, L., Ayoub, A., and Medina, R. (2001). "Development of a testing protocol for woodframe structures". CUREE Publication No. W-02, Richmond, CA.

Kawai, N. (1998). "Pseudo dynamic tests on shear walls.'' Proceedings of the 5th World Conference on Timber Engineering, 412–419. Montreux, Switzerland.

Kivell, B.T., Moss, P.J., Carr, A.J. (1981). "Hysteretic modeling of moment resisting nailed timber joints." Bulletin of New Zealand National Society for Earthquake Engineering, 14(4), 233-243.

Lam, F. (2005). "Structural performance of Japanese post and beam building". Technical report, Univ. of British Columbia, Vancouver, BC.

Lam ,F and Foschi, R (2003). "Computer Model – Structural Performance of Japanese Post and Beam Walls". Technical report, Univ. of British Columbia, Vancouver, BC.

Lam, F., Prion, H.G.L. and He, M. (1997). "Lateral resistance of wood shear walls with large sheathing panels." Journal of Structural Engineering, ASCE, 123 (12), 1666-1673.

Li, H. and Foschi, R. O. (1998). "An inverse reliability method and its application." Structural Safety. 20, 257-270.

Li, Y. and Ellingwood, B.R. (2004). "Assessment of Wood Residential Construction Subjected to Earthquakes". Proceedings of 13th World Conference on Earthquake Engineering. Paper No. 2537, Vancouver, BC.

McCutcheon, W.J. (1985). "Racking Deformations in Wood Shear Walls." Journal of Structural Engineering. ASCE, 111(2), 257-269.

Michalewicz, Z. (1996). Genetic Algorithm + Data Structure = Evolution Programs. 3rd rev. Springer-Verlag, NY.

National Research Council. (NRC, 1995). "National Building Code of Canada." National Research Council, Ottawa, ON.

Nelder, J.A. and Mead, R. (1965). "A simplex method for function minimization." Computer Journal, 7, 308-313.

Newmark, N. M. (1959). "A method of computation for structural dynamics". Transactions of America Society of Civil Engineers, ASCE, 85, 67-94.

Okabe, M., Barrett, J. D. and Fumoto, H. (2004). "Effect of wood density on structural performance of shear walls for post and beam construction". Proceedings of 8th World Conference on Timber Engineering, Lahti, Finland.

Pardoen G., Waltman, A., Kazanjy R. P. Freund, E. and Hamilton C. H. (2003). "Testing and Analysis of One- Storey and Two- Storey Shear Walls under Cyclic Loading". CUREE Publication No. W-25. Richmond, CA.

Peterson, J. (1983). "Bibliography of lumber and wood panel diaphragms." ASCE Journal of Structural Engineering, 109(12): 2838–2852.

Prion, H.G.L. and Foschi, R. O. (1994). "Cyclic behavior of dowel type connections." Proceedings of 1994 Pacific Timber Engineering Conference, Queensland University of Technology, Australia, Vol. 1, 19-25.

Prion, H.G.L. and Filiatrault, A. (1996). "Performance of timber structures during the Hyogo-ken Nanbu earthquake of 17 January 1995". Canadian Journal of Civil Engineering, 23(3), 652-664.

Popovski M. (2000). "Seismic performance of braced timber frames". Ph. D thesis, University of British Columbia, Vancouver, BC.

Porter, K.A., Beck, J.L., Seligson, H.A., Scawthron, C.R., Tobin, L.T., Young, R. and Boyd, T. (2002). "Improving loss estimation for woodframe buildings." CUREE Publication No. W18, The CUREE-Caltech woodframe project, Richmond, CA.

Riddell, R. and Newmark, N.M. (1979). Statistical Analysis of the Response of Nonlinear Systems Subjected to Earthquakes, Structural Research Series No. 468, University of Illinoois at Urbana-champaign, Urban, IL.

Robertson, R. A. (1980). "Discussion of racking Strength of Light-Frame Nailed Walls", Journal of the Structural Division, ASCE 106(ST 9), 1981-1985.

Rosenblueth E. (1975). "Toward optimal design through building codes." Journal of the Structural Division, ASCE 102(ST3), 591-607.

Roswsky, D.V. (2002). "Reliability-based seismic design of wood shear wall." Journal of Structural Engineering. ASCE 128(11), 1439-1453 .

Sakamoto, L. and Ohashi, Y. (1988). "Effect of horizontal diaphragm on hehaviour of wooden dwellings subjected to lateral load – experimental study on a real size frame model", Proceedings of the 1988 International Conference on Timber Engineering, Vol. 2, 112-117, Seattle, WA.

Sakamoto, L. and Ohashi, Y. (1988). "Seismic response and required lateral strength of wooden houses and its applications." Proceedings of the 1988 International Conference on Timber Engineering, Vol. 2, 243-247, Seattle, WA.

Scales, L.E. (1985). Introduction to Non-Linear Optimization, Springer-Verlag, NY.

Sjoberg, B.D. (2003). "Probabilistic Analysis Software for Structural Seismic Response." Ph.D thesis, Univ. of British Columbia, Vancouver, BC.

StatLib. (2002) "Subroutine MINIM." http://lib.stat.cmu.edu/apstat/47. CSIRO and Rothamsted Experimental Station. Last updated on October 31, 2002. Visited on July 25, 2003.

Stefansescu, M. (2000). "Lateral resistance of traditional Japanese post-and-beam frames under monotonic and cyclic loading conditions." M.A.Sc thesis, Univ. of British Columbia, Vancouver, BC.

Stewart, W.G. (1987). "The seismic design of plywood sheathed shear walls." Ph.D thesis, University of Canterbury, Christchurch, New Zealand.

Stewart, W. G., Dean, J.A. and Carr, A. J. (1988). "The earthquake behaviour of plywood sheathed shearwalls". Proceedings of the 1988 International Conference on Timber Engineering. Vol 2, 248-261, Edited by Itani, R. Y. Seattle, WA.

Structural Engineers Association of California (SEAOC). (1995). "Performance Based Seismic Engineering of Buildings". Structural Engineers Association of California, Sacramento, CA.

Sugiyama, H., Uchisako, T., Andoh, N., Arima, R., Hirano, S. and Nakamura, N. (1988). "Comparison of lateral stiffness of frame obtained from full-scale test and that estimated by racking tests in Japanese type of wooden frame construction". Proceedings of the 1988 International Conference on Timber Engineering. Vol. 1, 804-810. Edited by Itani, R. Y. Seattle, WA.

Tissell, J. R. (1993). Structural Panel Shear Walls. Research Report No. 154. American Plywood Association, Tacoma, WA.

Tsukuba Building Test Laboratory Center of Better Living. (2001). Testing Method for Wooden Shear Walls and its Shear Strength Coefficient (bairitu). Technical Report. Tsukuba, Japan. (Test Method is authorized by Japan Japanese Ministry of Land, Infrastructure and Transport).

Tuomi, R.L. and McCutecheon, W.J.(1978). "Racking strength of light-frame nailed walls." Journal of the Structural Division. ASCE, 104(ST 7). 1131-1141

Vamvatsikos, D. and Cornell, C. A. (2002). "Incremental dynamic analysis." Earthquake Engineering and Structural Dynamics. 31(3):491-514.

van de Lindt, J. W. (2003). "Evolution of wood shear wall testing, modeling, and reliability analysis: bibliography". Practice Periodical on Structural Design and Construction. 9(1), 44-53.

van de Lindt, J. W., Huart, J. N. and Rosowsky, D. V. (2005). "Strength-based seismic reliability of wood shear walls designed according to AF&PA/ASCE 16". Journal of Structural Engineering, 131(8): 1307-1312.

van de Lindt, J. W., and Walz, M. A. (2003). "Development and application of wood shear wall reliability model". Journal of Structural Engineering, 129(3): 405–413.

Ventura, C. E., Taylor, G.W., Prion, H.G.L., Kharrazi M.H.K. and Pryor, S. (2002). "Full-scale Shaking Table Studies of Woodframe Residential Construction." Proceedings of the 7th US Conference of Earthquake Engineering (CD-ROM), 334. Boston, MA.

Wilson, E. L., Farhoomand, I. and Bathe, K. J. (1972). "Nonlinear dynamic analysis of complex structures".. Earthquake Engineering and Structural Dynamics. 1, 241-252.

Yamaguchi, N., Karacabeyli, E., Minowa, C., Kawai, N., Watanabe, K. and Nakamura, I. (2000). "Seismic performance of nailed wood-frame shear walls". Proceedings of World Conference on Timber Engineering, Paper No. 8-1-1. Whistler, BC.

Yasumura, M. (1990). "Seismic behavior of braced frames in timber construction". Proceedings of International council for building research studies and documentation working commission W18A- Timber structures. Lisbon, Portugal.

Yasumura, M. (2000). "Dynamic Analysis and Modeling of Wood-framed Shear Walls". Proceedings of World Conference on Timber Engineering (CD-ROM). Paper No. 7-1-3. Whistler, BC.

Yun, S, Hamburger, R.O. and Cornell, C.A. and Foutch, D.A. (2002). "Seismic Performance Evaluation for Steel Moment Frames." Journal of Structural Engineering. ASCE 128(4), 534-545.

Zacher, E.G. (1994). "Past seismic Performance of Timber Buildings." Proceedings of Research Needs Workshop: Analysis, Design and Testing of Timber Structures Under Seismic Loads. Forest Product Laboratory. University of California, CA.

Zhang, J. and Foschi, R. O (2003). "Performance-based design and seismic reliability analysis using designed experiments and neural networks." Probabilistic Engineering Mechanics, 19(3): 259-267. (Fifth International Conference on Stochastic Structural Dynamics)

APPENDIX I. TWO EXAMPLES OF MONTE CARLO METHOD CONSIDERING WEIGHTED RANKING

Two examples are demonstrated to verify the efficiency of the Monte Carlo method considering weighted ranking. One example is to simulate a lognormal distribution with a mean of 1.6487 and a variation of 2.1612. 30 pseudo random numbers were generated to follow this distribution. They were ranked as illustrated in the original Monte Carlo method (Figure A. 1 top). Same set of numbers are processed with the weighted ranking method and the results are shown in the bottom half of Figure A.2.

Another example is the simulation of the distribution of the variable, z, which is a function of x and y, shown as

$$z = \frac{1}{9} x^2 e^y \qquad \text{(A.1)}$$

where

x follows a lognormal distribution with a mean of 1.6487 and a variation of 2.1612;

y follows a uniform distribution between 0 and 1.

The distribution of z can be simulated with the original Monte Carlo method. Figure 5.6 gives the result simulated from 1000 set of data. To achieve the result with fewer samples, 16 values were sampled from the variable x and 10 values were sampled from the variable y. The function z is evaluated for each combination of x and y. There are 160 sets of z value in total (16x10). Directly and weighted ranking methods were applied to generate the distribution curves, respectively. The result is presented in Figure A.2.

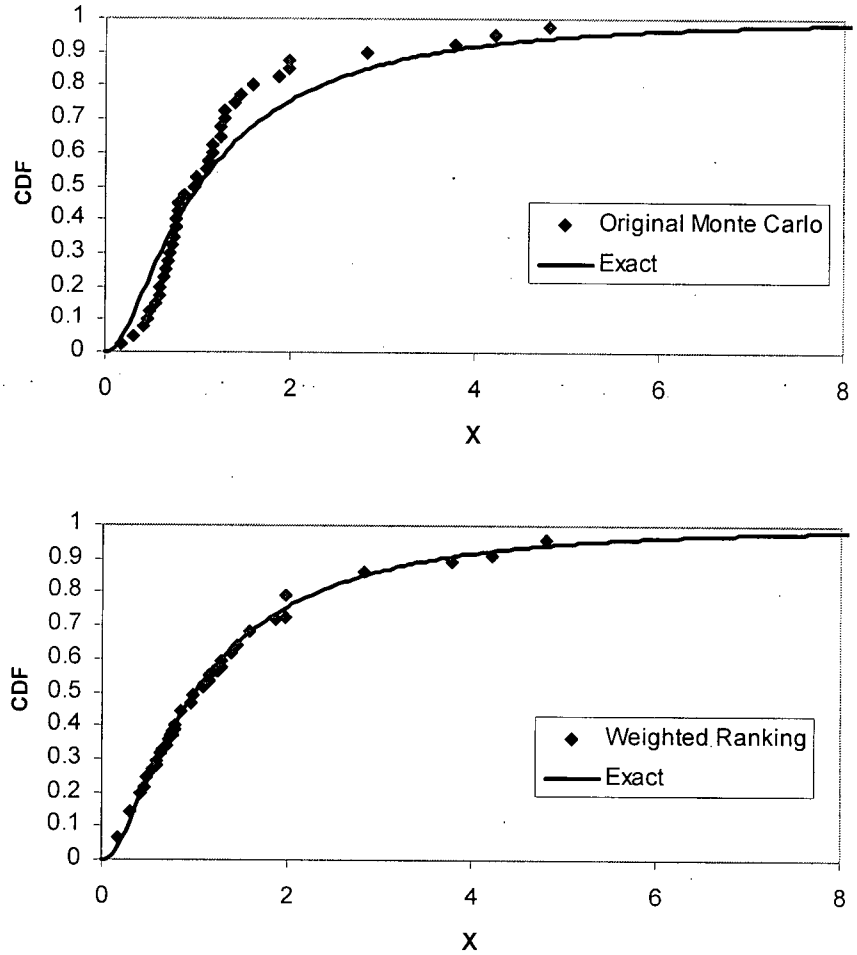

Figure A. 1 Simulating lognormal distribution with weighted ranking method

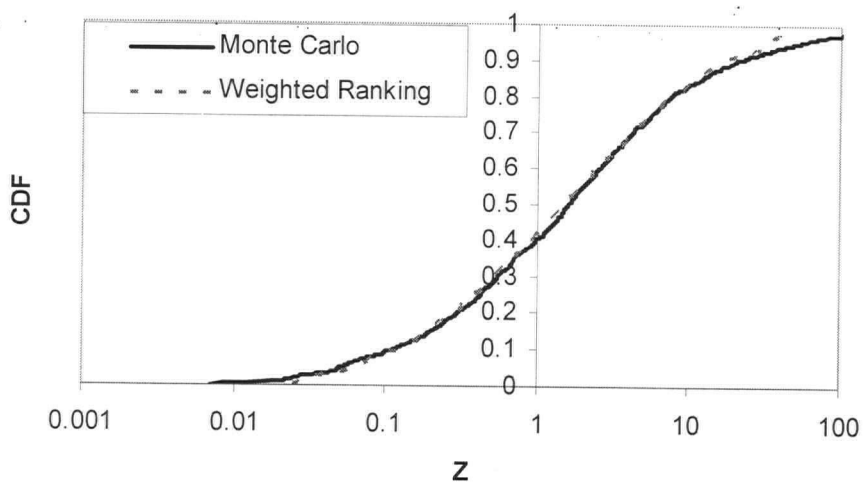

Figure A.2 Comparison between Monte Carlo and weighted ranking methods

APPENDIX II. RESULTS OF DRIFT DEMAND OF JAPANESE WALLS

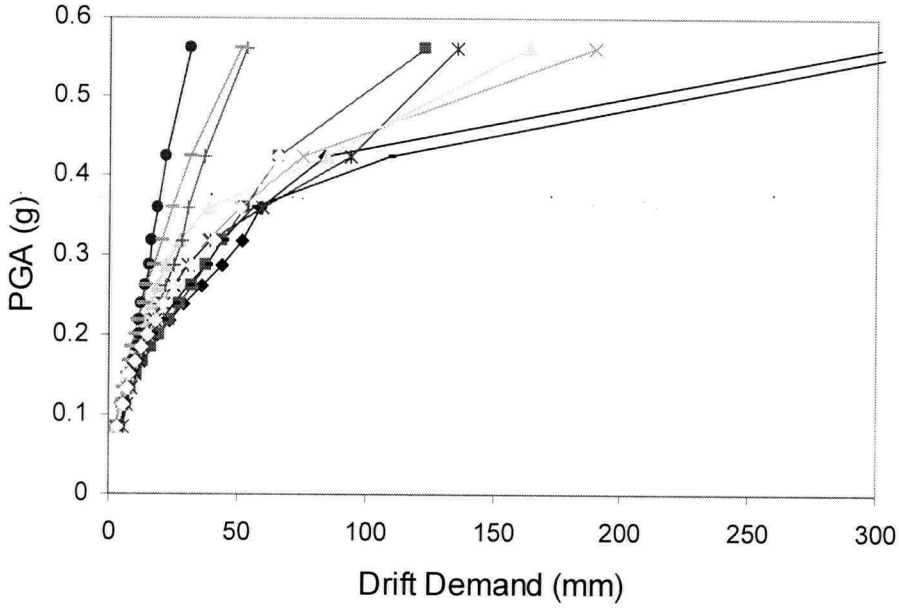

Figure A.3 Drift demand for Sugi braced walls (20 kN load)

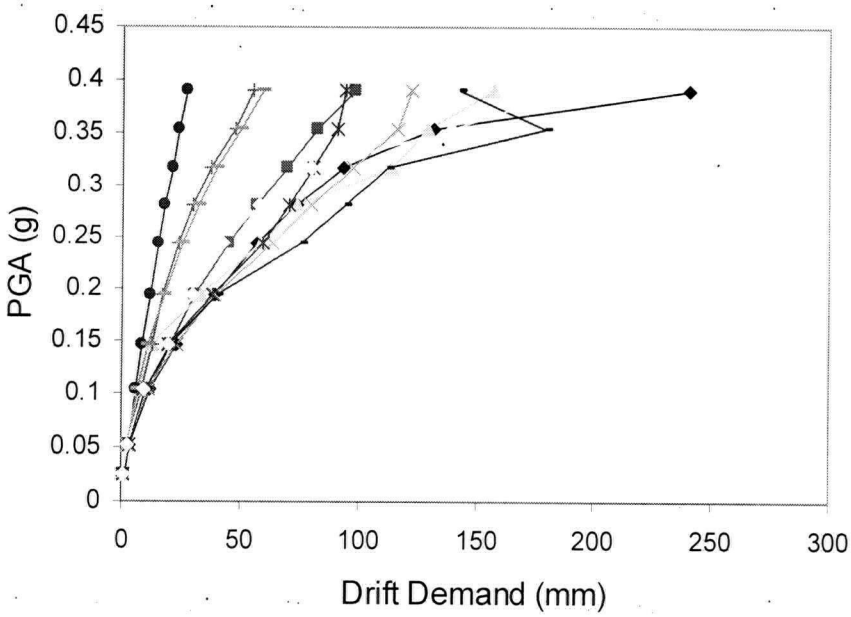

Figure A.4 Drift demand for Sugi braced walls (30 kN load)

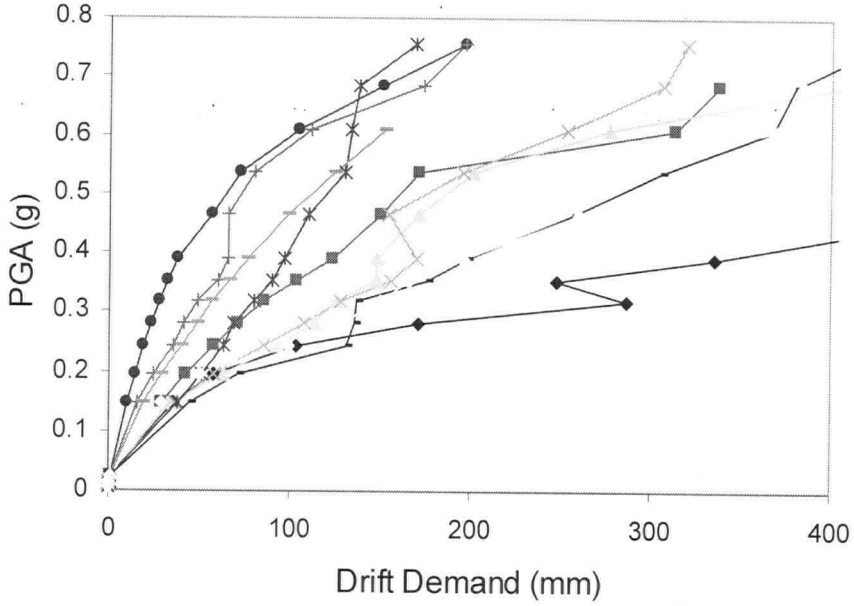

Figure A.5 Drift demand for Sugi braced walls (40 kN load)

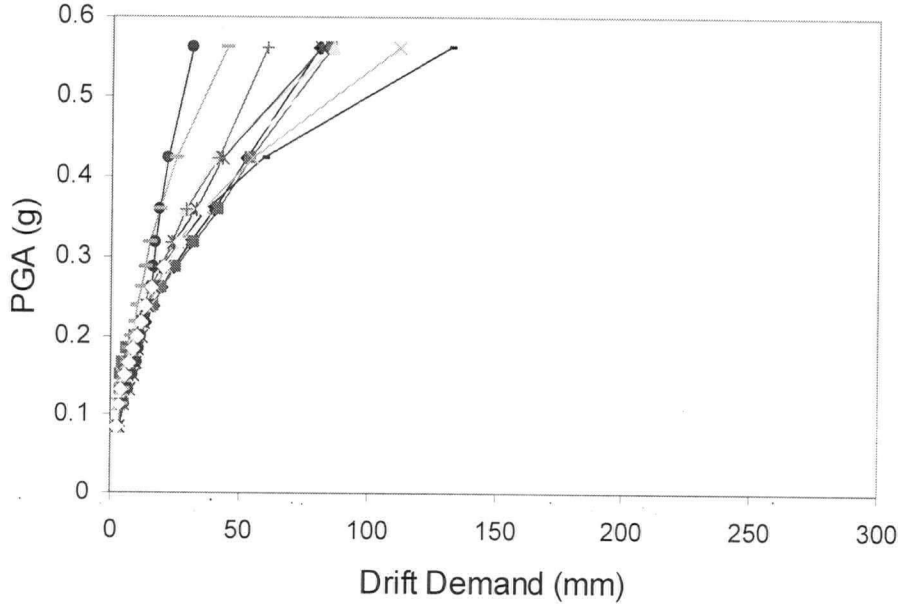

Figure A.6 Drift demand and for Sugi plywood walls (20 kN load)

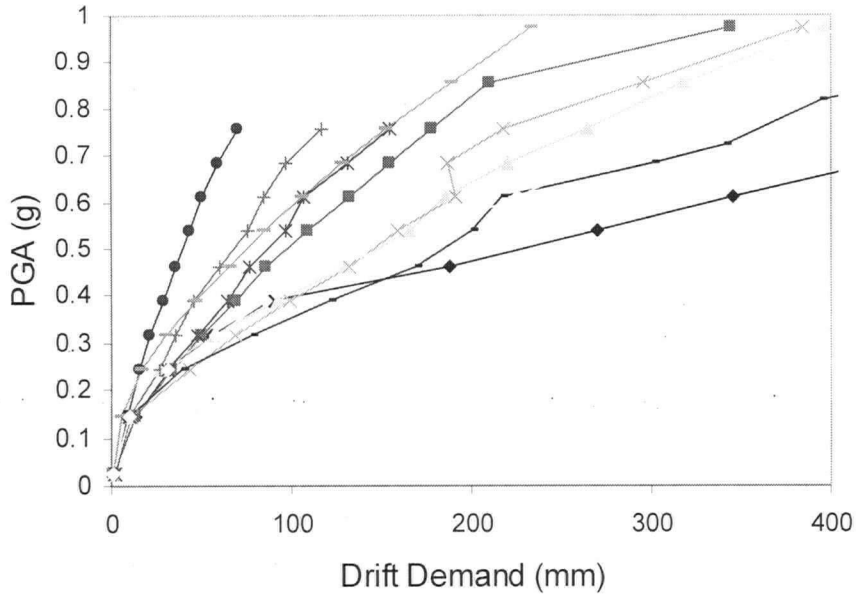

Figure A.7 Drift demand and for Sugi plywood walls (30 kN load)

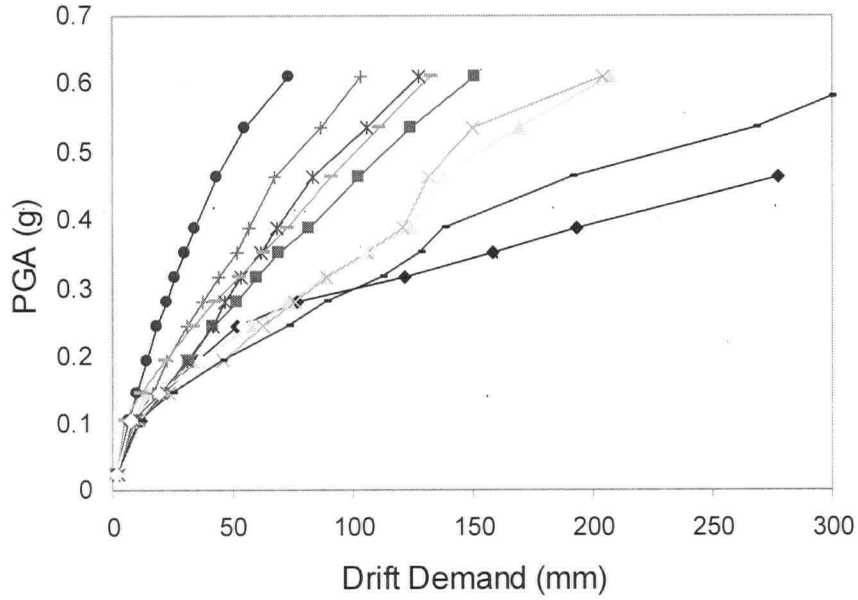

Figure A.8 Drift demand for Sugi plywood walls (40 kN load)

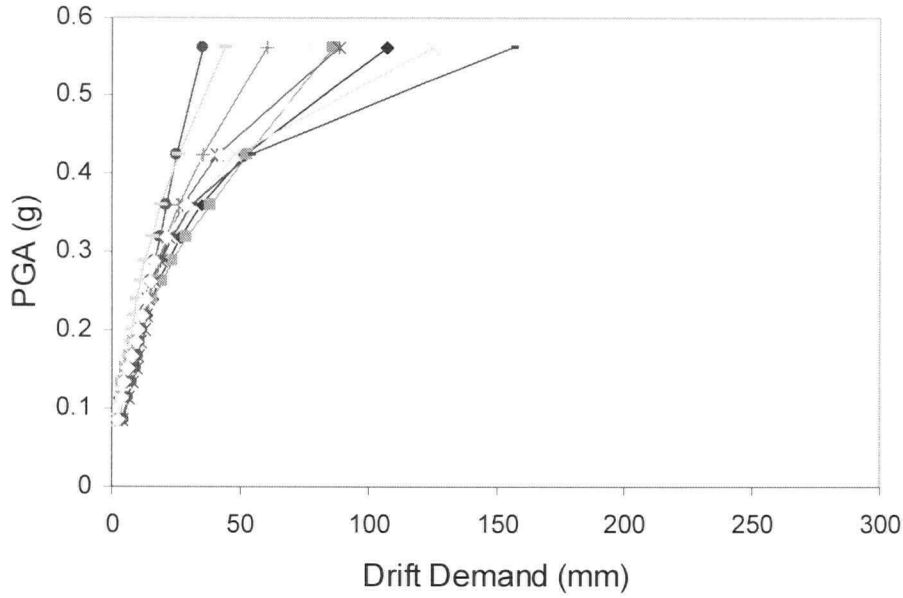

Figure A.9 Drift demand for Sugi OSB walls (20 kN load)

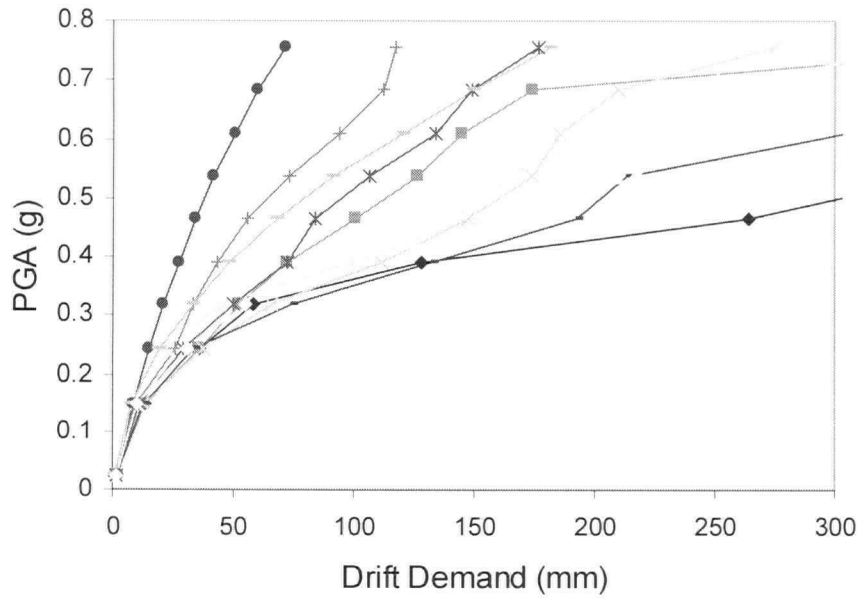

Figure A.10 Drift demand for Sugi OSB walls (30 kN load)

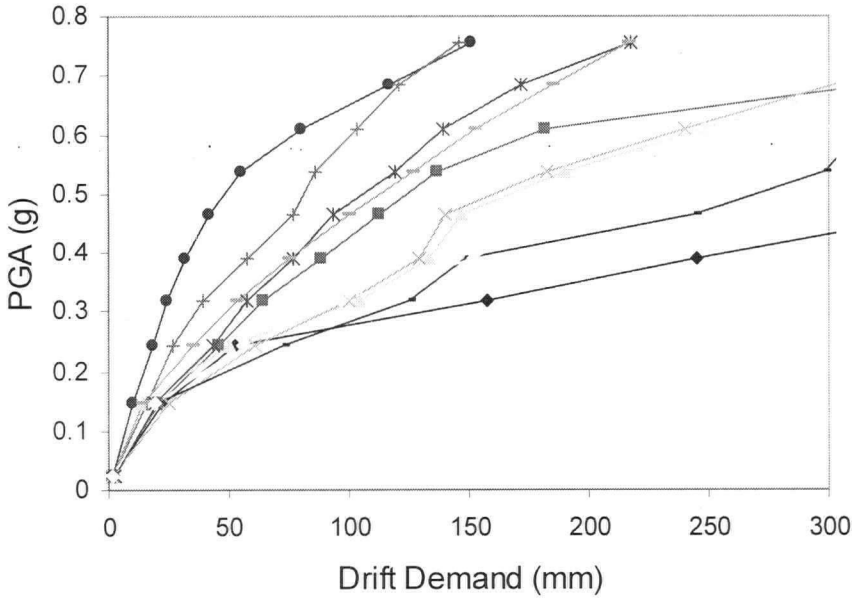

Figure A.11 Drift demand for Sugi OSB walls (40 kN load)

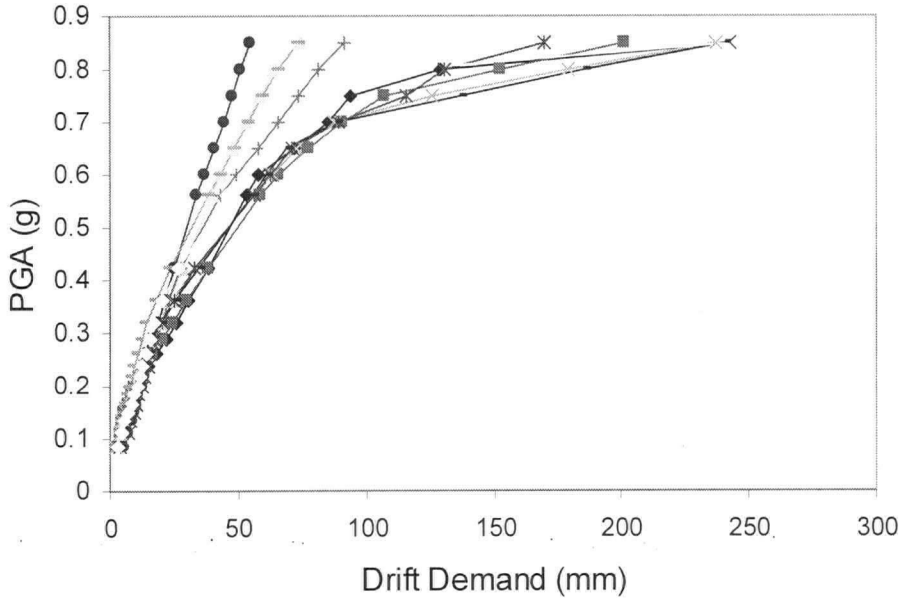

Figure A.12 Drift demand for Tsuga braced walls (20 kN load)

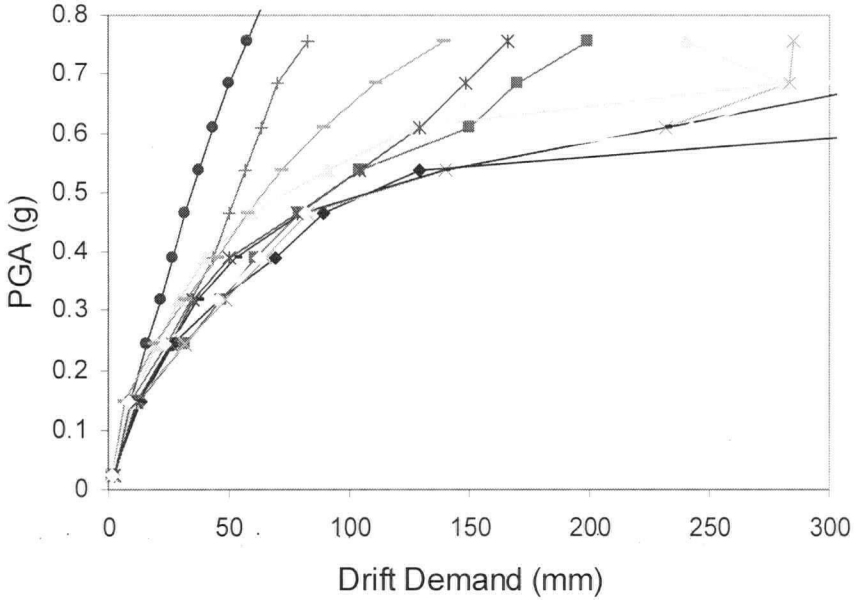

Figure A.13 Drift demand for Tsuga braced walls (30 kN load)

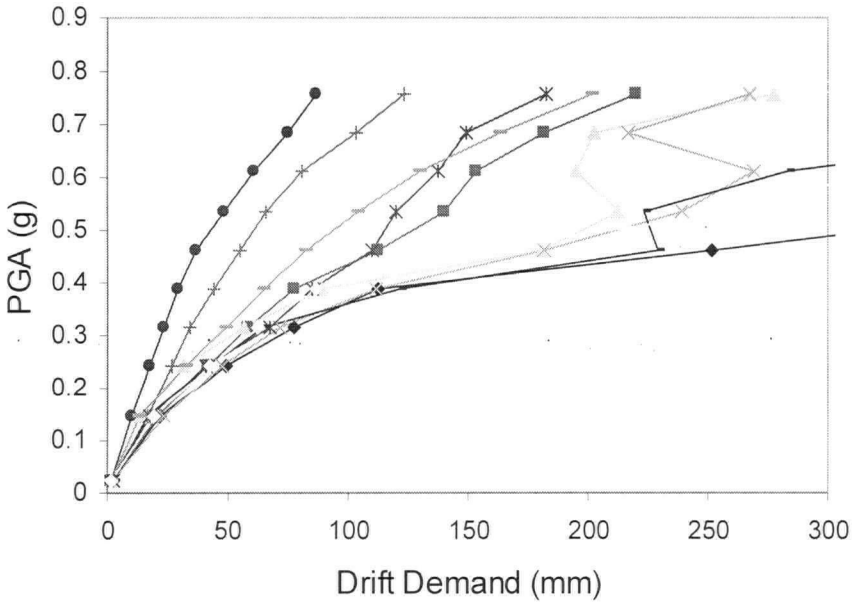

Figure A.14 Drift demand for Tsuga braced walls (40 kN load)

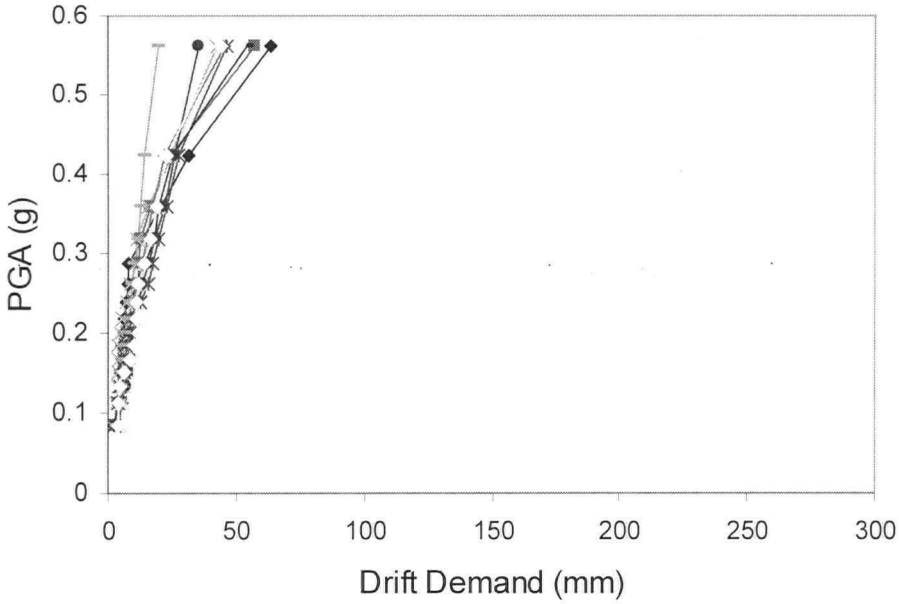

Figure A.15 Drift demand for Tsuga plywood walls (20 kN load)

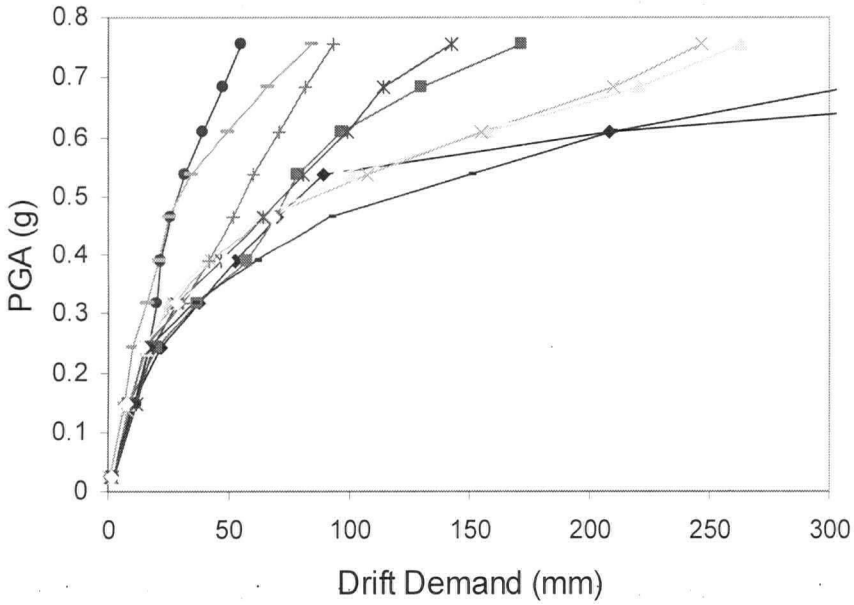

Figure A.16 Drift demand for Tsuga plywood walls (30 kN load)

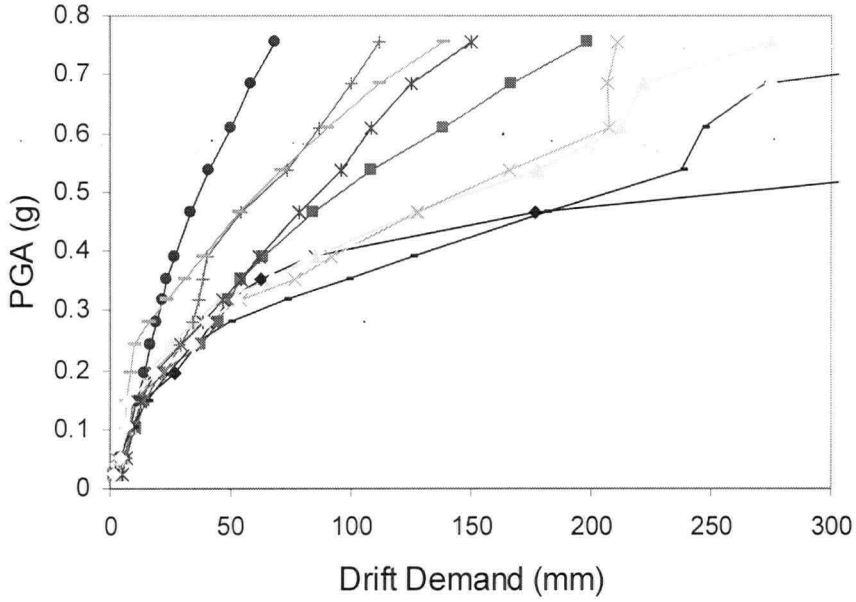

Figure A.17 Drift demand for Tsuga plywood walls (40 kN load)

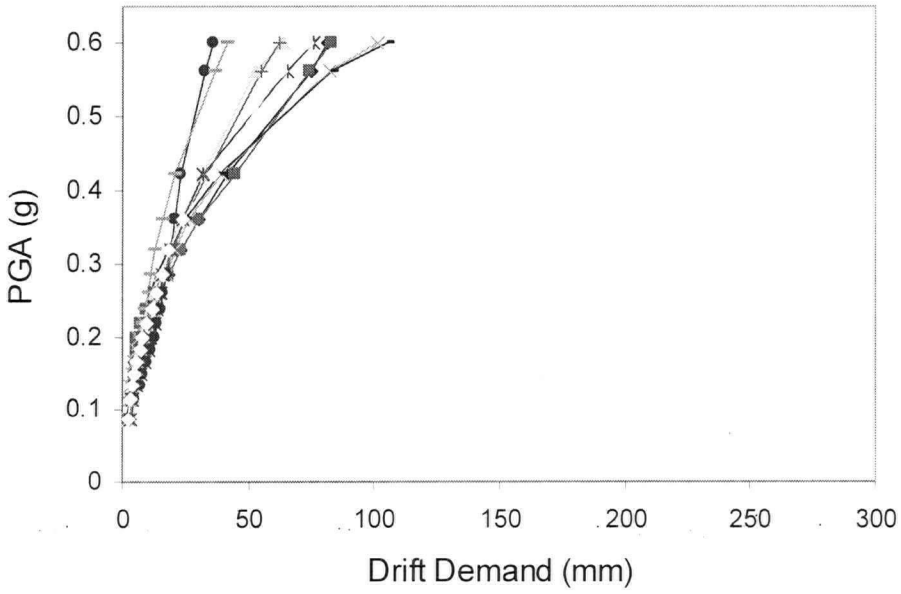

Figure A.18 Drift demand for Tsuga OSB walls (20 kN load)

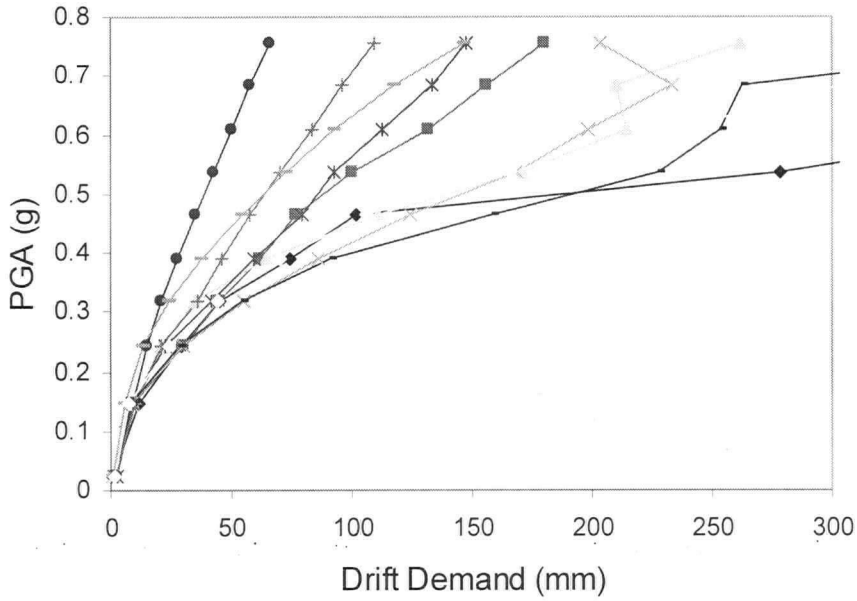

Figure A.19 Drift demand for Tsuga OSB walls (30 kN load)

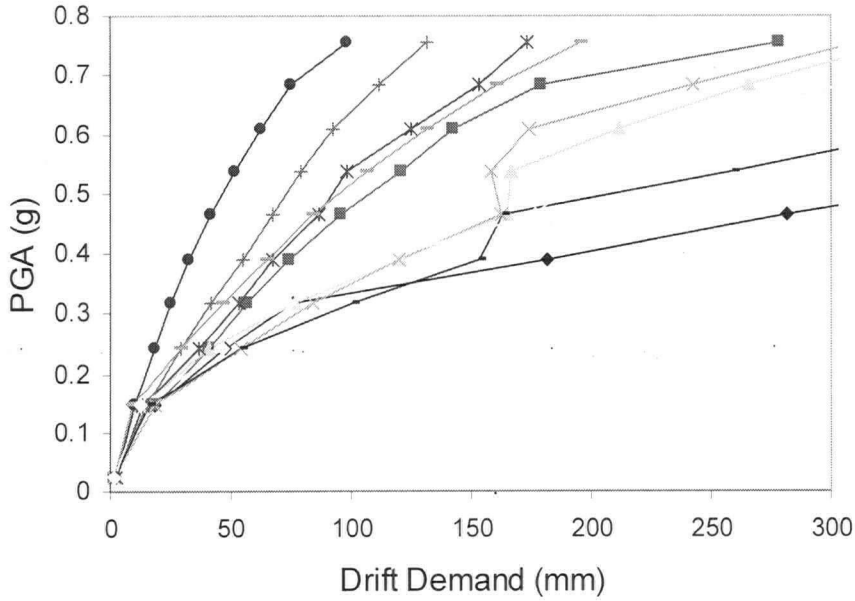

Figure A.20 Drift demand for Tsuga OSB walls (40 kN load)

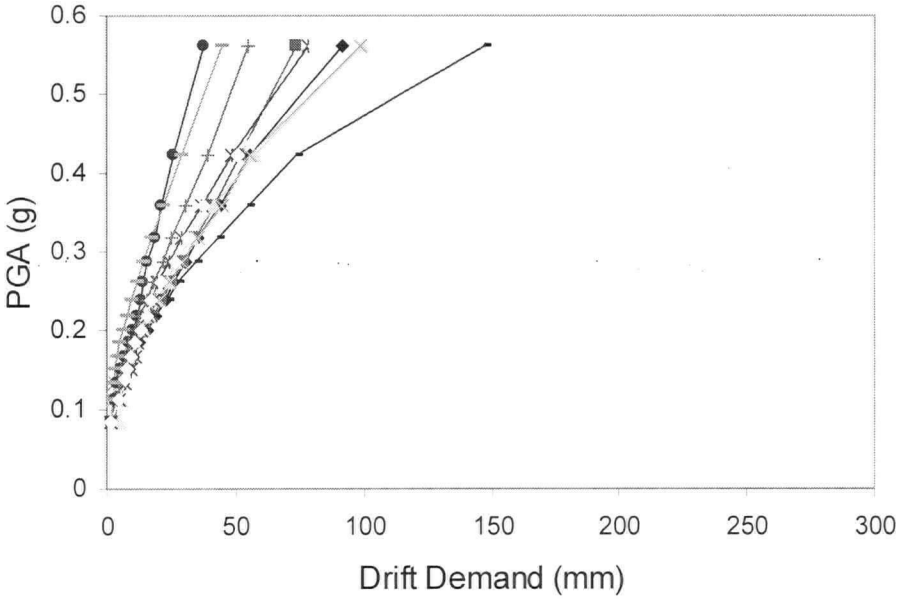

Figure A.21 Drift demand for Whitewood braced walls (20 kN load)

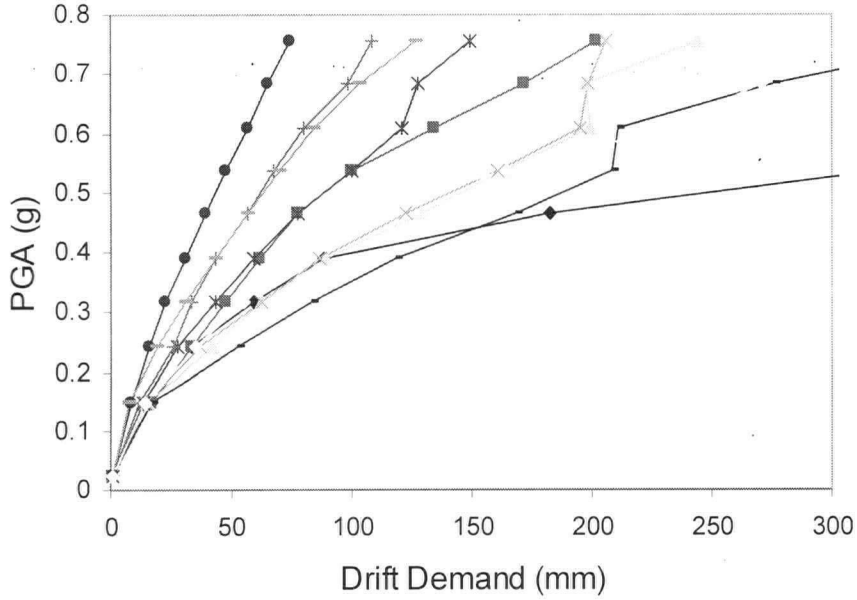

Figure A.22 Drift demand for Whitewood braced walls (30 kN load)

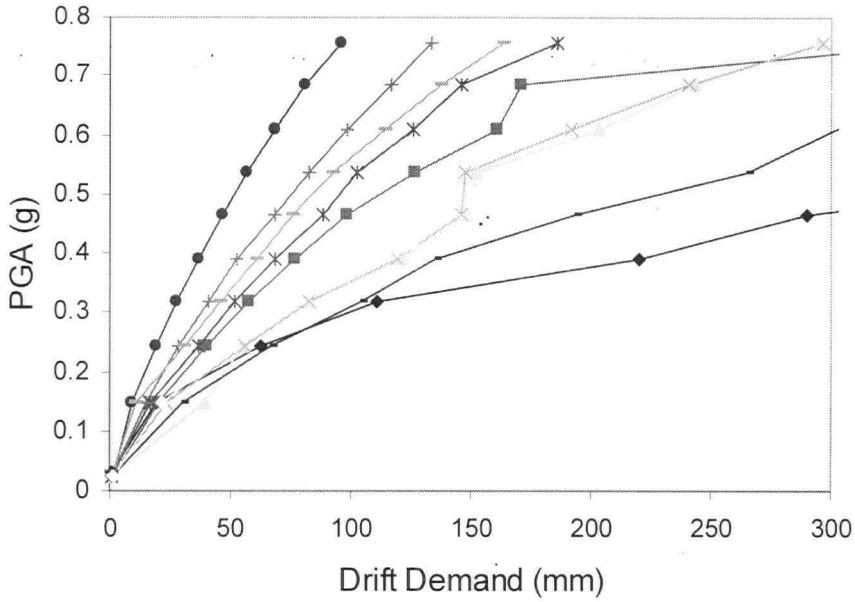

Figure A.23 Drift demand for Whitewood braced walls (40 kN load)

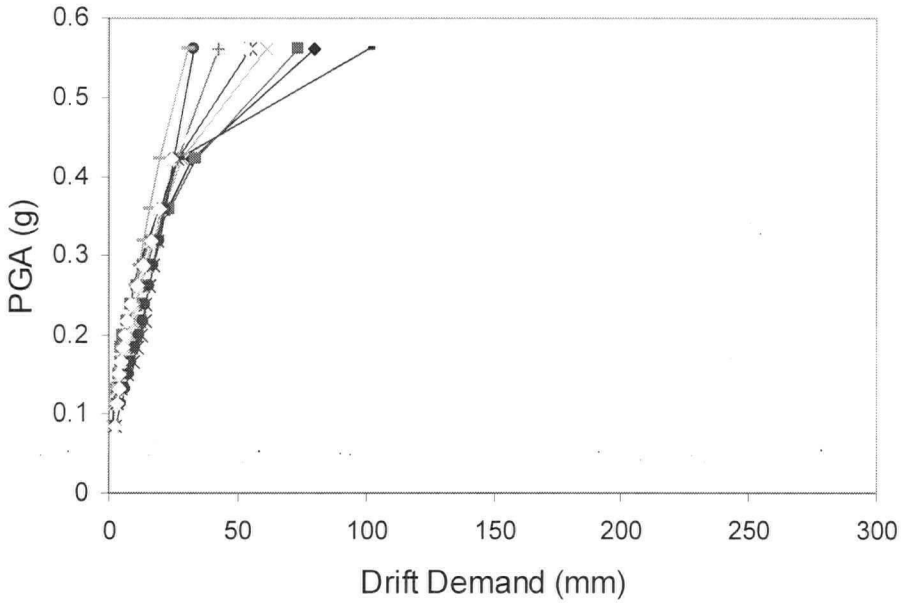

Figure A.24 Drift demand for Whitewood plywood walls (20 kN load)

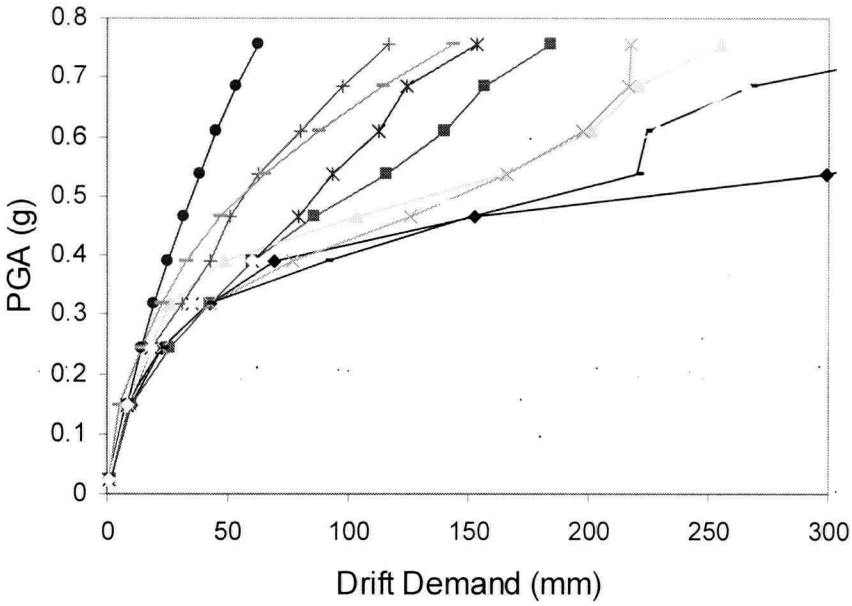

Figure A.25 Drift demand for Whitewood plywood walls (30 kN load)

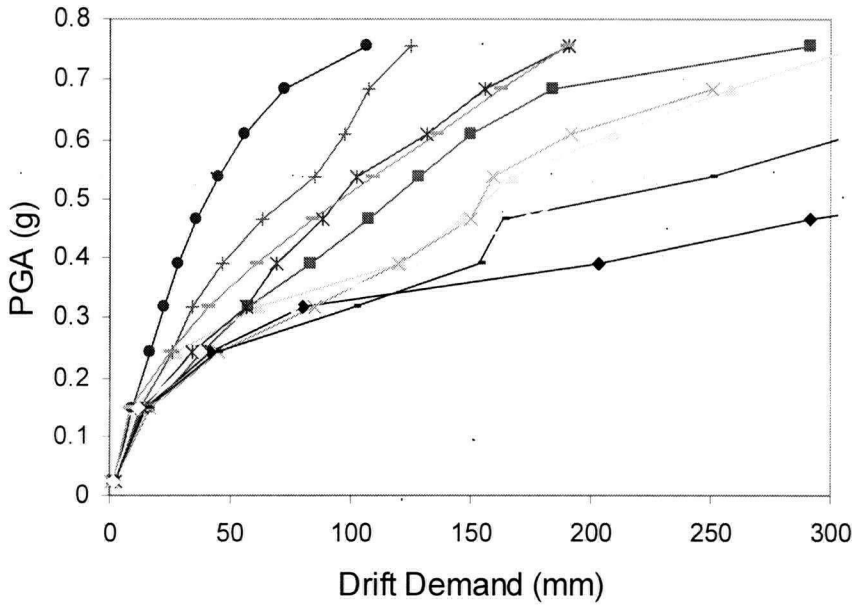

Figure A.26 Drift demand for Whitewood plywood walls (40 kN load)